R-14-30

A demonstration project on controlling and verifying the excavation-damaged zone

Experience from the Äspö Hard Rock Laboratory

Lars O Ericsson, Johan Thörn
Chalmers tekniska högskola

Rolf Christiansson, Tomas Lehtimäki, Henrik Ittner
Svensk Kärnbränslehantering AB

Kent Hansson, Geosigma

Christian Butron, Sweco

Oskar Sigurdsson, OS Geological Consulting

Pär Kinnbom, PK konsult

January 2015

Svensk Kärnbränslehantering AB
Swedish Nuclear Fuel
and Waste Management Co

Box 250, SE-101 24 Stockholm
Phone +46 8 459 84 00

ISSN 1402-3091
SKB R-14-30
ID 1453521
January 2015

A demonstration project on controlling and verifying the excavation-damaged zone

Experience from the Äspö Hard Rock Laboratory

Lars O Ericsson, Johan Thörn
Chalmers tekniska högskola

Rolf Christiansson, Tomas Lehtimäki, Henrik Ittner
Svensk Kärnbränslehantering AB

Kent Hansson, Geosigma

Christian Butron, Sweco

Oskar Sigurdsson, OS Geological Consulting

Pär Kinnbom, PK konsult

Extended summary

Over the years SKB has carried out extensive studies on the presence and physical behaviour of an excavation damaged zone, the so called EDZ, which may surround a tunnel. The SKB reference method for excavation of a nuclear waste repository is the drill-and-blast method even if other methods are studied and analysed. The field investigations presented in this report address one of the regulatory comments (SSM 2011) that "SSM believes it is important that SKB can show that the requirements made by the design premises on the EDZ can be met in tunnelling under production conditions in Forsmark". The report describes the requirements for and results of an excavation in one of the tunnels, TAS04, at Äspö Hard Rock Laboratory, Oskarshamn, Sweden. The project has had special emphasis on the EDZ in the floor of the tunnel.

The work in this project has adopted a broad approach emphasizing experience from field work, the applied evaluation methods, the most significant findings and recommendations. This in turn has meant that a very large amount of background material is gathered in separate appendices.

Furthermore, this project has been focused on quality measures to ensure that requirements on tunnel excavations are met and methodological studies of methods for verification of the resulting excavation damage.

Objectives

The project objectives were:

- Propose the requirements needed to execute tunnelling with the drill-and-blast method so that the EDZ is minimized and also propose the required QA/QC measures and the documentation needed to verify that the requirements are met.
- Develop a characterization method to confirm the initial state regarding the extent of excavation-induced fractures.
- Develop a method for characterization of the hydraulic properties of the EDZ and demonstrate by field experiments its suitability for application in a tunnel environment.
- Propose means and methods to verify that post-closure safety requirements regarding the EDZ are met.

Scope of works

The proposed strategy for verification of the extent of the EDZ and scope of works has been developed based on the following principles and methods:

- Verification that the execution of blasting complies with requirements on drilling, charging and detonation by documentation and analysis of deviations.
- Geometrical control of the tunnel contour to ensure that tolerances in contour control are complied with.
- Follow-up inspection using geophysical methods on the tunnel floor after blasting. Mainly ground-penetrating radar has been used.
- Mapping of the tunnel floor for supplementary visual assessment of the extent of the excavation damage.
- Development of a conceptual model showing the tunnel floor's topography, fracturing and the estimated extent of the EDZ.
- Hydraulic characterization of the EDZ in short boreholes (1–2 metres) by means of injection tests and cross-hole interference tests.
- Development of a hydraulic conceptual model of the EDZ.

An overview of the input data, analysis, modelling and evaluations carried out is summarized in Figure ES-1.

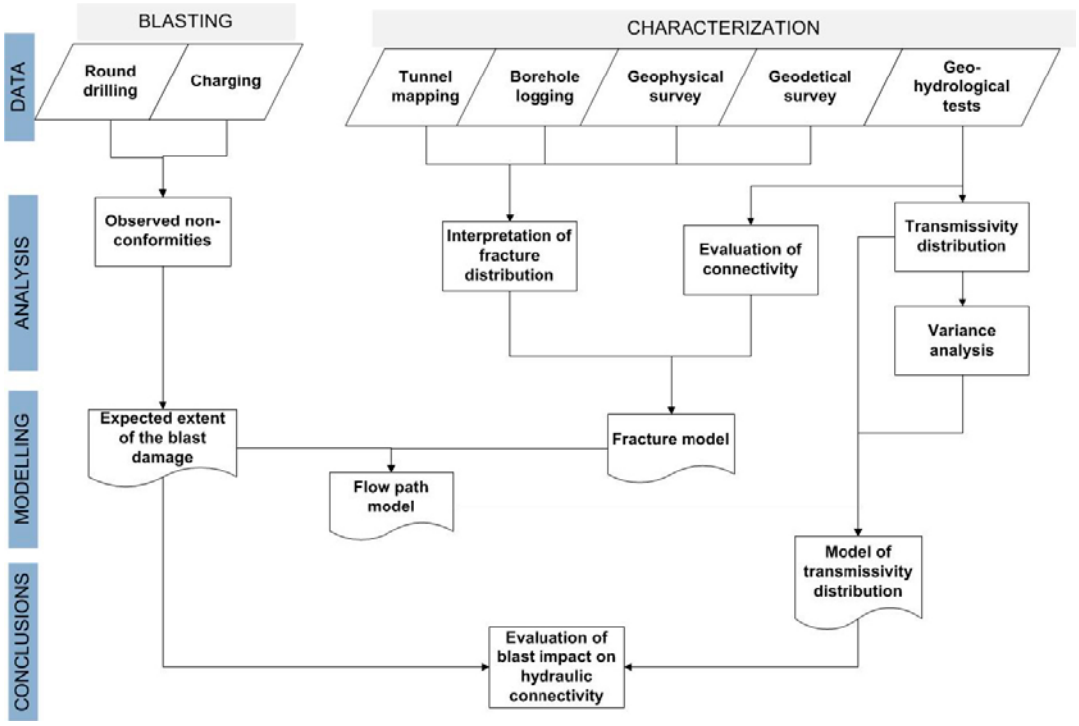

Figure ES-1. *Overview of data flow and interpretations in this project.*

Excavation method

The tunnel was excavated with careful drill & blast method. The blast design was adopted from a previous excavation study at the Äspö Hard Rock Laboratory that had proven to cause very limited excavation damage. The follow-up of the excavation works concluded that the requirements on perimeter control (drilling precision) and charged weights of explosives was met to a high degree. The least successful drilling was in the tunnel floor. 50% of the tunnel floor exceeded the requirement of a maximum look out angle of 30 cm outside the theoretical tunnel floor. No pre-grouting was needed for this experimental tunnel.

Site conditions

The site conditions at the actual tunnel at 410 m depth was characterised by tunnel mapping and coring of 42 holes along 20 metres of the tunnel floor. 7 holes are 2.0 m deep and the others are 1.0 m. The lithology is dominated by fine grained granite and diorite/granodiorite. The dominant natural fracture sets are steeply dipping, approximately parallel and perpendicular to the studied tunnel, as well as gently dipping fractures. The mean total inflow to the 20 m long tested part was 0.54 L/min and the pore pressure varied significantly between the 42 boreholes in the floor. There were 9 sections in which pore pressures were estimated to be equal to or higher than 250 kPa, relative to the atmospheric pressure. A maximum hydraulic pressure was determined to 865 kPa in a section. The tunnel is oriented parallel to the maximum horizontal in situ stress. The stress composants perpendicular to the tunnel is in the range of 11–12 MPa. This is estimated to have a minor influence on the tunnel stability in this hard, crystalline rock. However, the calculated vertical displacement based on a simple 2D elastic model indicate the potential for a maximum heave of the floor of approximately 1.0 mm. This convergence might contribute to the development of excavation induced fracturing in the floor.

Geophysical investigations

The GPR EDZ method has been used to study how deep the EDZ penetrates. This method provides valuable information in evaluation of excavation quality and general rock damage level. Interpreted distinct reflectors also provide an indication of EDZ formation close to the tunnel surface, as well as the presence on larger structures, whether natural or excavation-induced. The equipment used

for the GPR survey of the tunnel floor was GSSI's (Geophysical Survey Systems, Inc.) SIR-3000 GPR system with a shielded ground-coupled 1.5 GHz bandwidth antenna. The data was collected by positioning the antennae against the cleaned and dried tunnel floor in lines parallel to the tunnel with an increment of 10 cm covering the whole width of the tunnel. Interpretation of distinct reflectors from each measurement line was done by selecting reflectors that could be followed in more than 4 parallel lines. This gives a 30 cm "cut-off". Any discontinuity where there is a contrast in electrical properties could cause a reflection. Consequently, all reflections are not necessarily caused by fractures.

The resistive rock is optimal for GPR analysis due to relatively low attenuation. Cracks and fractured areas can be spotted as far as 1 m below the surface. Detectability (how small structures can theoretically be detected) is calculated from the wavelength as a function of depth. In this study, detectability varies between 6 and 30 cm (depth range 0.05–1 m), which means that in the deeper parts of the studied object a feature has to be at least 30 cm in diameter in order to be detected as a reflector. The depth determination for reflectors is based on the radar wave velocity (travel time) in the media, which is governed by its dielectric properties. The average value of wave velocity that was used (0.12 m/ns) gives a good estimate of depth for reflectors with few percentage errors. It is possible to determine the orientation (strike and apparent dip) of the reflectors, and the results can also be used to study reflector length variation or reflector density variation. The horizontal maximum length of the interpreted 130 reflectors is 3.8 m in the direction parallel to the tunnel and 2.0 m in the perpendicular direction. There is most observed reflectors in the first part of the tunnel that is dominated by the very brittle fine-grained granite.

From the 3D model, partly shown in Figure ES-2, where all results in this study are included, it is possible to determine the orientation (strike and apparent dip) of the reflectors, and the results can also be used to study reflector length variation or reflector density variation. The model shows that most of the interpreted reflectors are sub-horizontal, and the apparent dip varies from 0 to a maximum of approximately 40 degrees in some cases. The GPR method has limitations in detecting fractures in a larger angle (45–60 degrees) to the surface where the measurements are carried out.

Investigations of fractures in wire-sawed slots at the tunnel surfaces have also been conducted, see Ittner and Bouvin (2015). A total of 5 slots were made, four of which were in the TAS04 tunnel and two were in the tunnel floor in the same area as in this study. Fracture mapping in the slots was done by applying a dye penetrant to the sawed surface, which makes the fractures more visible and permits mapping of even small fractures. The fractures were divided in the interpretation into two groups, excavation fractures and natural fractures, and are marked with different colours in the resulting photographs. When the fractures interpreted from the sawed surfaces are viewed together with the interpreted reflectors from the GPR results, some observations the can be made regarding the GPR interpretation uncertainties and method resolution.

From Figure ES-3 it is obvious that more features are visible in the sawed surface than can be interpreted from GPR. The resolution in GPR does not allow detection of small and very tight fractures, which use of the dye penetrant does. Looking at the right-hand side of Figure ES-3 there seems to be a continuous sub-horizontal fracture (marked with yellow arrow) that is not detected by the GPR. This could be explained by two facts. First, the fracture seems to be dry at this part of the cut. On the left part of the surface (marked by the yellow circle) there is a similar fracture, but wet, and an interpreted reflector coincides with it. Second, above this fracture there is a fracture swarm as well as excavation fractures that could attenuate the GPR signal and thus prevent detection.

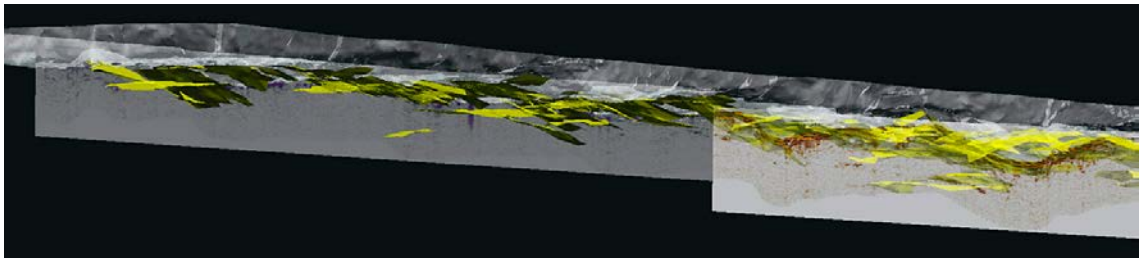

Figure ES-2. *A 3D view of interpreted reflectors. In the background are the outermost radar profiles.*

Figure ES-3. *A photograph showing a sawed slot in the floor of TAS04 at tunnel length 34 m. The interpreted fractures from Ittner and Bouvin (2015) are marked with green (natural fractures) and yellow (excavation fractures). The light blue lines are GPR reflectors that intersect this section.*

The attenuation effect can also be seen at the left below the previously mentioned fracture, where no reflector exists. Looking closer at the large sub-horizontal fracture marked by a yellow circle, we see a small difference in the location of the reflector. This may be due to the dip error discussed earlier, but it may also result from the fact that the radar wave velocity used in GPR interpretation is too high in this case.

Hydraulic tests

The hydraulic testing has focused on sealed off section transmissivities, specific capacities and flow connectivities in the context of characterization, without considering flow modelling issues. Since the assessment of long-term safety is based on saturated conditions, the testing and analysis methods do not include unsaturated situations, even though the tunnels and niches are open and in atmospheric contact. In the development of an appropriate hydraulic test method, several aspects have been considered, e.g. choice of test location, equipment robustness, equipment mobility, measurement resolution, initial and boundary conditions of testing, confinement, hydro-mechanical couplings and test durations. Furthermore, for the evaluation and interpretation of test responses in terms of flow and pressure changes, it has been essential to consider boundary conditions, heterogeneity, anisotropy (hydraulic and structural), spatial variability and scale dependence. Different practical aspects and their implications for test analysis have also been highlighted.

In this study it has not been possible to determine the transmissivity of single fractures beneath the tunnel floor in the depth range of a potential EDZ. Therefore, the study has focused on measuring flow in short vertical boreholes, which in turn are divided into several shorter test sections by means of packers. Different hydraulic evaluation methods have been used in the study. In order to ensure saturated conditions near the tunnel floor, a positive hydraulic boundary condition was maintained at the floor by means of a constant water level above or close to the tunnel floor and with the aid of pumps in the ponds. The injection or packer tests that have been used in this project were performed in uncased short boreholes in order to permit interpretation of a section transmissivity of individual layers by isolating them with the aid of packers. In total 210 injection tests were carried out. Even though the concept can be disputed, the method is widely used for approximately estimating the hydraulic characteristics of fractured rock (see e.g. Singhal and Gupta 1999 or Gustafson 2012).

Due to the existence of positive boundary conditions as well as the very short packer intervals (slimness in project r_w/L varies from 0.027 to 0.38), a sensitivity analysis was carried out in order to suggest a suitable determination method for the steady-state injection tests. In order to treat boundary condition uncertainties in a conservative way, the evaluation of steady-state section transmissivities have mainly been done using the Moye's formula.

The transient evaluations have been done using the software Aqtesolv V4.50.002, which contains a library of different evaluation models. The tests were carried out in fractured rock, but the evaluation models regard the rock as an equivalent porous medium. This means, that the injected flow is

assumed to be distributed uniformly in all directions from the injection section (space filling). This assumption is, however, rarely fulfilled in fractured hard rock. The transient evaluations of the injection tests have been done both for selected injection sections and observation sections.

Different evaluation activities have been carried out to determine hydraulic connectivity along the tunnel floor or beneath the floor. The pressure responses from the injection tests were analyzed in qualitative ways. Another option for interpreting connectivity conditions has been to assess the variability of the specific capacities or section transmissivities along the tunnel floor. This has been done by means of semi-variogram analysis and kriging. The kriging has been carried out in 2D for each test interval. Furthermore, depth dependence between different layers in the floor has been assessed according to specific capacity values.

The equipment for the hydraulic tests was designed to perform measurements in short holes drilled in tunnels. The equipment was developed to meet the following specifications: 1) it must be capable of measuring transmissivities between $5 \cdot 10^{-10}$ and $5 \cdot 10^{-7}$ m^2/s at an assumed pressure disturbance of 500 kPa and measurements along the drilled holes must be made from the borehole opening (tunnel floor), 2) it must be possible to display numeric values and produce simple graphs with selected parameters versus time, 3) a measurement must include both an injection and a recovery phase.

There is some risk that measurements made near the tunnel floor could cause jacking or elastic deformations in the fractures if the injection pressures are too high. Furthermore, the selected injection pressure should be high enough in relation to the error of the hydraulic formation pressure so that it has a minimal effect on the evaluation of the test. However, injection pressures must not be so high that turbulent flow is obtained. In our test set-up, it has been estimated that laminar flow in single fractures occurs if the mean aperture does not exceed 0.3 mm, i.e. fracture transmissivities are lower than $T = 3 \cdot 10^{-5}$ m^2/s (Zimmerman and Bodvarson 1996, Gustafson 2012). In order to determine the over-pressure that could be used in the injection tests, initial measurements were made of the deformations in selected sections with different injection pressures. Based on the results of the initial measurements, the over-pressure used in relation to the hydraulic formation pressure was decided to about 200 kPa for sections 0.00 to 0.10 m and 0.10 to 0.20 m, and to about 500 kPa for the deeper sections.

The steady-state analysis focused on section transmissivities determined using Moye's formula. Hydraulic conductivities and specific capacities were also determined. The interpreted transmissivity results versus borehole depth are shown in Figure ES-4. The figure shows that the estimated transmissivity is high in the uppermost sections, which are often hydraulically connected with the tunnel floor. The values decrease with depth. Relatively high transmissivities were estimated for sections down to the section 0.40 to 0.60 m in many of the boreholes. It should be noted that according to a sensitivity analysis in the project section transmissivities at depths below 0.2 and in relative terms may be overestimated by a factor of about 2–3 compared with the more superficial layers.

Pressure disturbances in observation holes were analyzed during the injection tests. To summarize, the evaluation of the pressure responses in observation holes and the analysis of leakage to the tunnel floor gave the following results: 1) The shallowest tests, 0 to 0.10 m, show a high frequency of leakage paths to the tunnel floor in the immediate surroundings of the test section. 2) In the interval 0.10 to 0.60 m, some of injection sections are hydraulically connected with adjacent boreholes. However, the frequency of connections decreases with depth. 3) For sections below 0.6 m, the pressure disturbance estimates showed similar results, i.e. the frequency of connections decreases with depth. 4) The longest hydraulic connections between two boreholes were about three metres, as estimated from a single test. 5) If the length calculations are based on measurements in several injection tests in neighbouring holes, the total connecting length was about seven metres. However, no pressure responses from one single test were registered for this entire length.

A geostatistical interpolation of the data obtained from all the single-hole injection tests was conducted in order to analyze the correlation structure of transmissive conditions in the rock mass close to the tunnel floor. A combination of the blasting design and the kriging results shows that the most transmissive areas are located around the bottom charge area of the blasting rounds, where most damage is expected to occur, and that the axial connectivity is not continuous but exhibits an intermittent/periodic behaviour. Furthermore the specific capacities or section transmissivities are much higher (several orders of magnitude) close to the tunnel floor, but the occurrence of these higher values is more frequent for the bottom charge areas compared with the column charge areas.

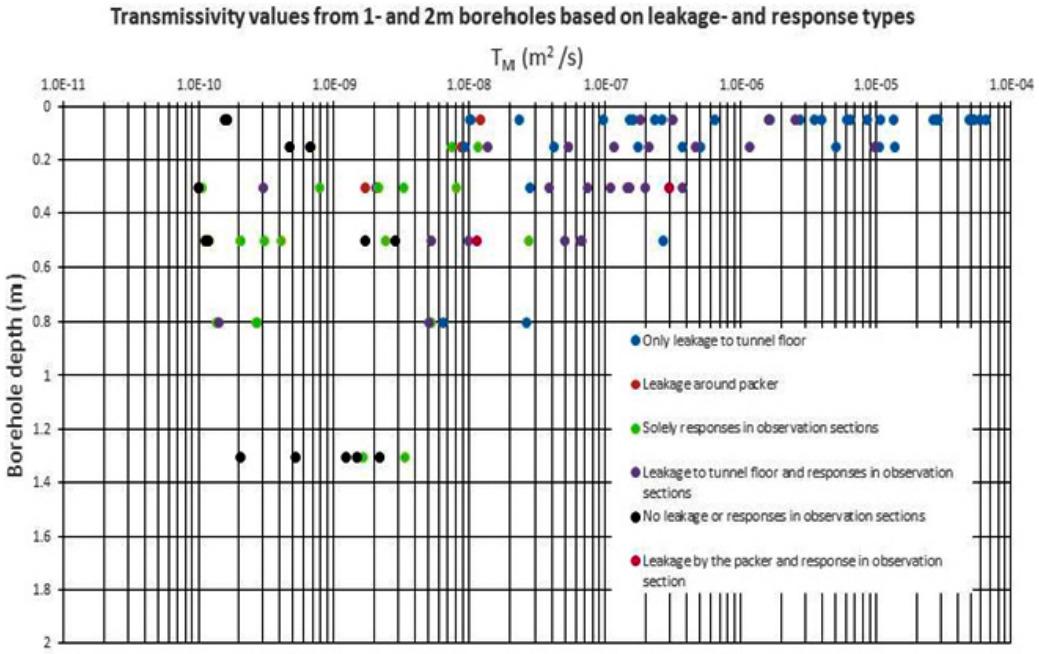

Figure ES-4. *Estimated transmissivities for each section in all boreholes versus borehole depth. According to a sensitivity analysis in the project section transmissivities at depths below 0.2 and in relative terms may be overestimated by a factor of about 2–3 compared with the more superficial layers.*

An additional assessment of the confidence in permeability differences and depth dependence was performed as a simplified significance analysis. The analysis assumed the calculated section transmissivity values. Furthermore, the transmissivity values were assumed to follow a log-normal distribution. Figure ES-5 shows that the log-normal mean values for bottom charge areas are significantly (confidence level of 95%) higher than the values for the column charge areas at the uppermost level 0.0–0.1 m. At deeper levels, the discrepancies between the two charging classifications are not so obvious.

The previous paragraph suggests that the floor exhibits a zonation in terms of permeability conditions. If anyhow the flow regime is assumed to be uniform along a prospective EDZ in a tunnel floor, it is possible to average a transmissive property based on local measurements. The arithmetic mean is usually applied in cases where the local measurements represent test volumes (blocks) in parallel. In the case of test volumes in series, the averaged transmissive property is represented by the harmonic mean (see e.g. de Marsily 1986). Simple calculations of the averaged transmissivities at the test site give the following results, as shown in Table S-1. The tunnel has been divided into 20 transects with widths 0.87–1.31 m along the floor. The transects have been assigned representative arithmetic means (occasionally only one value is available). Then the harmonic mean transmissivities have been calculated for the investigated floor in the tunnel section. The calculations have only been done for a depth interval where indications of EDZ (max. 0.6 m) were possible according to previous interpretations. The table shows that if the uppermost 10 or 20 cm are removed from the floor, the transmissivity will be drastically reduced along the tunnel.

Table S-1. Averaged transmissivity, T_{Moye} , along a 20 m tunnel section at the test site TAS04. Averaging has been carried out for different test intervals, 0–0.6 m, 0.1–0.6 m, 0.2–0.6 m and 0.4–0.6 m in order to show the effect of blasting damage.

Test sections, Depth interval (m)	Harmonic mean, T_{Moye}, (m^2/s)
0.0–0.6	2.5 E–07
0.1–0.6	1.4 E–08
0.2–0.6	1.3 E–09
0.4–0.6	3.6 E–10

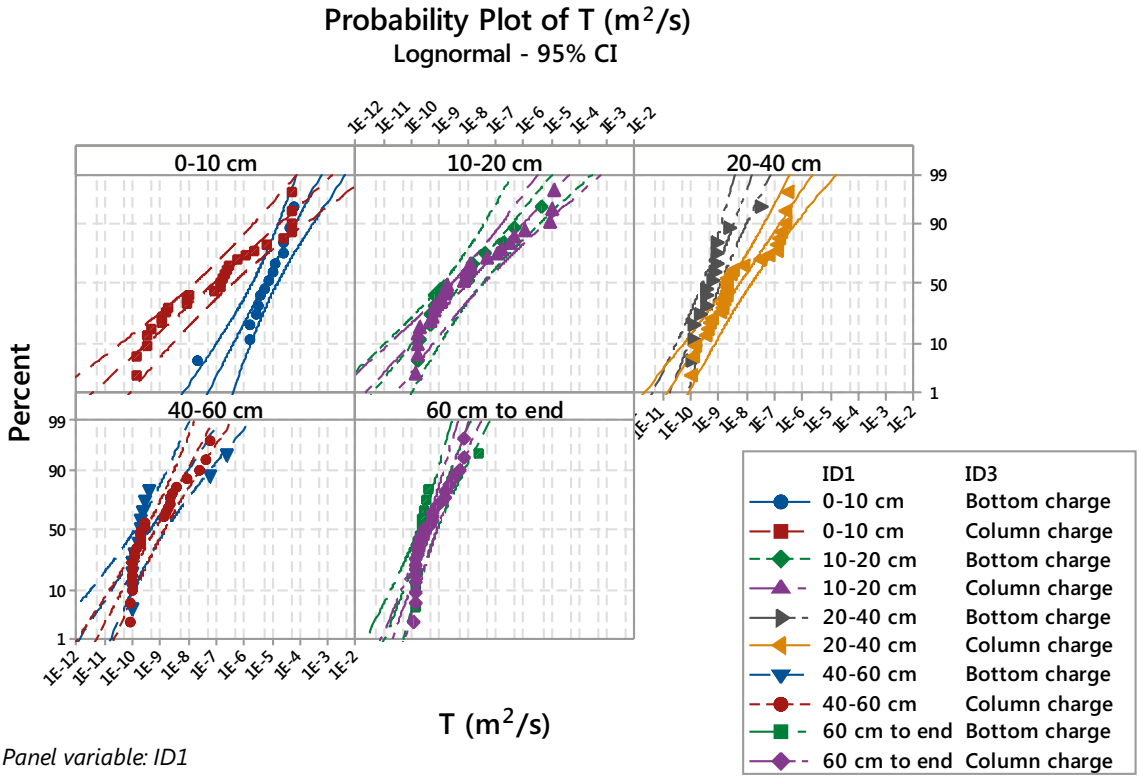

Figure ES-5. *Probability plots of the interpreted transmissivity values obtained from tests conducted in different sections with bottom charge areas and column charge areas, respectively. The lines show the 95% confidence interval.*

Conclusive general observations

The extensive investigations along 20 m of the TAS04 tunnel floor at Äspö HRL generally show that:

- Blast-induced fractures occur at low frequency. The highest fracture density is in the bottom charge at the end of each blast round due to higher charge weight.
- Blast damages in the tunnel floor exhibit a zonation with respect to the bottom charge and the column charge. The depth of the excavation-induced fractures beneath the floor is interpreted to be on average 0.3 m for a column charge of 0.5 kg/m and 0.5 m for the short bottom charge (1.8 kg/m).
- Both blast-induced and stress-induced fractures will form sub-parallel to the tunnel contour. The full extent and connectivity of the fractures can only be explored by indirect methods, such as hydraulic testing in boreholes or the use of geophysical methods in addition to geological mapping.
- The majority of injection tests with transmissivity > 10^{-8} m^2/s leaked to the tunnel floor. These flow paths are interpreted to be correlated with excavation-induced damage.
- The connectivity between induced fractures is limited.

Conclusions and recommendations

The current blast design used seems to be sufficiently good from the point of view of minimizing the blast-induced damage. However, breakage was not efficient with the current blast design. Oversized boulders and the need for reblasting of some perimeter holes occurred frequently. Greater efforts are required to optimize the blast design for efficient breakage as well as to limit the EDZ. More research is therefore recommended on the fragmentation process in a blast round, especially in brittle crystalline rock under high confinement. In addition, a greater understanding of the influence of geological conditions (rock brittleness and fracturing) on blast efficiency and development of the EDZ would be valuable.

Regarding the quality assurance and control, QA/QC, it is recommended that procedures be established for continuous improvements in consultation with the miners if project-specific demands on perimeter control are to be met. The approach of controlling the execution of the excavation works with checklists for the Contractor, use of modern loggers in drilling and charging equipment and Client follow-up inspection is fundamental in verifying that the design requirements on drilling and blasting are met. Experiences from the project show that high precision in drilling and charging with string emulsion can be achieved and documented using modern logger technology in the drilling and charging equipment. However, further development of the logger systems and processing software is needed in order to verify the results of logged emulsion in individual holes on an industrial scale.

This project has developed equipment for hydraulic testing and outlined testing and analysis procedures that have provided data permitting the successful characterization of the hydraulic properties of the rock mass in the tunnel floor. Fracture transmissivity is high in the upper 0.1–0.4 m of the tunnel floor, especially in the inner part of each blast round due to the heavier charge weight in the bottom charge. The connectivity of the most transmissive fractures is short and is normally connected to the tunnel floor. The longest connectivity observed in this project was approximately 7 metres, and it is usually less than 3 m.

This study proposes an investigation strategy to verify the extent and properties of interest of the EDZ. The following main recommendations are:

- The same test section length should be considered for the boreholes. The length of test sections ought to be 0.4–0.5 m. The use of a borehole extender enables testing directly under the floor. There is however a possibility that the most shallow injection tests leaks to the floor.
- The injection pressure applied in hydraulic tests must be adapted to site conditions so that hydraulic fracturing is avoided.
- The GPR method is proposed to be used for verification of excavation results with regard to the EDZ. The survey should be conducted on a cleaned and dried tunnel surface with high accuracy, both horizontally (dense measurement point spacing) and vertically (dense sampling point interval and high radar frequency). The measurement lines are set parallel to the tunnel and line spacing should be sufficiently dense. The site-specific GPR settings should be determined in advance, allowing the application of the GPR EDZ method for mapping the lateral distribution of the EDZ and the maximum depth of the EDZ. Geological mapping of the tunnel is useful in analyzing the GPR results. Selection of reflectors is useful in order to get an image of the sub-horizontal fracture distribution and lengths.
- The fracture network in and below the tunnel floor should be co-interpreted with GPR surveying, tunnel mapping and core mapping. It is also recommended that the terminology for tunnel and core mapping be harmonized, especially with regard to open fractures.
- Televiewer investigations in pilot holes or ultrasonic measurements of drill cores provide complementary and supporting information

Given the blasting design applied in the present project, the following recommendations for the management of the EDZ in a safety assessment are suggested:

- The rock mechanics situation with stress and strain response to the excavation has to be considered, even although stress-induced spalling is unlikely to occur.
- Conductive conditions due to blasting effects and rock stress redistribution should be considered as superimposed on natural conditions and may increase hydraulic conductivity in the repository tunnel floors.
- The relative pressure response may be regarded as a proxy parameter for describing the interference between injection and observation sections, also considering the measuring point distances. The injection test results, of the current study, show that most of the superficial 0–0.1 m sections are hydraulically connected with the tunnel floor. However, below this level the relative pressure responses show a significant decreasing trend versus depth to approximately 0.5 m (section midpoint). The few values below 0.5 m show a more constant relative pressure response. In the context of creating DFN models for the tunnel floor and its surroundings, the relative pressure responses could be used for calibration purposes.

- If the shallowest 10 to 20 centimetres are removed from the floor, transmissivity will be drastically reduced along the tunnel. Appropriate methods could be blasting of a bench or mechanical scaling.
- Measurement of hydraulic properties should focus on obtaining data on transmissivities or specific capacities using a specified test section length and injection duration time (i.e. equivalent values). Evaluation of the testing should consider initial conditions, hydraulic boundary conditions and test-scale aspects, treating different kinds of uncertainties in a robust way.
- GPR results show that water-saturated/filled gently dipping fractures cause most of the reflectors, and the GPR information makes it possible to estimate the lengths and apparent orientations of the reflectors. The GPR results can be superimposed on fracture mapping results and provide data for statistical fracture analysis and DFN modelling.

Sammanfattning

Denna rapport behandlar frågan om utbredning och egenskaper för den skadade zonen runt en tunnel, Excavation Damage Zone (EDZ). Arbetet baseras på studier i en tunnel som byggdes på Äspölaboratoriet 2012. Sprängdesign och kvalitetsstyrningsprogram under tunnelbyggnaden baserades på tidigare erfarenheter från Äspö.

Uppföljning gjordes inom 20 m av en tunnel med fotogrammetrisk inmätning av tunneln, geologisk karaktärisering genom kartering av tunnel och 42 korta kärnborrhål som borrades i tunnelgolvet, 1–2 m djupa samt mätning med högfrekvent markradar (GPR) i profiler längs tunneln, profilavstånd 10 cm. I dessa hål utfördes injektionstester i fem sektioner, totalt 210 injektionstester. Samtidigt registrerades tryckresponser i de övriga hålen, vilket gav 205 interferenstester. Mättade förhållanden för borrhålstesterna säkerställdes genom att nivåkontrollera vattensamlingar i golvets lågpunkter. I samband med injektionstesterna observerades eventuellt läckage till tunnelgolvet. I förarbetet utfördes några hydromekaniska tester för att säkerställa att injektionstrycket inte orsakade hydraulisk spräckning/lyftning.

Värdefulla allmänna observationer är främst:

- Sprängdinducerade sprickor har låg frekvens, relativt mest sprängdinducerade sprickor finns inom område för bottenladdning i slutet av varje salva. Där uppskattas skadedjupet till ca 0,5 m, medan skadedjupet för resten av salvan inom pipladdningen bedöms vara ca 0,3 m.
- Trots låg magnitud på in situ bergspänningar kan man inte utesluta att dessa kan ha viss påverkan på skadezonen, eftersom det teoretiskt uppstår en liten hävning av golvet när tunneln tas ut. Både spännings- och sprängningsinducerade sprickor utvecklas främst sub-parallellt med tunnelgolvet.
- Omfattning av och konnektivitet för inducerade sprickor kan bara bedömas med indirekta metoder, såsom hydraultester i borrhål eller kombination av geologisk och geofysisk dokumentation.
- De flesta injektionstesterna med transmissivitet > 10^{-8} m^2/s läckte till tunnelgolvet, troligen via sprickor som inducerats eller påverkats vid tunneluttaget (av sprängning och/eller spänningsomlagring).
- De högsta transmissiviteterna återfanns ytligt, samt i läge för bottenladdningen.
- Konnektiviteten mellan inducerade sprickor är begränsad.

Viktigaste rekommendationerna är:

- Sprängdesignen är tillräcklig för att minimera sprängskador, men behöver effektiviseras för att minska omskjutningar.
- Kvalitetsrutiner för bergarbetena behöver utvecklas och effektiviseras. Nyttjande av loggrar i modern borr- och laddutrustning bör utredas mer.
- Karaktärisering avskadezonen bör göras med en kombination av geologisk kartering, geofysiska mätningar (GPR) samt hydrauliska injektionstester. Flera utvecklingsområden påpekas, bl a:
  - Enhetligare terminologi mellan tunnel- och borrhålskartering
  - GPR kan bedöma påverkansdjup under tunneln och identifiera individuella reflektorer. Dessa reflektorer kan ge delunderlag till DFN-modellering. Det är dock viktigt att bestämma fysikaliska parameterar på berget för kalibrering av GPR.
  - Hydrauliska tester (injektion och interferens) bör göras så konsistent lika som möjligt i alla hål och sektioner (testlängder och -tider). Randvillkor måste vara kända. Man får förvänta sig att ytliga injektionstester läcker till tunnelgolvet.
- Konnektiviteten längs tunneln är beroende av naturliga sprickors frekvens, samt inducerade sprickor av sprängning och bergmekanisk spänningsomlagring som öppnar naturliga sprickor eller inducerar nya. Dessa förhållanden måste vara kända vid utvärdering av den skadade zonens hydrauliska egenskaper.
- Om man med lämplig metod kan ta bort de översta 2–3 dm av golvet försvinner de sektioner där de högsta transmissiviteterna uppmätts. Den bergmekaniska konsekvensen av en sådan åtgärd bedöms vara insignifikant.

Contents

Appendices

All appendices below can be downloaded from www.skb.se/publications
Direct link: http://www.skb.com/publication/2480345/

1. Borehole data
2. 3D model
3. Charging data for each individual hole
4. Table extracted from the Boremap mapping of the boreholes in the floor of TAS04.
5. Geological map from the RoCS-mapping of the floor of TAS04 with positions and names of boreholes marked.
6. 3D modelling of fractures from RoCS-mapping of tunnel floor intersecting fractures from Boremap mapping of boreholes
7. Photographs of the tunnel floor of TAS04 at each borehole location
8. Photos of cores from the boreholes in the floor of TAS04
9. Practical aspects of test analysis
10. Evaluation of injection tests in tunnel floor considering EDZ
11. The impact of wellbore storage on the evaluation of hydraulic tests
12. Analysis of hydraulic tests that exhibit leakage on the tunnel floor
13. Lower and upper limits for the calculation of transmissivity from the injection tests
14. Description of injection equipment involving technical specifications
15. Check of pressure sensors against air pressure
16. Deformation measurements at different injection pressures.
17. Evaluation of rock deformation based on hydraulic tests at different pressures
18. Radius of influence. Test time
19. Data handling and protocols
20. Measured data and evaluation of each injection test
21. Water levels in boreholes during pumping from pits, before packer installation
22. Diagram of pressure data in observation holes, weekly and daily plots
23. All pressure responses in observation sections, comments to the Excel sheet
24. Hydraulic transmissivity
25. Hydraulic conductivity in sections
26. Specific capacities in sections
27. Comparison of some methods to estimate hydraulic parameters based on injection tests in shallow tunnel boreholes
28. Injection tests. Pressure responses in observation sections and leakage to tunnel floor
29. Statistics on hydraulic connections between injection sections and observation sections in the tunnel floor
30. Variogram of the base-10 log transmissivity values obtained from injection tests
31. Interpolation by kriging of the base-10 log transmissivity values obtained from injection tests
32. Sensitivity test for Section T (Moye) and K (Moye) according to measurement interval and depth
33. Harmonic mean calculations along the tunnel from section transmissivity data

1 Background and objectives

1.1 Background

The bedrock is subject to gravitational and tectonic stresses. Any excavation in the bedrock causes some kind of disturbance or damage to the rock closest to the excavated surface. This is caused by stress redistribution due to altered geometry and effects of the excavation method. The stress concentrations around the tunnel could be so high that the tangential maximum stress exceeds the strength of the rock. This initiates spalling. However, the damage to the rock could also be caused by the excavation method itself. This report focuses on how tunnelling using the drill-and-blast method causes damage to crystalline rock in a geological environment where in situ stresses are not high enough to initiate spalling. Examples of blast- and stress-induced damage to a tunnel wall are shown in Figure 1-1.

1.2 Objectives

SKB (2013) presented plans for further development of production methods adapted to the requirements made concerning rock excavation, stability and tightness. "The goal is primarily to be able to specify performance requirements in the construction documents for accesses as well as methods to verify that the requirements are satisfied. The performance requirements and their verification will be further developed to satisfy the specific requirements that apply regarding the rock below the level for the top seal". This project aims to meet this goal regarding tunnel excavation and verification by ensuring that the requirements on the Excavation-Damaged Zone (EDZ) are met. The main objectives are:

- Propose the requirements needed to execute tunnelling with the drill-and-blast method so that the EDZ is minimized and also propose the required QA/QC measures and the documentation needed to verify that the requirements are met.
- Develop a characterization method to confirm the initial state regarding the extent of excavation-induced fractures.
- Develop a method for characterization of the hydraulic properties of the EDZ and demonstrate by field experiments its suitability for application in a tunnel environment.
- Propose means and methods to verify that post-closure safety requirements regarding the EDZ are met.

The proposed strategy for verification of the extent of the EDZ has been developed based on the following principles and methods:

- Verification that the execution of blasting complies with requirements on drilling, charging and detonation by documentation and analysis of deviations.
- Geometrical control of the tunnel contour to ensure that tolerances in contour control are complied with.
- Follow-up inspection using geophysical methods on the tunnel floor after blasting. Mainly ground-penetrating radar has been used.
- Mapping of the tunnel floor for supplementary visual assessment of the extent of the excavation damage.
- Development of a conceptual model showing the tunnel floor's topography, fracturing and the estimated extent of the EDZ.
- Hydraulic characterization of the EDZ in short boreholes (1–2 metres) by means of injection tests and cross-hole interference tests.
- Development of a hydraulic conceptual model of the EDZ.

The total scope of works is presented in greater detail in Chapter 3.

Figure 1-1. *Left: A smoothly blasted tunnel wall. The perimeter holes for blasting are seen as lighter lines. The irregular surface of the wall is primarily caused by the vertical blast-induced cracks. Right: stress-induced spalling from a 1.8 m diam. Borehole (looking up the hole). The spalled zone is approximately 10 cm deep.*

1.3 Definitions

1.3.1 Excavation-damaged and -disturbed zones

The damage around tunnels differs depending on rock type, and the description of this zone in the literature has therefore been different depending on the rock type involved (McEwen 2005). In crystalline rocks, a distinction was made between the **Excavation-Disturbed Zone (EdZ)** and the **Excavation-Damaged Zone (EDZ)** (Martino and Chandler 2004, Bäckblom and Martin 1999).

A distinction using a general description of the most dominant properties for each zone, which is used in current literature, was proposed by Bernier et al. (2005).

- The EdZ is a zone with hydromechanical and geochemical modifications, without major changes in flow and transport properties.
- The EDZ is a zone in which hydromechanical and geochemical modifications induce significant changes in flow and transport properties. These changes may, for example, include one or more orders-of-magnitude increase in flow permeability.

The EdZ and EDZ are the perturbed rock zones around an underground opening following excavation. These zones occur because of the inevitable effects of excavation, and the effects will be exacerbated to a greater or lesser extent by the excavation mode, i.e. whether by blasting or by the use of a tunnel boring machine (Hudson et al. 2009).

The formation of some form of EdZ and EDZ is inevitable. This is due to the three primary effects of excavation (Hudson and Harrison 1997):

- displacements occur because stressed rock has been removed, allowing the remaining rock to move (due to unloading),
- there are no normal and shear stresses on an unsupported excavation surface, and hence the excavation boundary must be a principal stress plane with one of the principal stresses (of magnitude zero) being normal to the surface. Generally, this will involve a major perturbation of the pre-existing stress field, both in the principal stress magnitudes and in their orientations,

- at the boundary of an excavation open to the atmosphere, any previous fluid pressure existing in the rock mass will be reduced to zero (or more strictly, to atmospheric pressure). This causes the excavation to act as a 'sink', and any fluid within the rock mass will tend to flow into the excavation.

The magnitudes of the effects will depend on the rock mass circumstances, the method of excavation and any mitigating strategies used in the rock engineering. The main concern in the radioactive waste context is the potential creation of new fractures and/or the opening of existing fractures that might contribute to enhanced fracture connectivity and hence increase the permeability of the rock mass and associated potential radionuclide migration via increased water flow.

1.3.2 Blasting terminology

Rock blasting is the controlled use of explosives to excavate, break down or remove rock. Tunnelling by the drill-and-blast method is described as a cycle, Figure 1-2. Drilling and blasting is followed by ventilation, mucking out, scaling, rock support and surveying before the next round. The length of a round is determined by the size of the boom. Typical round lengths are 4.5–5 m.

The drilling of the blast round includes several groups of holes that are charged with explosives. The blast design include distribution of boreholes, charge weights/borehole and initiation sequences. Centrally positioned in the tunnel face is the cut. The cut is a cluster of boreholes close to each other. Some of these holes are drilled with a larger diameter (approximately 100–150 mm), compared to the rest of the boreholes (45–52 mm). The large-diameter holes are not charged. The cut is always the first blast interval. Outside the cut are the production holes, which are fired after the cut. The holes in the row closest to the contour holes are called helpers. The distance between the rows is called burden. The charge weight in each row must be strong enough to break the burden. The helpers are fired before the contour. The charge weight is reduced toward the tunnel contour and consequently the spacing (burden) between the rows. The sum of all drilling or charging for a round divided by the excavated volume is called specific drilling (m/m^3) respectively specific charging or powder factor (kg/m^3).

The drilling of the contour holes has to be slightly angled outside the tunnel contour to provide sufficient room for the booms to collar for drilling of the next round. The space needed for the booms is at least 25–30 cm. The consequence is that the cross-sectional area of the tunnel varies systematically along every round, see Figure 1-3. This is called the look-out angle.

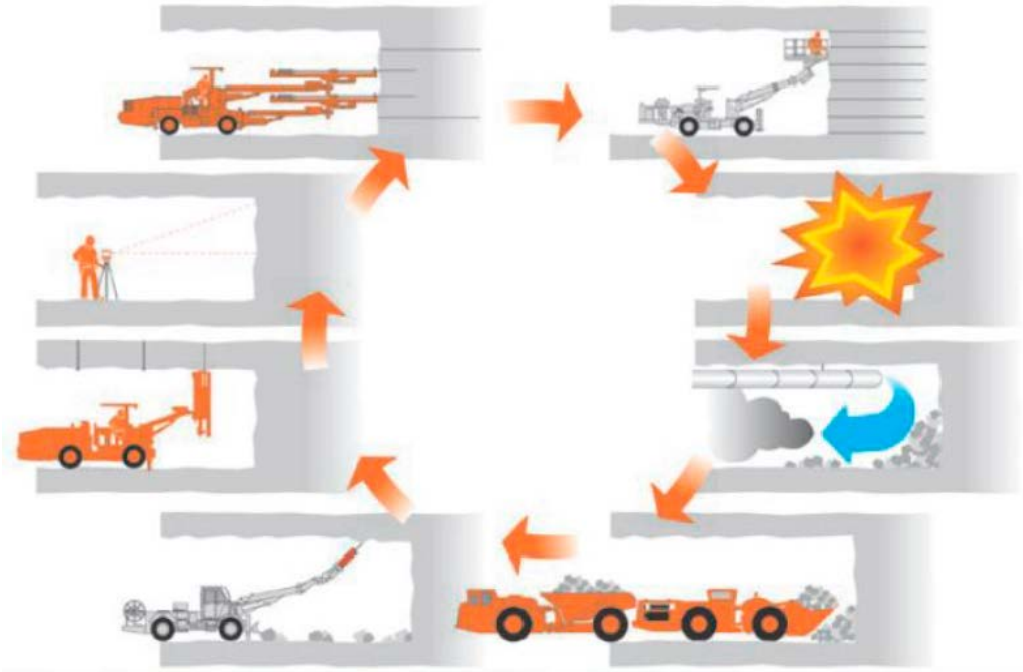

Figure 1-2. *The drill-and-blast cycle starts with drilling a round (top left).*

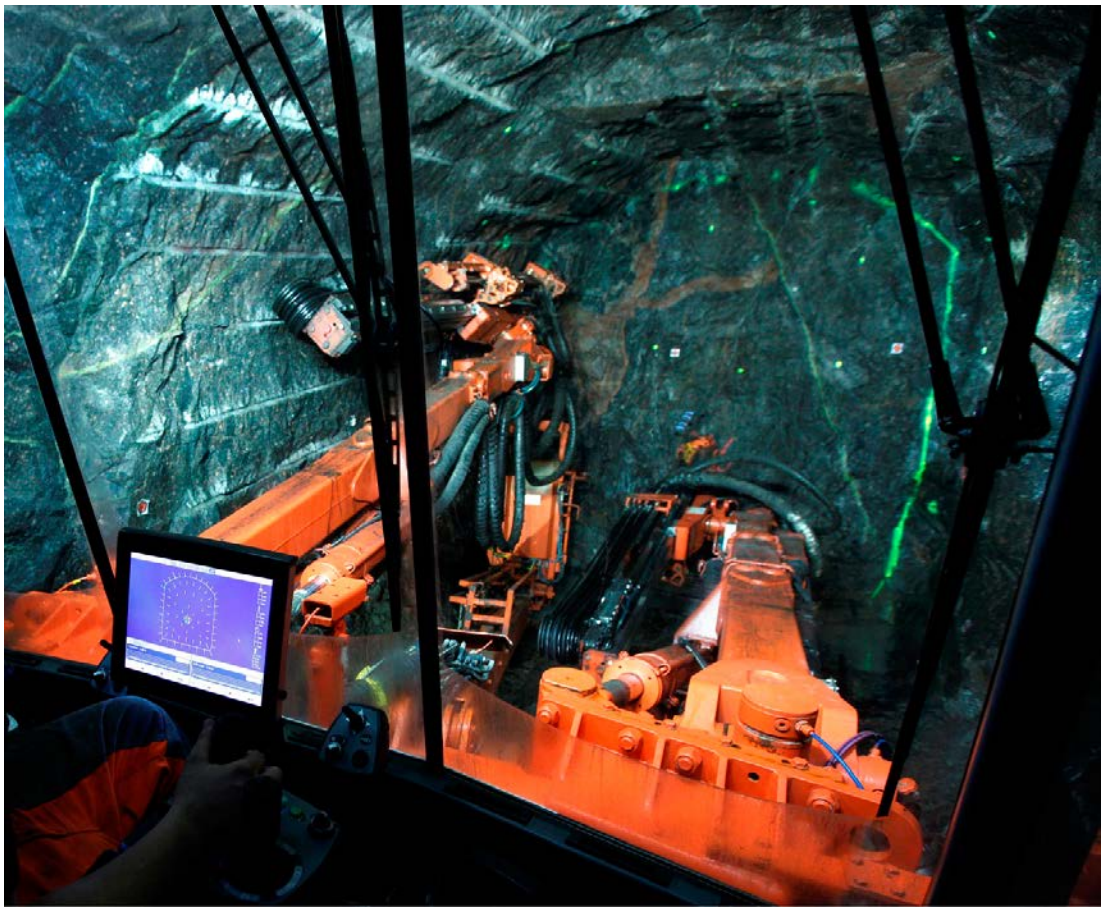

Figure 1-3. *Drilling of a blast round with a two-boom jumbo. Note the contour holes and the step between two rounds caused by the look-out angle.*

The detonation of the explosives is a rapid chemical reaction that transforms the explosives to gas. The velocity of detonation (VOD) depends on the type of explosive and the length or weight/m in the borehole. A typical VOD is 3.5–5.5 km/s. The detonation causes a compressive wave towards the tunnel face that can cause some crushing of the borehole wall. The rock shows contraction after the elastic wave and fails in the tension mode. The gases that are formed during the detonation can now penetrate into these fractures, breaking even more rock, and through the rock into the tunnel. The degree of damage to the tunnel contour depends on many factors; see for example Olsson and Ouhterlony (2003). The blast-induced damage results in fractures with different length and frequency, depending on the charge weight. The bottom charge creates the greatest damage, see Figure 1-4. The damage from blasting on the tunnel contour can vary from a few fractures to extensive fracturing depending on local geology and the charge concentration in the boreholes. Note that borehole deviations influence charge geometry (distribution of explosives in the rock) and consequently also local charge concentrations.

The blast is initiated by a detonator placed in the bottom of the borehole. Detonators with several different delay times are normally used in a blast round to optimize the breakage and to ensure that the blast sequence starts in the centre of the tunnel face, the cut. There is always a group of empty large-diameter boreholes (diam. > 100 mm) in the cut.

The detonator is normally placed in a primer to ensure the detonation of the full hole. The primer has a limited length (200–400 mm) and a high weight/length ratio compared with the remaining explosives in the borehole. The primer together with the designated explosives in the bottom of the borehole is called the bottom charge and the remaining explosives in a borehole are called the column charge. The bottom charge has a high weight/length ratio compared with the column charge.

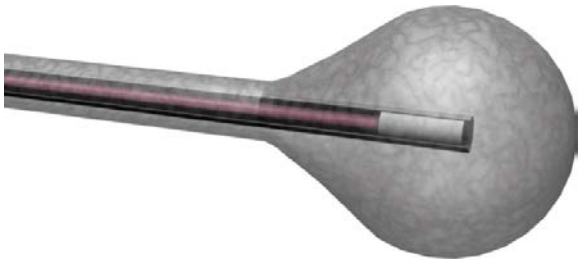

Figure 1-4. *Fracture envelope for a blast hole. The gray flask-shaped surface contains in principle all radial and conical blasting fractures directed back into the remaining rock. The fractures that break the burden are obviously longer (Olsson et al. 2009).*

Blast design aims at optimizing the distribution of explosives in the blast round. The different time intervals between the detonators serve to detonate the different borehole rows step-wise from the cut and out towards the tunnel contour. The amount of explosives detonated in a given interval controls the ground vibrations from the explosions in the boreholes. Therefore, each row can be split up to detonate at different delay times. The distance between the holes in one row that is detonated in the same interval depends on the charge weight in the boreholes. Reduced hole spacing permits a weaker charge and consequently less fracturing. This is especially important if the excavation damage to the tunnel contour is to be minimized. There is some correlation between specific drilling and specific charge (powder factor). If one of these parameters is increased, the other parameter can be reduced slightly.

1.4 The impact of the EDZ on the safety assessment

In SR-Site (SKB 2011), design premises concerning the EDZ were formulated as follows.

- **Excavation-damaged zone (EDZ) in deposition tunnels:** Excavation-induced damage should be limited and not result in a connected effective transmissivity, along a significant part (i.e. at least 20–30 m) of the disposal tunnel and averaged across the tunnel floor, higher than 10^{-8} m^2/s.
- **EDZ in shafts and ramp, rock caverns and tunnels other than deposition tunnels:** Below the location of the top seal, the integrated effective connected hydraulic conductivity of the backfill in tunnels, ramp and shafts and the EDZ surrounding them must be less than 10^{-8} m/s. This limit need not be met in sections where e.g. the tunnel or ramp passes highly transmissive zones. There is no restriction on the hydraulic conductivity in the central area.

SKB (2011) also defines the "top seal", the upper part of the accesses with no restriction on hydraulic conductivity (Figure 1-5). The depth of the top seal can be adapted to the expected depth of permafrost during the assessment period, but must not be deeper than 100 m above repository depth.

The possibility that the EDZ will cause significant changes in flow and transport properties has been analyzed in SKB's safety assessment. SKB (2011, Section 10.2.4) concludes that "An obvious mechanical impact is the creation of rock cavities for the repository" and draws the following conclusion regarding the additional mechanical consequences of the EDZ: There is ample evidence that a potential EDZ formed during excavation will have less than the maximum allowed transmissivity as set by the design premises, and data suggest that a continuous EDZ would not develop at all. However, given that the occurrence of the EDZ can at present only be assessed by indirect measurements, it would appear justified to consider an EDZ according to the design premises, i.e. with an axial transmissivity of 10^{-8} m^2/s, as a basic assumption for further analyses. Furthermore, it would also appear justified to explore how transmissive an EDZ needs to be in order to significantly impact other safety functions while also exploring the impact of no axially continuous EDZ at all. In concluding the result of the assessment it is stated that (SKB 2011, Section 15.5.16) "the sufficiency of the upper transmissivity limit of 10^{-8} m^2/s is indeed demonstrated in SR-Site. …, the analysis also shows that a more transmissive EDZ could affect risk since the number of failed canisters starts to increase, although moderately, when the transmissivity is increased. The EDZ seem to be even less important for radionuclide transport."

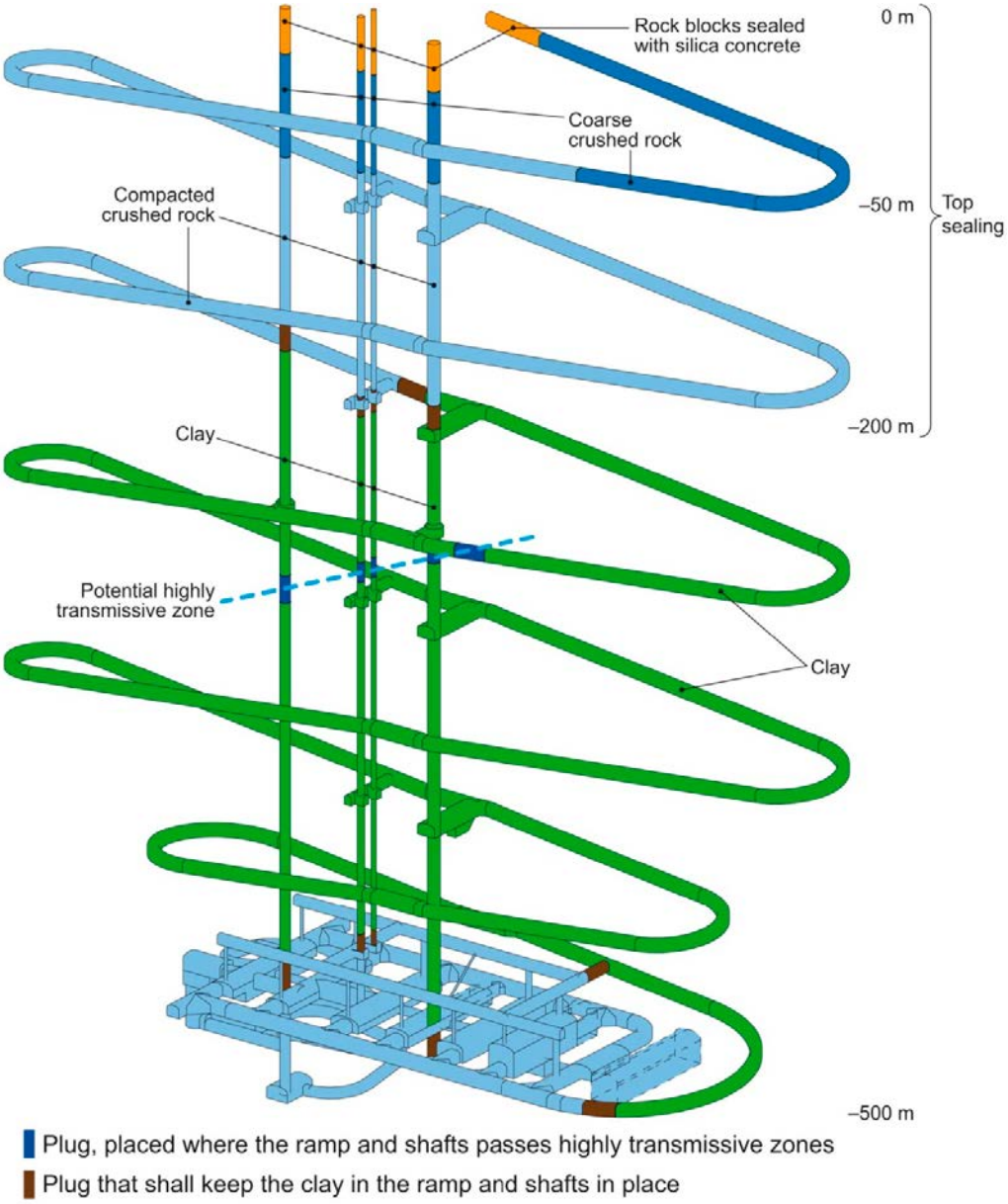

Figure 1-5. *Illustration of "top seal" (SKB 2011).*

1.5 This report

SKB has carried out extensive studies on the development of the EDZ, see Chapter 2. The reference method for excavation is the drill-and-blast method (Bäckblom et al. 2004). The current state of knowledge was summarized in the RD&D report by SKB (SKB 2013). Experience from rock excavation for the fine sealing tunnel in the Äspö HRL (Karlzén and Johansson 2010) was applied to the extension of the Äspö HRL. The results obtained were reformulated in technical requirements for tendering specifications for procurement of the rock construction works. This also included the prescribed blasting plan (drilling and charging plans) for the different tunnel areas. In addition, electronic detonators were prescribed to be used in the contour holes. The tunnelling was mostly carried out during 2012 and was concluded with rock support and fitting-out during the first 4 months of 2013.

This report describes the requirements for and results of the excavation of the new tunnels with a special emphasis on the EDZ in the floor of one of the new tunnels. This study addresses one of the regulatory comments (SSM 2011) that "SSM believes it is important that SKB can show that the requirements made by the design premises on the EDZ can be met in tunnelling under production conditions in Forsmark".

SKB (2011) concluded that “there is currently no reliable direct method that can quantify the connected effective transmissivity along a tunnel, apart from judging the likelihood that no continuous EDZ has developed at all. SKB plans to develop several procedures for ensuring that the damage in deposition tunnels conforms to the design premises. Procedures to control and inspect the drilling, charging and ignition sequences will be developed and included in the monitoring and control programmes for the underground openings. The influence of rock conditions on the EDZ will be evaluated within the framework of the observational method and the associated monitoring programme, i.e. combining results from geological characterization, geophysical techniques and geological modelling”. This report aims to demonstrate how these procedures can be utilized in the tunnelling works via quality control procedures and integrated investigations.

The work in this project has adopted a broad approach emphasizing experience from field work, the applied evaluation methods, the most significant findings and recommendations. This in turn has meant that a very large amount of background material is gathered in separate appendices.

It is essential to point out one limitation in the work; this project has not carried out any groundwater flow modelling to confirm the hydraulic flow regime of the EDZ in the studied tunnel.

This project has been focused on quality measures to ensure that requirements on tunnel excavations are met and methodological studies of methods for verification of the resulting excavation damage. The purpose is not to discuss how the findings from this project can be applied to the construction of a future repository.

2 Experience prior to commencement of the project

SKB has conducted several studies related to the EDZ both at the Stripa mine and at the Äspö Hard Rock Laboratory. This Chapter provides a broad overview of the research work done within this area, with a focus on experience from crystalline rock.

2.1 Literature review

The first systematic studies of blast damage in Sweden were carried out by Sjöberg et al. (1977). Cores were drilled out from the roof of a tunnel in granite where blasting had been carried out with different charges. The damage was defined as at least two fresh fractures per borehole metre.

The international Stripa Project, 1980–1992, studied the natural and engineered barriers in an abandoned iron ore mine in the central part of Sweden. One of the concerns during the period 1986 to 1992 was the Excavation-Damaged and -Disturbed Zone. The summary report by Gray (1993) provides an overview of the results. The main conclusions of the Stripa tests were that the hydraulic conductivity determined by Lugeon tests is interpreted to be $1 \cdot 10^{-8}$ m/s down to 0.3 m in the roof and walls and $2 \cdot 10^{-8}$ m/s down to 0.8 m in the floor. The hydraulic conductivity of the blast-damaged zone, as reported by Gray (1993), was found to vary up to 4 orders of magnitude within a few metres. The results are from a tunnel covering a length of approximately three drill-and-blast rounds in saturated conditions and from a tunnel that was twice considerably heated. Furthermore, the tunnel was not newly excavated, but close to 10 years old when the test was performed and had been subject to two heating experiments.

One of the earliest efforts to compile current knowledge on the impact of the Excavation-Damaged Zone was the workshop on "Excavation Response in deep Radioactive Repositories" organized by OECD/NEA in Winnipeg, Canada 1988. Winberg (1991) compiled current knowledge, including the results of major experiments at the Stripa mine, Sweden. He also reviewed some modelling approaches regarding the hydraulic properties of the EDZ. In general, the extent and properties of the damaged zone around a tunnel were simplified to be homogeneous in the axial direction of the tunnel and in general most extensive and permeable in the floor. This was supported by field experiments, for example in Stripa and in the URL, Canada.

The most important experiments carried out with the drill-and-blast method in crystalline rock are from from Stripa and the Äspö HRL, Sweden, the URL, Canada, Grimsel, Switzerland and Onkalo, Finland. Bäckblom (2008) summarizes the findings. The depth and hydraulic conductivity of the EDZ vary between the floor and the walls, and depending on whether the tunnel has been subject to stress-induced spalling or not. Many of the tests have been carried out within a limited length of a tunnel, sometimes only in one borehole array in one section. The hydraulic conductivity of the EDZ is reported to be in the range of 10^{-6}–10^{-5} m/s if stress-induced spalling has occurred. Other tests without any reported spalling indicate a hydraulic conductivity range of 10^{-12}–10^{-5} m/s. The higher conductivity values are normally found closest to the tunnel contour. The large span in the latter case is likely due to differences in both blast design and site conditions. A list of relevant EDZ experiments is presented in Section 2.2.

Hudson et al. (2009) discussed the factors relating to the EDZ, see Figure 2-1:

- the rock mass response to tunneling, i.e. creation of the inevitable EDZ disturbance,
- excavation method (creation of additional EDZ disturbance),
- characterization methods (required so that the EDZ can be specified and modelled as necessary)

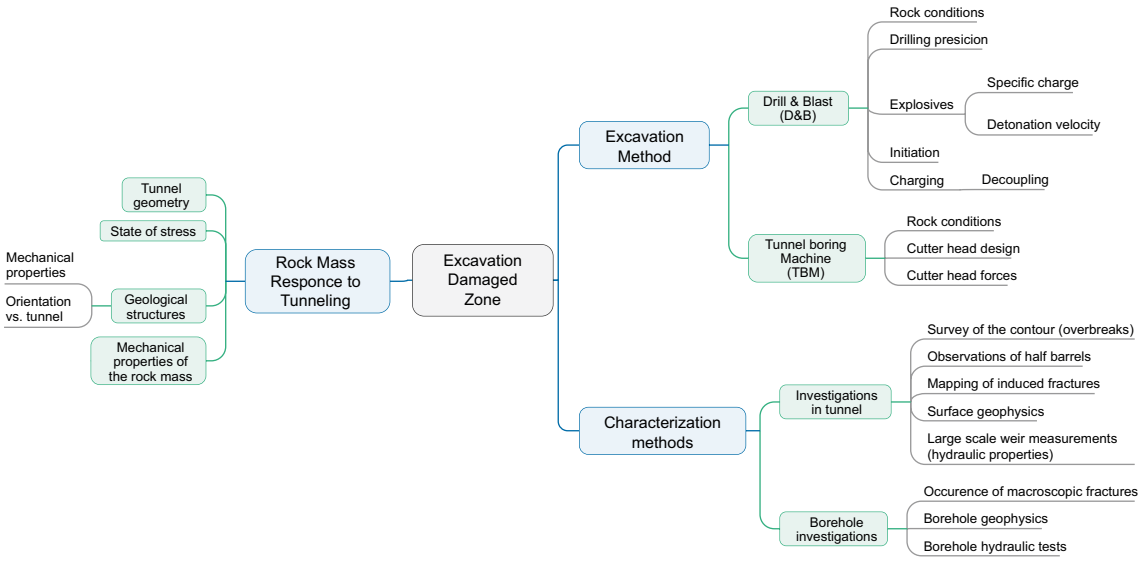

Figure 2-1. *Overview of rock mass response to tunnelling, its dependence on excavation method and characterization methods for the EDZ. (Hudson et al. 2009).*

2.2 Overview of EDZ experiments

The major experiments of interest for understanding the extent and properties of the EDZ resulting from the drill-and-blast method in crystalline rock are:

- Stripa – Rock Sealing Experiment (Gray 1993)
- AECL – Room 209 connected permeability experiment (Chandler et al. 1996)
- AECL – The Mine-by tunnel connected permeability test (Chandler et al. 1996)
- AECL – Tunnel Sealing Experiment (Chandler et al. 2002)
- AECL – The Blast Damage Assessment Project (Martino et al. 2004)
- SKB – The ZEDEX project at Äspö HRL (Emsley et al. 1997)
- SKB – The Backfill and Plug Tests at Äspö HRL (Ludvigsson et al. 1999)
- SKB – Experiences of blasting of the TASQ tunnel. (Olsson et al. 2004)
- SKB – Examination of the EDZ in the TASS tunnel (Olsson et al. 2009)
- SKB – Hydraulic features of the EDZ – Laboratory investigations (Ericsson et al. 2009)
- Posiva – The EDZ09 project and other EDZ studies (Mustonen et al. 2010)
- Nagra – Excavation Disturbed Zone Experiment (Frieg and Blaser 2012)

2.3 Project-specific experience from the Äspö HRL utilized in this study

During 2007–2008 a new tunnel was excavated by SKB at the 450 m level of the Äspö HRL. The tunnel has a cross-sectional area of 19 m^2 and is 90 m long. One of the aims of the tunnel project was to investigate how carefully the blasting could be done, applying state-of-the art research on blast designs (Christiansson and Karlzén 2010). This was done by careful monitoring of the key components in the drill-and-blast plan such as drilling precision, charging amounts and initiation sequences (Karlzén and Johansson 2010). These efforts permitted good traceability in the tunnel excavation works.

The final tunnel met the stipulated requirements on contour control with respect to restricted over-break from the intended bentonite clay backfill. The lookout angle was kept within 25 cm, resulting in a maximum variation in local oversize of 2 m^2. The average overbreak was 16% of the tunnel cross-sectional area.

The use of electronic detonators increased the number of visible half pipes from perimeter holes. The extent of the blast-induced damage (EDZ) was investigated in a part of the tunnel wall by Olsson et al. (2009). The investigated area was 1.5 m high, 8.0 m long and 0.7–0.9 m deep. This part of the wall was taken out by means of the wire saw technique and cut into 75 slices 0.1 m thick. Mapping of these rock slices was used to develop a 3D model of the fracturing in the tunnel wall, Figure 2-2. The conclusion was that there was no continuous EDZ caused by blasting. The blast-induced damage from the contour holes consists mainly of small fractures sub-parallel to the tunnel wall, Figure 2-4.

Ericsson et al. (2009) compiled the length distribution of the fractures in the model. Ericsson et al. (2009) also carried out laboratory testing of intact rock from the rock slices. They found a small trend for reduced sonic velocity within 25 cm from the tunnel wall and increased matrix porosity within 30 cm from the tunnel wall. Microscope studies of the same samples indicate opening of old microfractures with mineral precipitation and formation of only a few new (fresh) microfractures.

These experiences from successful blast design were implemented into the Äspö Expansion project 2012. The project, and how blast design and QA/QC procedures were implemented, is presented in Chapter 4.

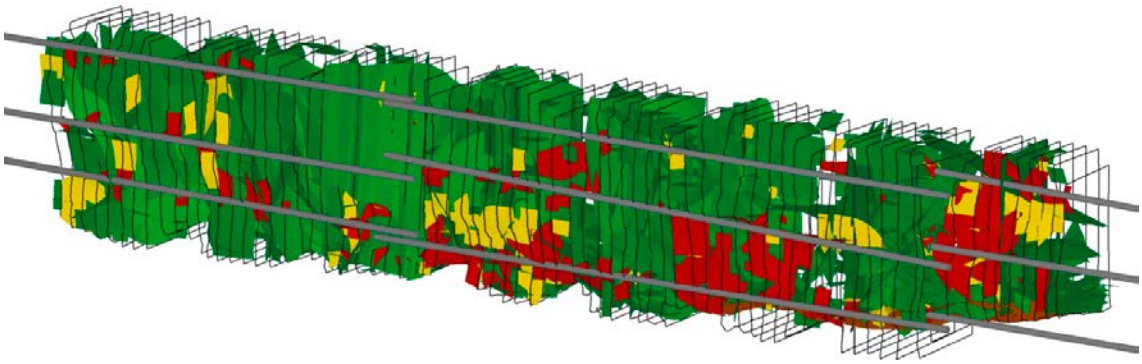

Figure 2-2. *All modelled fractures, section outlines and blast holes (Olsson et al. 2009). Green = natural fractures. Red = direct blast-induced fractures (origin from a perimeter hole). Yellow = fresh fractures without mineral precipitation, assumed to be blast-induced.*

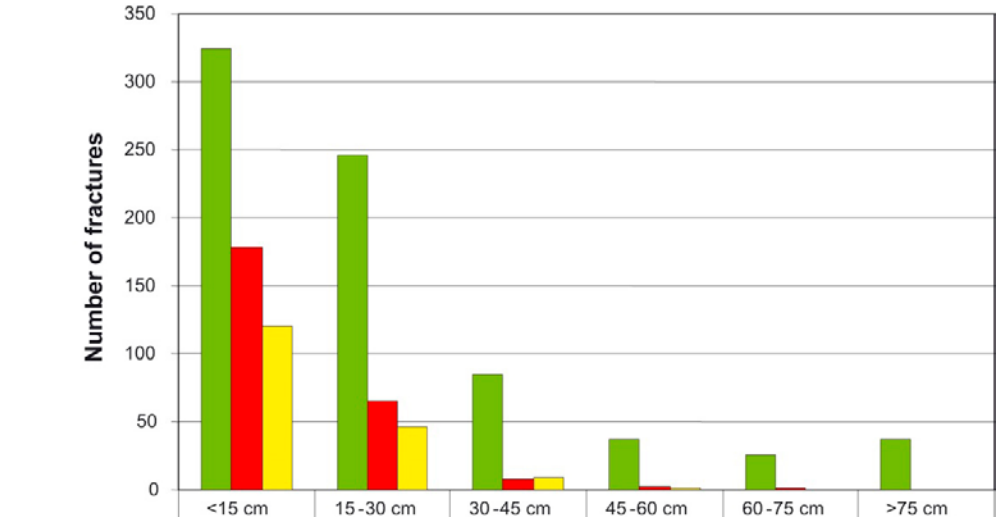

	<15 cm	15-30 cm	30-45 cm	45-60 cm	60-75 cm	>75 cm
Natural	325	246	84	37	26	37
Dir Blast Ind	178	66	8	2	1	0
Induced	121	46	9	1	0	0

Figure 2-3. *Length distribution of the modelled fractures in Figure 2-2. Natural (green), direct blast-induced (red) and induced (yellow) fractures in the 3D model (Ericsson et al. 2009).*

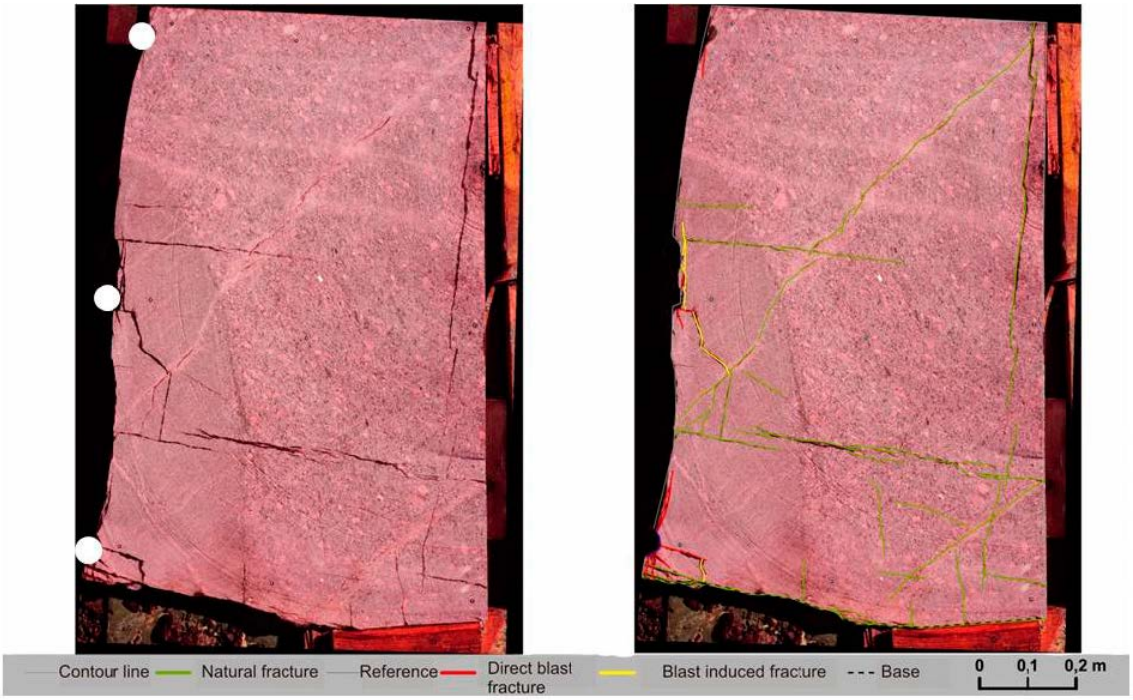

Figure 2-4. *The figure shows a 2D image of the occurrence of fractures from one of the rock slices perpendicular to the wall in a tunnel excavated by careful blasting. The location of the contour boreholes shown in Figure 2-2 is shown in the left-hand photo. The distribution of blast-induced fractures is discontinuous and connected to the charge boreholes. There are secondary blast-induced fractures which terminate against natural fractures. Increased axial fracture connectivity due to blasting and blast-induced fractures is estimated to be insignificant due to the sparse distribution of these visible fractures. Natural fractures may be affected at the tunnel perimeter.*

3 Scope of works

3.1 The demonstration project

The Äspö Hard Rock Laboratory (HRL) is a unique research facility for geological disposal. SKB is conducting a series of experiments at depths down to a maximum of 450 m together with Swedish and international experts.

Experiments will be carried out at the Äspö HRL also in the future, to support the continued development of the methodologies and technologies necessary to construct the Final Repository for Spent Fuel. These experiments have necessitated the construction of two main tunnels and several short tunnels at the lower levels of the Äspö HRL (400–450 m level), see Figure 3-1. The construction of these tunnels is referred to as the Äspö Expansion Project. The Expansion project was carried out in 2011–2012, with most of the excavation works carried out during 2012. The requirements for blasting were set based on the production methods used for any similar public tunnel, using a modern drill jumbo and charging equipment for two-component string emulsion. An important aspect was the QA/QC requirements on the excavation works that were stipulated at the tendering stage and applied throughout the construction works. The tunnelling required systematic grouting in many locations. These works are described in more detail by Olofsson et al. (2014). Some areas were drier, for example the 36 m long tunnel TAS04 required no grouting. It was decided to use that tunnel to test different investigation methods to evaluate the extent and hydraulic properties of the Excavation-Damaged Zone (EDZ). TAS04 has a cross-sectional area of 19 m^2 with a width of 4.2 m and a height of 4.8 m, the same as in the reference design for a KBS-3 deposition tunnel. This project was carried out between chainage 16 and 36, i.e. the inner 20 m of the tunnel.

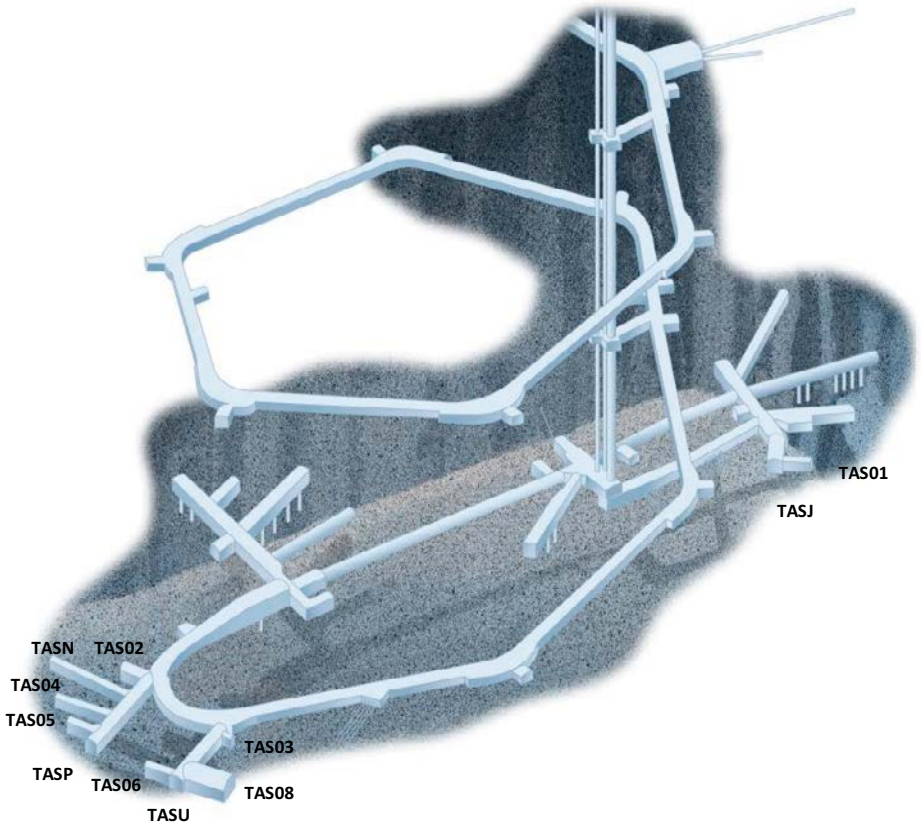

Figure 3-1. *General location of the Äspö Expansion Project. The location of the TASU and TASP tunnels is referred to as the 410 Level, and the TASJ tunnel is located at the 450 Level. This project focuses on the results from the experimental tunnel TAS04 excavated from TASP in the lower left-hand corner of the figure.*

3.2 QA/QC for construction works

The blast design was based on previous experience of successful blast design from construction of an earlier tunnel at the Äspö HRL (Christiansson et al. 2009, Christiansson and Karlzén 2010). The basic principle is to ensure precision in both drilling and charging. A reduced charge is important to reduce excavation damage, but this increases the demand on drilling precision to ensure that the charge geometry (distribution of explosives in the rock) is as planned. In addition, simultaneous initiation of the contour holes in particular reduces the risk for blast damage (Olsson and Ouchterlony 2003, Ouchterlony et al. 2010). The principles applied in this project are shown in Figure 3-2. The requirements on the excavation works are given in Section 4.3. The procedures to ensure the quality of the works are described in Section 4.4.

3.3 Characterization methods

3.3.1 Surveying for perimeter control

The tunnel floor geometry was documented as a 3D-modell using a photogrammetry method (SKB MD 150.010). This provides geometric information on the spatial position and the shape of objects, in this case the tunnel contour. The method is based on taking photographic pairs of the object that is to be mapped (i.e. the floor of TAS04) from two positions such that *conjugate points* (corresponding points) intersect. The *local model space* in 3D is then computed from the photographs using the software ShapeMetrix. The local 3D model was converted to the local site coordinate system ÄSPÖ96 using the surveyed coordinate points. Further description of the surveying method is provided in Section 6.1.

3.3.2 Geological mapping

The geological mapping of the TAS04 tunnel floor was done using the RoCS method (SKB MD 150.011, in prep.). This method is based on photographs, which are used to make a 3D-model with surveyed coordinate points. First photographic pairs are taken of the object that is to be mapped (i.e. the floor of TAS04). The photographs are combined to make a 3D model, which is associated with surveyed coordinate points in Äspö in the local site coordinate system ÄSPÖ96 so that the model can be oriented in a known space. This 3D model is then used as a basis for mapping in the RoCS software, where the parameters of the individual objects that are being mapped are described and saved in a database. The RoCS mapping includes a description of rock types, rock boundaries/contacts, fractures, deformation zones, the occurrence of water/water leakage as well as Rock Mass Rating (RMR).

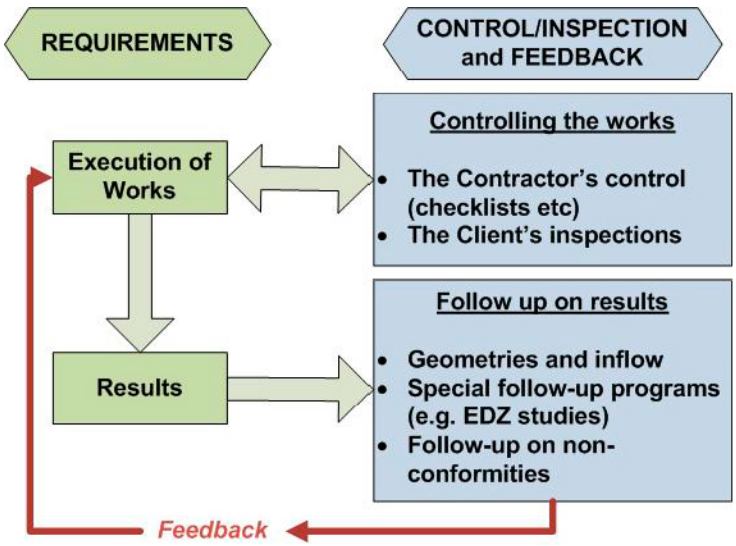

Figure 3-2. *Overview of the principles for QA/QC.*

The geological mapping of the 42 cored boreholes was done using the Boremap method (SKB MD 143.006), in accordance with Section 6.1.2; "Kartering av kärnborrhål, baserad på borrkärna (aktivitetstyp: GE038)", i.e. "Mapping of cored borehole, based on core (activity type: GE038)". In addition, all holes were filmed with a simple borehole viewer. Further description of geological mapping is provided in Section 6.1.

3.3.3 Geophysical investigations

Geophysical investigations consisted of Ground Penetrating Radar (GPR) measurements in TAS04 on the tunnel floor. The GPR survey was performed using GSSI (Geophysical Survey Systems, Inc.) SIR-3000 GPR system and a 1.5 GHz bandwidth, shielded, ground-coupled GPR antenna. The antenna was positioned against the cleaned and dried tunnel floor with best possible contact for data collection. Recording of the data was triggered by a calibrated line encoder. The antenna was positioned on measurements lines using a laser liner. Measurements were performed in lines parallel to the tunnel with an increment of 10 cm covering the whole width of the tunnel. The tunnel was measured in two parts at two different times. The first part covered tunnel lengths 7–21 m and was performed before drilling of the holes for hydraulic measurements. This first measurement consisted of 41 parallel lines. The second part, which was performed after drilling of the holes, covered tunnel lengths 21–36 m (end of tunnel) and consisted of 39 parallel lines.

The recorded GPR data were analyzed in two different ways. First, the unprocessed data were analyzed according to the GPR EDZ method as described by Kantia et al. (2010).Then data were processed in a more conventional interpretation. The radar image analysis methodology was tested including reflector selection from each profile, combining single line reflectors into reflector planes from several parallel lines and visualization in 3D. The geophysical works and results are presented in Chapter 7.

3.3.4 Hydraulic investigations

Specially designed equipment was developed for the hydrogeological investigations in 42 boreholes, 76 mm in diameter, drilled vertically in the floor within 20 m of the TAS04 tunnel. The majority (35 of the holes) were 1.0 m deep and the rest (7 holes) were 2.0 m deep (see Appendix 1 for details). The following criteria for the injection tests were established:

- The equipment must be capable of measuring transmissivities between $5 \cdot 10^{-10}$–$5 \cdot 10^{-7}$ m^2/s at an assumed pressure disturbance of 500 kPa. The flow interval that must be detected at that pressure is 1.0–1,500 mL/min.
- Measurements along the boreholes must be made from the borehole collar (tunnel floor).
- The packer system must have a rubber sealing length of 50 mm.
- A double packer system with 100 mm and 200 mm section lengths and a single packer system were specially manufactured.
- The equipment must be able to display numeric values and produce graphs with selected parameters versus time.
- A measurement must include both an injection and a recovery phase.

The equipment is described in Section 8.2.1. A borehole extender was bolted to the tunnel floor to permit injection tests to be performed from zero depth in the boreholes. Monitoring of possible interference from the injection tests was carried out in the other boreholes. The monitoring system is described in Section 8.2.2. Injection tests were carried out at 5 different depth intervals in all 42 boreholes, for a total of 210 injection tests. The testing details and results are presented in Section 8.4 to 8.6. Specially manufactured short packers were installed in all boreholes and connected to the Hydro Monitoring System (HMS) at the Äspö HRL. The system is described in Section 8.2.2. This installation made it possible to measure the formation pressure in the tunnel floor, see Section 6.3.1, as well as to detect any pressure disturbance from injection tests. The sealing length of the short packers was 100 mm and they were installed just beneath the tunnel floor.

The water flowing into the tunnel filled up the local depressions in the uneven floor, see Figure 3-3. Small pumps were installed to control the water table in these local water ponds and ensure constant head boundary conditions and saturated conditions during the injection tests, see Section 6.3.3. The locations of these pumps are shown in Figure 6-14. These pumps also made it possible to get a good measure of the total inflow of water to the test section, see Section 6.3.3.

3.3.5 Analysis approach

The key issue for the analysis was whether the blast design and the execution of the excavation works were adequate to meet the requirements on the hydraulic properties of the EDZ, see Section 1.4. This means that the investigations by means of geological, geophysical and hydrogeological methods must be fit for purpose. Therefore, the chosen characterization methods must support each other. The reliability of the methods used was another key issue, as well as the data evaluation approach. Finally, the use of independent data sources for the evaluation of blast impact on hydraulic connectivity in the studied tunnel floor was the major challenge. The different data sources and the analysis and modelling steps are outlined in Figure 3-4.

All data and interpretations were combined in a 3D model. The 3D model was used to compare different types of information, such as geological characterization, blast records and characterization data. The model is found in Appendix 2.

Figure 3-3. *Example of the uneven tunnel floor after cleaning (looking into the tunnel). One of the depressions in the uneven floor was at the left side between chainage 26 and 28. This depression was probably caused by misalignment of the drilling. The photo also shows some of the steeply dipping NW trending fractures aligned nearly parallel to the tunnel axis (at the top in the photo).*

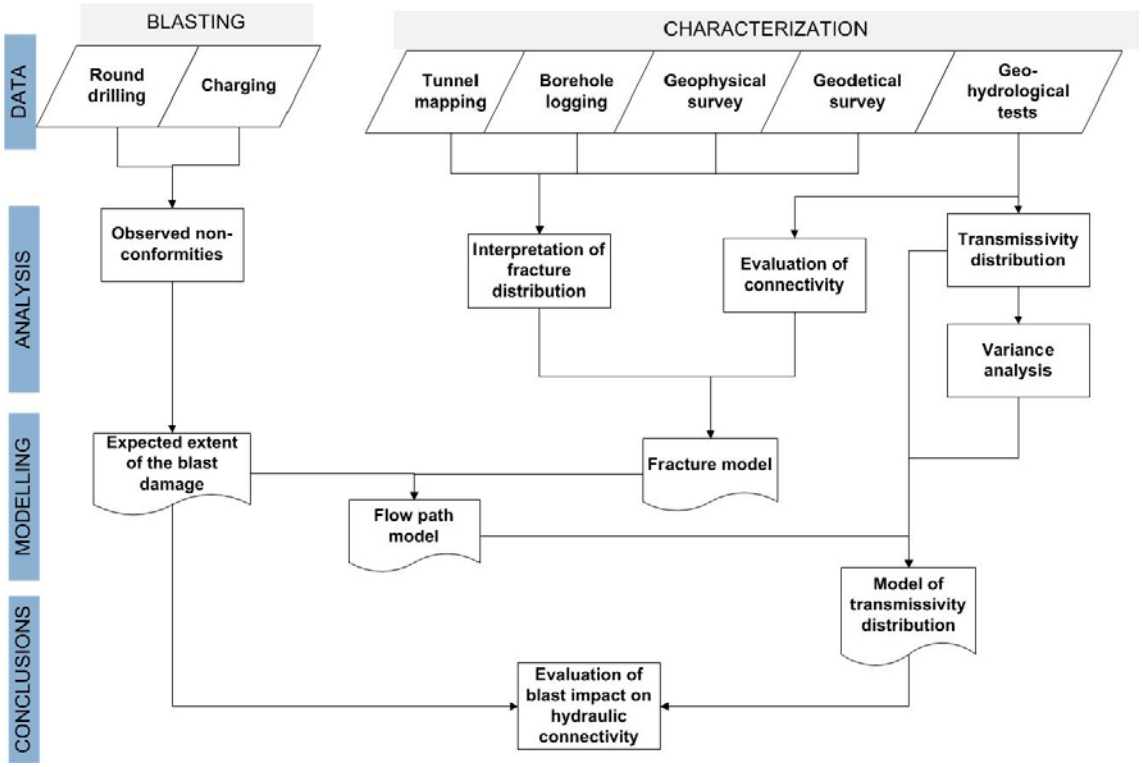

Figure 3-4. *Overview of data flow and interpretations in this project.*

4 Äspö reference project

4.1 Äspö tunnel expansion 2012

New demonstration experiments supporting the technology needed for the implementation of the design of the KBS-3 geological nuclear waste repository required the construction of two main tunnels TASP and TASU and several short tunnels at the 410-m level of the Äspö Hard Rock Laboratory (HRL), Figure 3-1. The lengths of the tunnels are given in Table 4-1.

Table 4-1. Length of the tunnels in Figure 3-1.

Transport tunnel	Experimental tunnel	Length (m)
TASP		60
	TASN	52
	TAS04	36
	TAS05	16
	TAS02	13
TASU		55
	TAS08	25
	TAS06	17
	TAS03	7
TASJ		19
	TAS01	15
Total		**308**

4.2 Site conditions

The bedrock at the Äspö HRL consists of diorite, intersected by granitic and pegmatitic dykes. The fracturing consists of three major fracture sets, two steeply dipping sets oriented NW and NE and one gently dipping set. The NW-trending set is the most dominant water-bearing fracture set at the Äspö HRL site.

The area at the 410 m level (Figure 3-1) exhibited mixed hydraulic conditions. There were a number of minor water-bearing structures. Pre-excavation grouting was required in many tunnel sections but not for TAS04, Figure 4-1.

The major horizontal stress is estimated to be 24 ± 5 MPa, probably in the lower range at the 410 m level. There are indications that the magnitudes of the minor horizontal stress and the vertical stress are similar, around 11–13 MPA at the 420–450 m level. A more detailed site description is provided in Chapter 6.

4.3 Blast design and tendering process

The principles of how inspection was carried out against specified requirements are illustrated in Figure 3-2. As-built inspection included the Contractor's inspection plans and checklists, as well as SKB's verification that these procedures were followed and that the requisite documentation was handed in. Inspection of tunnelling results could be done after the blasting, where the finished contour could be observed. With the support of the photogrammetric aid for tunnel mapping (see Section 6.1), geometrical verification of the tunnel contour could also be done in less than 24 hours after the excavation works, which permitted continuous feedback to the Contractor regarding how well he was complying with the contour requirements.

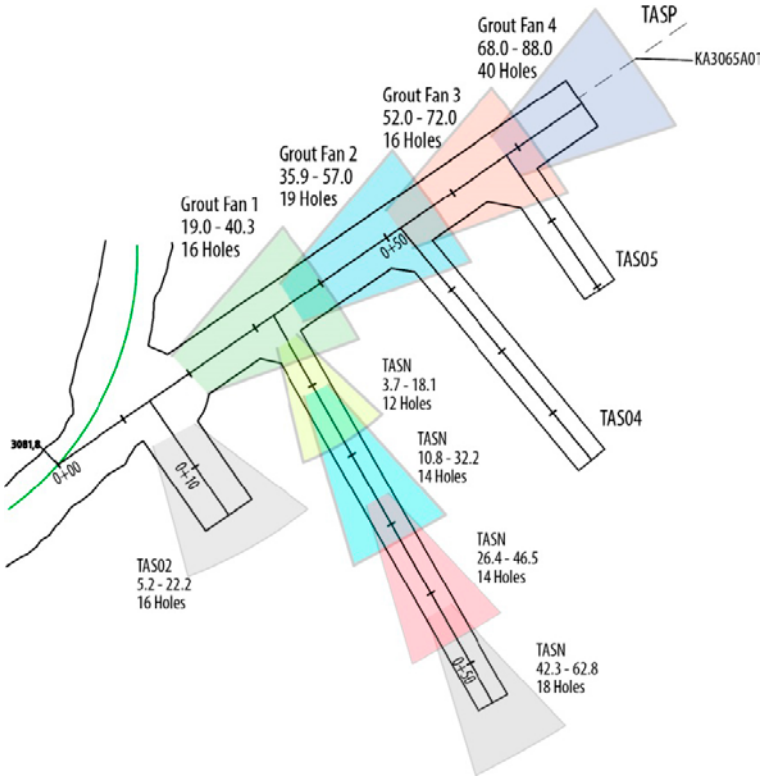

Figure 4-1. *Extent of pre-grouting in the vicinity of TAS04. The water-bearing structures are steeply dipping and strike sub-parallel to TAS04 (Figure from Olofsson et al. 2014).*

The blast design was based on previous experience of successful blast design from construction of an earlier tunnel at the Äspö HRL (Christiansson et al. 2009, Christiansson and Karlzén 2010). The basic principle is to ensure precision in both drilling and charging. A reduced charge is important to reduce excavation damage, but this increases the demand on drilling precision to ensure that the explosives are distributed as planned. In addition, the simultaneous initiation of the contour holes in particular reduces the risk for blast damage (Olsson and Ouchterlony 2003, Ouchterlony et al. 2010). The design table for the extent of the longest blast-induced crack proposed by Ouchterlony et al. (2010) was used as reference in the project.

The requirements stipulated for drilling and charging are presented in Table 4-2 and Table 4-3.

Table 4-2. Tolerances for drilling.

Tolerances for drilling	Radial deviation
Allowed collaring deviation for contour and helpers	± 7 cm
Allowed deviation in the theoretical endpoint for contour holes	± 20 cm

Table 4-3. Tolerances for charging with string emulsion in the different hole types. The average length of the bottom charge was 0.2 m.

Hole type	Charging tolerances	Bottom charge [kg]
Contour	0.350 ± 0.05 kg/m (string)	0.4
Helpers and bottom	0.500 ± 0.05 kg/m (string)	0.5
Production holes in TAS04	1.200 ± 0.10 kg/m (string)	–
Cut	1.800 ± 0.10 kg/m (fully charged)	–

It was also specified that reduced feeding force should be used when collaring any borehole to permit as straight drilling as possible. The degree of reduction was to be determined jointly by the Client and the Contractor, based on the specifications of the drill jumbo. All boreholes in a round should be cleaned by use of compressed air prior to charging. The Contractor should be prepared to grout any borehole in a round if water inflow was significant, as water in the hole could decrease the decoupling rate. He should always document ingress of water to boreholes in the round. Grouting was never needed in the TAS04 tunnel.

In summary, the requirements in the tendering specifications included:

- Requirements on contour control as shown in Table 4-2 which in turn set requirements on the drilling equipment.
- Requirements on charge concentrations as shown in Table 4-3. In contrast to previous tunnelling where cartridge explosives had been specified in the contour to ensure the prescribed charge concentration, string emulsion was now allowed in the contour as well, since this is the most common procedure in normal tunnelling. This created the necessary conditions for testing how well requirements on restrictions of the EDZ can be achieved in more industrialized tunnel production.
- Requirement on precision in detonators.
- Requirements on the logger systems on the drilling and charging equipment.
- Requirements on the Contractor's supervision of his works.
- Documentation requirements.
- Contractor's management system.

Prior to the start of construction, the Contractor's inspection plans and checklists for the tunnelling works were examined to ensure correct procedures for supervision and its documentation.

4.4 Strategy for QA/QC of excavation works

4.4.1 Optimizing the drill and blast plan

The basic blast design that was presented in the tendering process was adjusted by the Client to suit his equipment before the excavation works started. The blast design was then continuously further optimized and updated during the project. The process for updates of the design is described in Figure 4-2.

Different drill plans were used for different sections during the expansion of Äspö HRL. The theoretical section of the experimental tunnels TASN and TAS04 corresponds to that of the reference design for deposition tunnels, with a horseshoe shape, height 4.8 m and width 4.2 m. Figure 4-3 shows the basic drill plan design and the design used in the project for the experimental tunnels TASN and TAS04. Theoretical specific charge and specific drilling for both the basic and optimized blast designs are presented in Table 4-4.

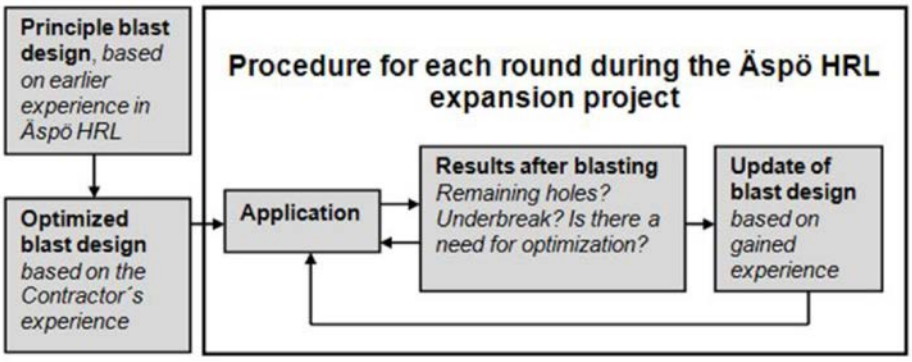

Figure 4-2. *Process for update of blast design during the Äspö HRL expansion project.*

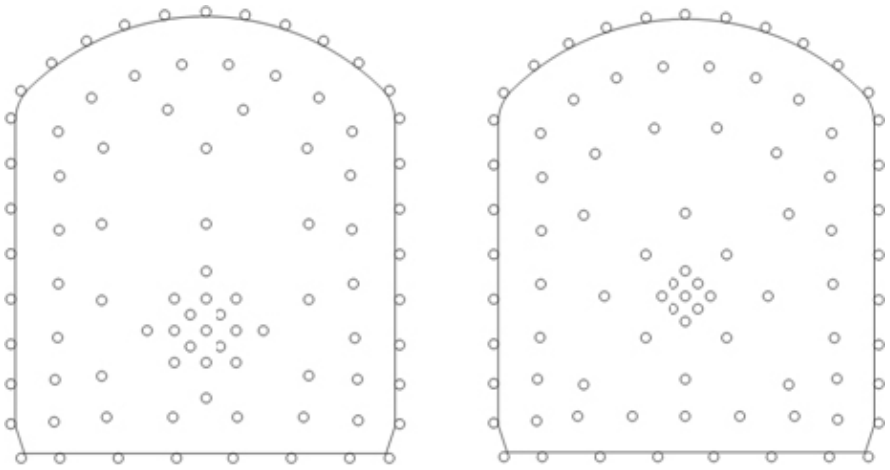

Figure 4-3. *Left: basic drill plan design for the experimental tunnels TASN and TAS04 proposed in the tender and right: the optimized design used in the project.*

Table 4-4. Specific charge and specific drill plan for the basic and optimized design.

	Basic blast design	Optimized design
Specific charge	2.7 kg/m^3	2.63 kg/m^3
Specific drill plan	4.04 m/m^3	3.92 m/m^3

Evaluation of possible blast damage was conducted with the aid of a table for damaged zone caused by emulsion explosives proposed by Ouchterlony et al. (2010), Table 4-5. The table was based on field experiments conducted in a quarry during 2006 with different concentrations of string emulsion charged in both horizontal holes and in plastic tubes in vertical holes.

The table by Ouchterlony et al. (2010) was modified for the actual hole diameter (48 mm) and explosive used, see Table 4-6 in order to be applicable to the Äspö expansion project.

Based on Table 4-6 the theoretical extent of blast-induced fractures could be determined for blast designs optimized by the contractor during the project before they were approved by SKB's supervisor. Figure 4-4 shows a visualization of the theoretical extent of the largest fractures generated by the charge concentrations used based on Table 4-6. The visualization was done with the iSURE software. iSure tunnel includes project files management, tunnel profiles, tunnel location, drill-and-blast design, and drilling and blasting patterns. This module offers pattern design at the end of the round, providing hole burden calculus and optimization of hole location. The design of the theoretical profile can be drawn manually or chosen from the standard profiles provided in iSURE. It is also possible to import a profile in .dxf format from AutoCad.

Table 4-5. Theoretical extenst of the largest blast-induced fracture (Ouchterlony et al. 2010). Charge concentration expressed as DxM/m and type of initiation (Nonel or simultaneous).

Theoretical damaged zone depth in m	Charge concentration, kg DxM/m (DxM is the reference explosive Dynamex M)	
	Nonel (Single)	Simultaneous
0.2	0.1	0.2
0.3	0.2	0.3
0.5	0.3	0.4
0.7	0.4	0.5
1.1	0.7	0.6
1.3	0.9	(0.7)
1.7	1.3	–
2.0	1.6	–

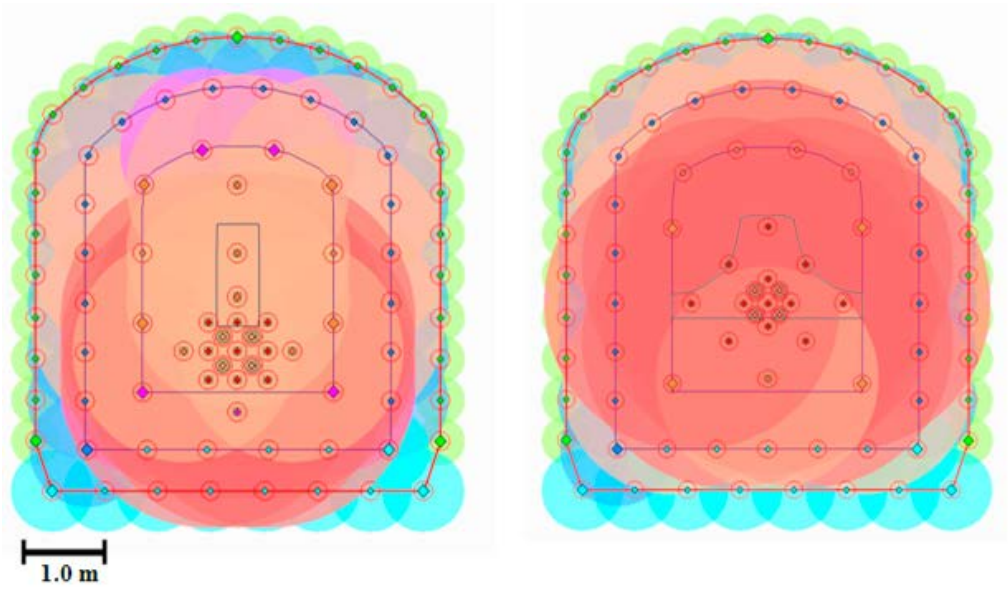

Figure 4-4. *Maximum theoretical extent of the longest blast-induced fractures. Left: principle drill plan design and Right: the optimized design applied in the project for the experimental tunnels TASN and TAS04. The colours represent the different hole types, while the radius of the circles represents the theoretical extent of the longest blast-induced fractures. Note that the theoretical extent of the longest fracture in the floor is 0.5 m for both designs. See Table 4-3 for charge concentrations.*

Table 4-6. The modified table used in the Äspö expansion project based on Ouchterlony et al. (2010). All values are for column charges. The explosive Kemiitti 810 has a density of 1.0 kg/m^3 and a concentration 0.78 DxM/m (DxM is the reference explosive Dynamex M).

Explosive	Charge concentration of string emulsion [kg/m]	Theoretical extent of the longest crack. (calculated with DxM = 0.8 for Kemiitti 810) [m]
KEMIITTI 810 350 g/m	0.35	≈ 0.25 (Simultaneous)
KEMIITTI 810 500 g/m	0.5	≈ 0.5/0.7 (Simultaneous /Single)
KEMIITTI 810 800 g/m	0.8	≈ 1.0 (Single)
KEMIITTI 810 1,200 g/m	1.2	≈ 1.35 (Single)
KEMIITTI 810 1,800 g/m	1.8	≈ 1.8 (Single)

In the drill pattern, the iSURE software can define a range of different drilling types such as contour holes, field holes, grouting holes, etc. They then use their specific pre-set parameters in the rig: less power is used for high accuracy in contour holes, whereas more power is used in field holes, for example.

In iSURE, measuring-while-drilling (MWD) data can be collected and reported and analyzed. The module collects data on 19 parameters. Among these are parameters such as air flow, feed pressure setting, rotation speed setting, anti-jamming state, drilling control setting etc. The MWD data can be studied and analyzed after drilling.

4.4.2 Overview of QA/QC procedures

The blast design included the approach to minimize the risk for extension of induced fractures from helper, cut and production holes. The quality assurance process applied in the Äspö expansion project included control of each step in the excavation cycle during the work as well as after verification that the functional requirements were met. In addition to the contractor's quality control of his work, SKB supervised the work process with the aid of logger data from the drilling jumbo and charging equipment as well as verification of tunnel geometry using photogrammetry and field inspections. The process is described in Figure 4-5.

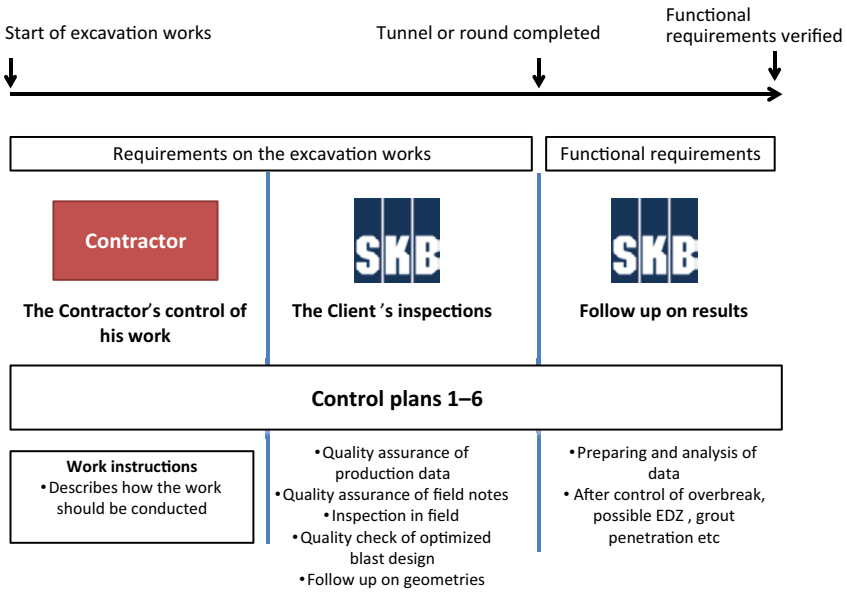

Figure 4-5. *Illustration of the process for quality assurance, applied in the Äspö expansion project.*

Each control activity was described in detail in one of a total of 6 control plans. The control plans included a short description, frequency of the control, how the activity was documented and responsible person for each activity. The control plans included control activities for the following steps in the excavation cycle:

- drilling,
- charging and blasting,
- grouting,
- scaling and rock bolt installation,
- shotcrete and wire mesh, and
- calibration and service of equipment

4.5 The Contractor's QA

4.5.1 Quality control of round drilling

Precise drilling is important in order to achieve a smooth contour and to minimize the extent of the blast-induced damage. With good drilling precision, the charge geometry (distribution of explosives in the rock) will be as planned. To achieve this, reduced feed pressure was applied when collaring the boreholes. In addition, the Contractor marked the theoretical contour on the face in order to ensure good collaring and also as a check of calibration of the drilling jumbo. The borehole diameter was 48 mm and the theoretical borehole length was 4.5 m, in practice there was a variation in hole length as the rounds were drilled to a predefined reference plane.

4.5.2 Quality control of charging

A possible extension of the EDZ due to any modification of the blast design was evaluated by the client's supervisor before acceptance. Calibration of the drilling jumbo and charging equipment was of high priority. Calibration of the charging equipment was performed with tubes of acrylic glass, Figure 4-7.

The charging equipment logged the volume of explosives charged into each borehole. By charging in a specific pattern, always starting with the same borehole, the amount of explosives per borehole could be determined. This made it possible to verify whether the requirements as shown in Table 4-3 were met.

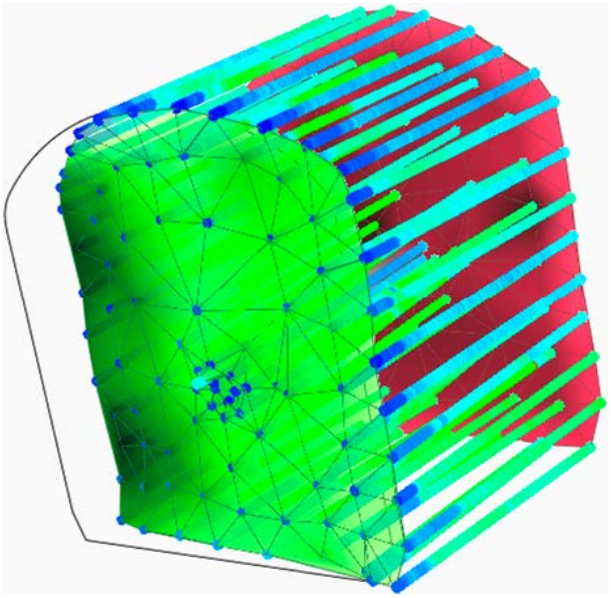

Figure 4-6. *Example of visualization of the drilling log from round #1 in TAS04 with the iSURE software. The visualization includes positioning of the holes, theoretical section, interpreted face structure and MWD data (In this example percussion pressure).*

Figure 4-7. *Calibration of the charging equipment using tubes of acrylic glass. Note the transition between the bottom charge and emulsion string.*

4.6 The Client's QA

4.6.1 The Client's inspections

The main task performed by the Client during the excavation works was to ensure that the Contractor followed his checklists and documented the results of his control plan in accordance with Section 4.4.2. In addition, the Client's supervisor evaluated the logs from drilling and charging and gave feedback on the degree of non-conformities, when required.

4.6.2 The Client's verification

Verification of complete results could only be done after completion of the excavation works and complete cleaning of the tunnel floor. An outline of the means and methods is provided in Section 3.3.

5 Construction records

5.1 Construction overview

A two-boom drill jumbo, Sandvik DT 920i, equipped with the iSure software, was used to drill the blast holes. The jumbo was delivered new from the factory at the beginning of the project to ensure the best possible conditions for drilling precision.

A Forcit charging unit model 201 was used for mixing, pumping and control of a two-component string emulsion (KEMIITTI 810 emulsion) that was used in all holes. Strings were applied in the contour, helper, production and bottom holes (Table 4-3). The holes in the cut were charged full. After the charging hose was inserted into the borehole, motorized electronic equipment was used to pull it out with a constant speed. This permitted high precision in the charging work. The mass of charged emulsion for each hole was recorded in chronological order by a charging logger. With the aid of a predefined charging sequence, the amount of explosives in each individual hole could be traced from the charging log. In downward-directed water-filled holes, charging was performed in lidded plastic tubes (40 mm in diameter) in order to avoid damage to the string. The tubes were used in the bottom holes of TAS04. In flowing upward-directed holes, charging was done with cartridges.

Initiation of the contour holes was performed with electronic detonators of the type i-Kon VS. Using this type of detonator, a time delay of <1 ms between initiators in the same intervals can be achieved. The production holes were initiated using pyrotechnical detonators from the Nonel LP system.

5.2 Construction records – production data

The construction documentation was used by SKB's supervisor to check compliance with the requirements on drilling, charging, geometry and blast damage control. The contractor delivered the following data and field notes for each round during the excavation of TAS04.

Drill log – in .dcl format. Original file from the drill jumbo for the iSURE Software.

Drill log – generated .csv file from the iSURE drill log. This file contains positioning data for the boreholes, drilled length etc.

MWD – generated .csv file from the iSURE drill log. Contains the MWD data for the drilled holes.

Round report summary – file in Microsoft word format generated from the original iSURE file. Contains a summary of the drilling of a round with both positioning and MWD data.

Observations during drilling – Drill plan image with field notes taken by the operator during drilling. Includes comments on moved holes, complementary holes and comments on the logged data.

Measurements of collaring positions and hole bottoms of contour holes (PLM,GEO and Excelfiles) – Coordinates for geodetically measured positions, also delivered plotted together with the theoretical contour.

Charging sequence – Drill plan image with field notes. Describes the order of charging for the contour, helper and bottom holes.

Charge log – Chronological log in .csv format generated by the charging equipment. Contains the amount of the emulsion charged in each hole.

Initiation plan – Describes the initiation sequence. Pdf format.

Drill and charge plan + blast journal in Excel format – Table with documentation of the drill and charging plan. The blast journal describes what was actually done.

Documentation of results after blasting – Drill plan image in .pdf format with field notes on locations of over- and underbreak and reblasts

5.3 Results

5.3.1 Results from compliance check of drilling

Results from the check of drilling precision at the end of contour holes are presented in Figure 5-1. In the 8 blast rounds of TAS04, 88% of the contour holes met the requirement of a maximum deviation of ± 20 cm from the theoretical endpoint. This check was however not possible to conduct for the bottom holes during the excavation work. The tunnel floor topography could later be determined based on photogrammetric documentation. The results were less encouraging, see Figure 3-3 and Figure 5-2. The limit of 35 cm overbreak was exceeded on almost 50% of the tunnel floor.

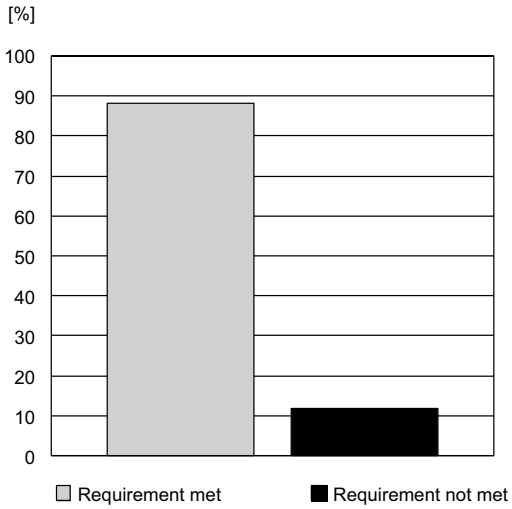

Figure 5-1. *Results from check of drilling precision for the contour holes (hole bottoms) in the 8 rounds of TAS04.*

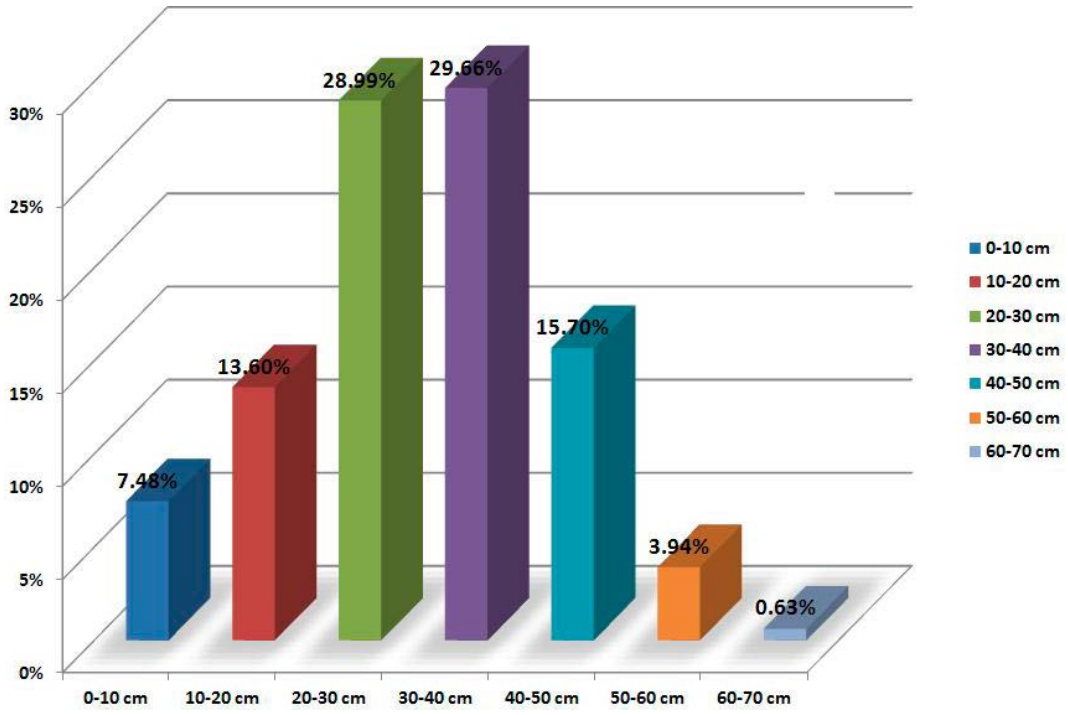

Figure 5-2. *The photographic documentation provides pixels. The documentation is based on analysis of the difference between the photogrammetrically documented floor and the theoretical (planned) level of the tunnel floor for each pixel.*

5.3.2 Results from compliance check of charging

Charging of the contour and helper holes was done in a specific order so that the charging log could be used to verify that the specifications on charging were in accordance with the tolerances presented in Table 4-3.

Evaluation of the results from charging was conducted based on the charging and drilling logs. In order to combine the recorded lengths from the drilling log together with the amount of charged explosives from the charging log, the charging sequence was also needed. Figure 5-3 shows an example of compliance checking of charging in the contour holes for round 1 in TAS04.

Table 5-1 presents the mean values for the achieved charging tolerances for the contour, helper and bottom holes in the 8 rounds for TAS04. The table also shows the specific charge achieved.

Charging data for each individual hole are presented in Appendix 3. There is a tendency for the logged amounts of emulsion explosives to be within the upper range of the tolerances for the bottom holes, when considering traceable charging data for individual holes. The actual specific charge values are close to the design value for the rounds for TAS04. The tendency is that the values are slightly higher than the design value. Even if the difference in percent is relatively great, the deviation from nominal weight is still very small. Figure 5-4 shows a visualization of the data seen from below the TAS04 for rounds 4 to 8 (where hydraulic tests and GPR measurements have been conducted).

The results presented in Figure 5-4 indicate that the evaluated charge concentrations (kg/m) are generally in the upper range of the tolerances or exceed the tolerances for the bottom holes. Charging data however indicate that the tolerances were only exceeded to a limited extent, compared with Table 5-1.

Table 5-1. The mean values of charged explosives per metre for the string-charged hole types together with the specific charge. The theoretical specific charge was 2.63 kg/m^3. The results suggest high general precision in the charging of string emulsion in the 8 rounds for TAS04.

Round Design value	Contour [kg/m] 0.35 ± 0.05	Helper [kg/m] 0.50 ± 0.05	Bottom [kg/m] 0.50 ± 0.05	Specific Charge [kg/m^3] 2.7
1	0.35	0.56	0.55	3.11
2	0.34	0.51	0.48	2.95
3	0.34	0.51	0.52	2.83
4	0.33	0.49	0.49	3.07
5	0.32	0.52	0.47	2.82
6	0.34	0.49	0.51	2.77
7	0.31	0.52	0.57	2.84
8	0.31	0.50	0.56	2.84

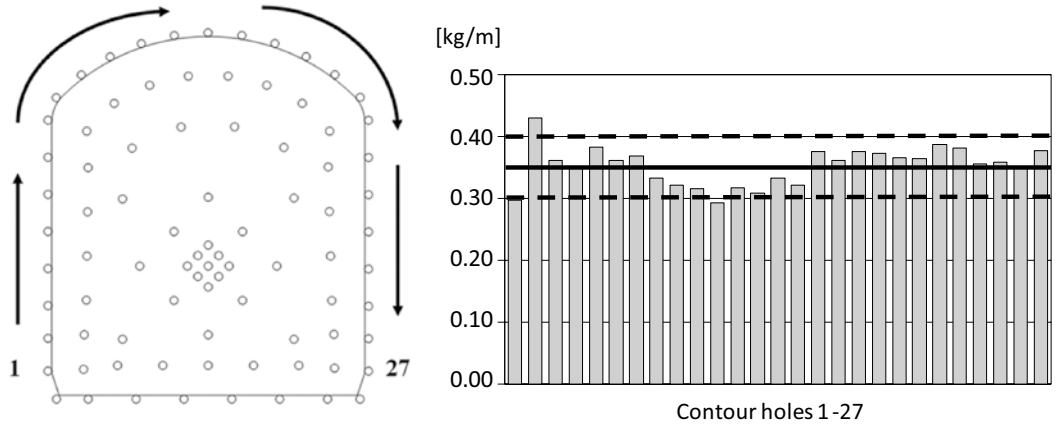

Figure 5-3. *Left: Order of charging of the contour holes, round 1 TAS04 (1–27 are the contour holes). Right: Results from the column charge of the contour holes in blast round #1 in TAS04. Tolerances, ± 0.05 kg/m, are shown together with the design mass of the string, 0.35 kg/m. Contour hole #2 was over-charged.*

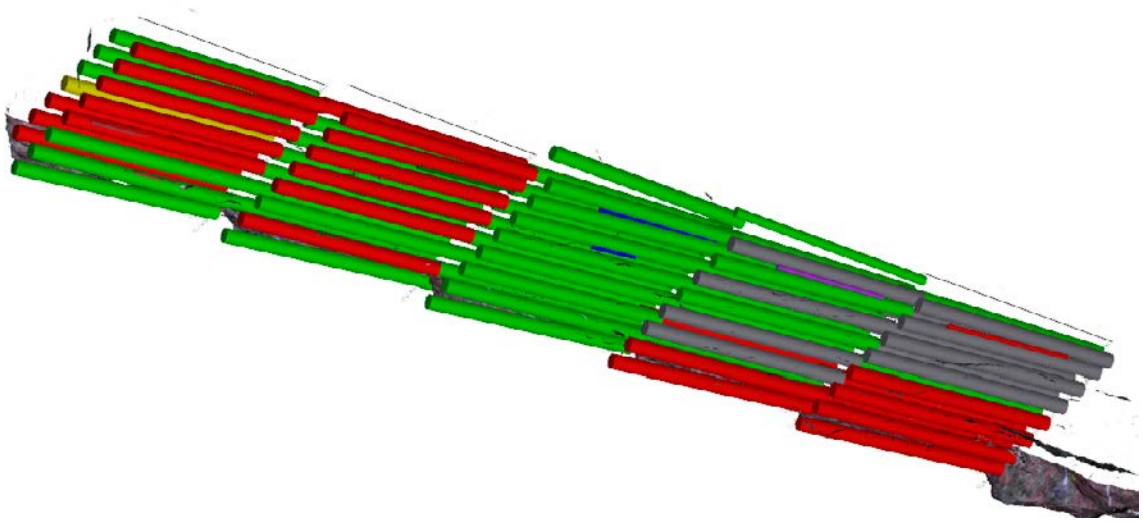

Figure 5-4. *Visualization of the charged concentrations in the bottom and helper holes in TAS04. Tunnel face towards left. Red colour marks holes where the tolerances have been exceeded, yellow marks holes where charges are less than the minimum tolerance, green marks holes with charged amounts within the tolerances and grey marks holes with uncertain data. Note that positioning is based on the theoretical drill plan.*

6 Geological characterization of the research tunnel

6.1 Mapping methods

Geological characterization of the experimental site serves as a basis for modelling the effects of tunnel excavation on the EDZ. Necessary components are descriptions of rock types, fractures, fracture zones and observed water inflow, both to the tunnel and the boreholes. A newly excavated tunnel with fresh surfaces is to be preferred, as well as cored boreholes from each rock type. The mapping procedures for tunnels and cores are described under the acronyms RoCS and BoreMap.

Characterization of fractures observed from a tunnel must consider the different conditions and scales for documentation. Mapping of fractures in a drill-and-blast tunnel requires god light conditions and free access to all surfaces for close observations or remote sensing technology. The excavation method may have opened up sealed fractures and induced the opening of new fractures from the blasting. The origin and properties of all fractures is therefore sometimes difficult to identify. The mapping must also consider the resolution required. It is obvious that a cut-off length for fracture traces has to be set for practical reasons, since fracture size follows an approximate power law distribution (increasing number of fractures with decreasing trace length). On the other hand, logging of drilled cores can be carried out under good conditions. The fracture length cannot be determined from individual cores, so all fractures are recorded. The fractures can easily be categorized as open, sealed, fresh, etc. The major uncertainty in mapping fractures in cores is to what degree fractures have opened or been caused by handling of the cores.

6.1.1 Tunnel mapping

RoCS is based on photogrammetric documentation of the tunnel surfaces. Photogrammetric pairs of photos are used to develop a 3D model of the tunnel. The cut-off length for fracture traces during tunnel mapping was approximately 1 m, where the fracture length is the trace length on the rock surface. Only fractures that show no indication of aperture are called tight, all other fractures are either tight to partially open, open, open to partially tight, re-opened or induced open fractures (fractures with no fracture fillings and fresh rock surfaces). The fracture width is defined as possible aperture plus possible fracture filling measured across the fracture. Oxidation rims (red staining/colouring) across fractures are measured in the same way and include the width of the fractures. Rock dykes/veins < 0.1 m in width are commonly regarded as fracture fillings and thus recorded as fractures.

The average orientation of structural features, besides the automatic orientation obtained from the 3D-model, was measured with a handheld compass. Magnetic north is used for reference and orientations of planar structures are given according to the right-hand rule. Thus, the orientation of the strike is measured when the dip direction is on the right-hand side. The orientation of linear structures is given as trend and plunge.

For the actual mapping of the floor, water leakage could only be observed if water could be seen flowing out of a fracture. No such observations were made during mapping of the floor of TAS04.

6.1.2 Core logging

Mapping of the borehole cores was done using the overview Boremap mapping method (SKB MD 143.006), activity type GE038. This includes rock types and fractures, where depth along the core, α-angle, aperture and width as well as other characteristics of the fracture (form, rawness, alteration and fracture filling) are mapped. As stipulated in the SKB MD 143.007, each uptake of core is marked on the core box, and if the core is broken in the handling the drillers mark the core box with an F (Fresh). This is used when mapping the core. If the is broken and there is no F marked on the box, no fracture filling is visible and the core bits fit perfectly together, the break is generally considered to be a drilling-induced break. When the core is broken along a fracture that has a fracture filling, and there is no F on the core box, the general assessment is that the fracture is a naturally broken fracture. When the core is not broken, but there is a fracture with mineral filling with a visible opening, the fracture is mapped with an aperture, which puts it in the category “partly open fracture”. Only fractures with filling that show no opening (aperture) are mapped as unbroken fractures.

The terminologies used by Boremap mapping and RoCS mapping differ in some ways, especially when it comes to fractures. An open fracture in RoCS mapping is called broken in Boremap mapping, and a tight fracture in RoCS mapping is called unbroken in Boremap mapping. This discrepancy is mainly due to differences in the definitions of fractures in the borehole core (see SKB MD 143.006), where open fractures are fractures that break the core, with or without aperture and/or mineral fillings. Visible fractures with fracture filling that do not break the core are called unbroken. In RoCS the terminology conforms more to mapping in the field, where open fractures are those that show aperture with or without mineral fillings and tight fractures show no aperture, but contain mineral fillings.

Lastly, the boreholes were filmed with a borehole camera for reference and possible rough orientation of major structures in the cores. The film is also useful as a support for the assessment of fracture origins, i.e. whether they are drill-induced or not.

6.2 Geological setting of the research tunnel

The chosen research tunnel (TAS04) is one of the new tunnels excavated in 2012 at the Äspö HRL. It is a side tunnel from TASP (see Figure 4-1) between the tunnels TASN and TAS05. The innermost part (between approximately 16 m and to the bottom of the tunnel at 37.5 m) was chosen to maximize the variability in rock types (see Figure 6-2) as well as fractures. There is also a distinct variation in the topography of the tunnel floor (see Figure 6-1), with more or less distinct ends of blast rounds.

6.2.1 Lithology

The rock in the tunnel floor can in general be divided into three main rock types; fine-grained granite, Äspö diorite and Ävrö granodiorite. Minor amounts of pegmatite dykes/veins also occur (see Table 6-1 and Figure 6-2.

An irregular deformation zone approximately 0.5–1 m in width cuts the TAS04 between approximately 28 and 30 m tunnel length striking approximately 190 degrees (magnetic north) and steeply dipping (85 degrees), see Appendix 4 and Figure 6-3 and Figure 6-7. The main deformation of that zone occurs along the boundaries and/or epidote-dominated fractures/cataclastic bands. More or less undeformed Äspö diorite occurs in between. Within the zone a number of irregular minor fractures are present, some of which are epidote-filled. The contact of the deformation zone towards the end of the tunnel coincides with Ävrö granodiorite, and towards the start of the tunnel the fine-grained granite stops at the deformation zone at the right-hand wall and the right-hand side of the tunnel floor (see Figure 6-7).

Figure 6-1. *Foto showing the tunnel TAS04 taken from the tunnel mouth at approximately 4 m and looking towards the end of the tunnel at 37.5 m, with the floor cleaned and shotcrete at the tunnel mouth to approximately 7 m. The photograph is taken before the drilling of the 42 boreholes in the floor.*

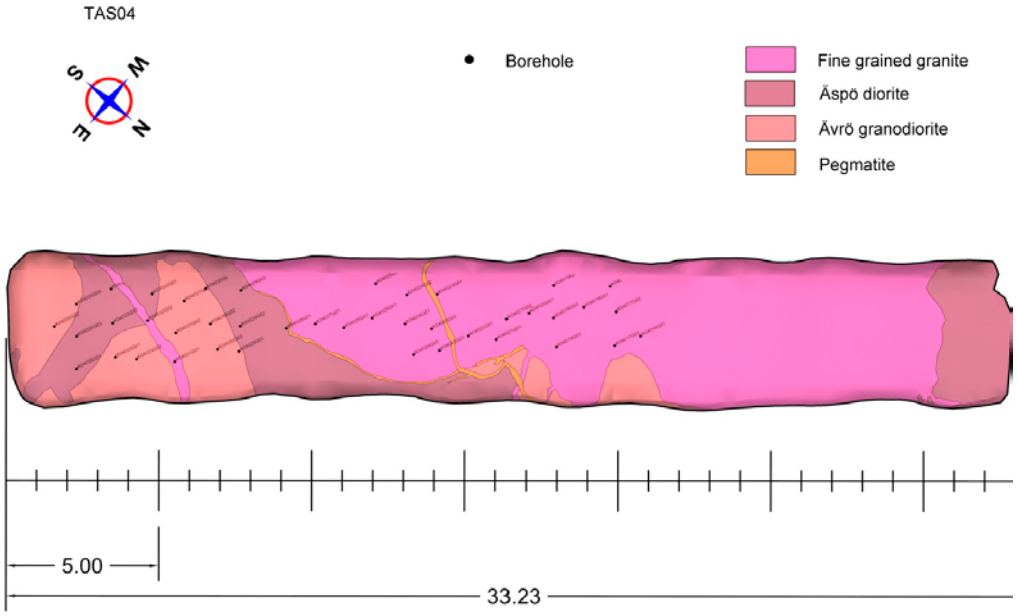

Figure 6-2. *Map of rock types in the floor of TAS04. Tunnel length from center of TASP is approximately 4.3–37.5 m. Boreholes are located between approximately 15 and 37.5 m. A deformation zone with orientation approximately 190/85 (strike is in magnetic North and dipping is to the West) is located between approximately 28 m in the left wall and 31 m in the right wall (see also Figure 6-7).*

Table 6-1. Area of mapped rock types in the floor of TAS04 (5–37.5 m)

Rock type	Area (m^2)	%	Comment
Fine-grained granite	98.00	56	Makes up the main body of the floor in TAS04
Äspö diorite	41.23	23	
Ävrö granodiorite	33.50	19	
Pegmatite	1.04	0.6	Irregular dyke
Pegmatite	0.68	0.4	Contact dyke/vein to fine grained granite ca 21–28 m
Fine-grained granite	1.87	1	Dyke

Figure 6-3. *The deformation zone in TAS04. Photograph taken towards the left wall between approximately 28 and 29 m, showing the two cataclastic bands that define the zone.*

Some of the fine-grained granite is somewhat coarser-grained and lighter red in colour. The contact between these two types of granite is very diffuse and irregular and could not be mapped with any certainty in the tunnel floor.

6.2.2 Fracturing

The RoCS mapping of the floor in TAS04 resulted in 372 fractures: 214 open fractures and 158 tight fractures. The dominant direction of the fractures can be seen in Figure 6-4.Tight fractures are shown in Figure 6-5 and re-opened fractures in Figure 6-6.

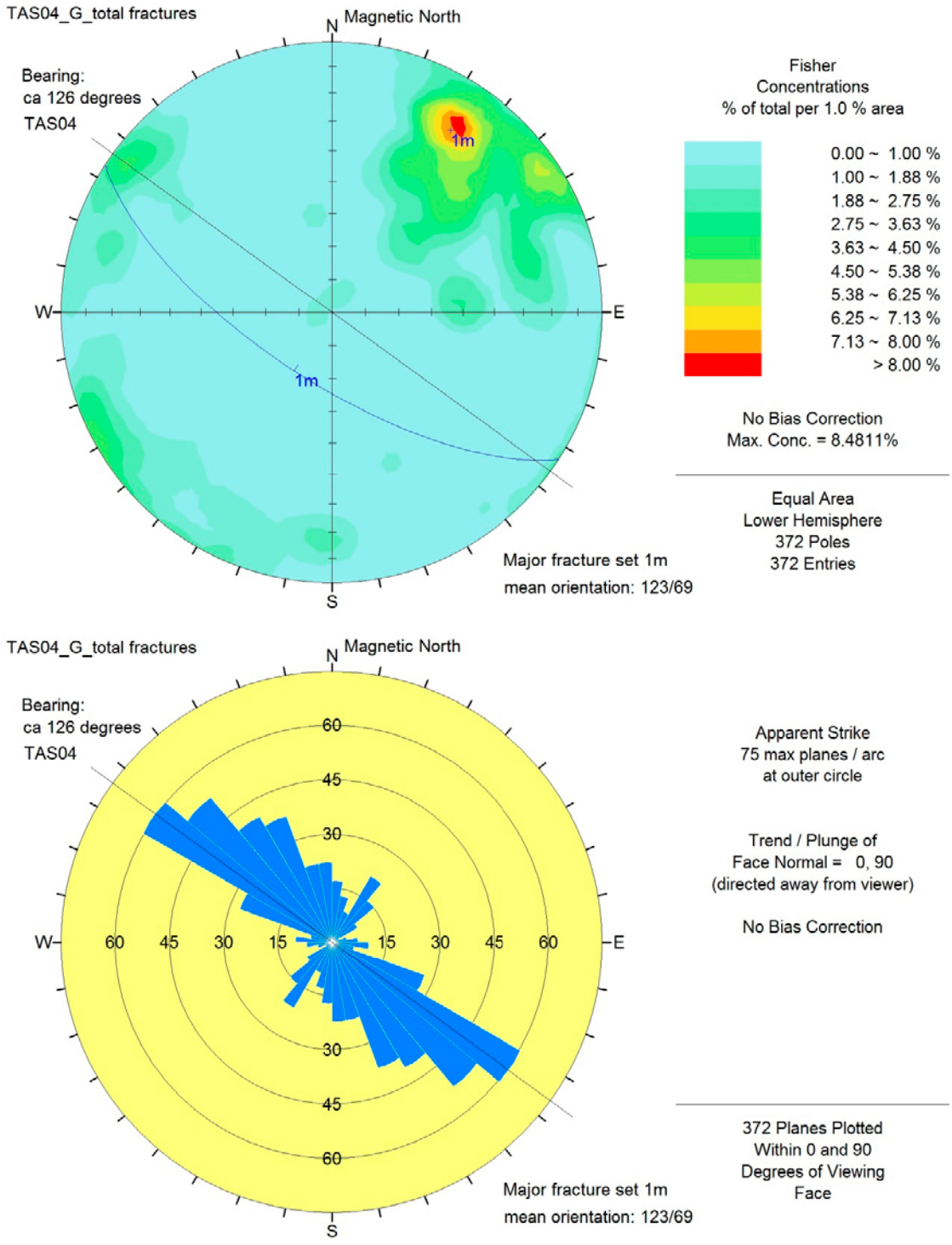

Figure 6-4. *Orientation of RoCS-mapped fractures from the floor in TAS04 presented in Schmidt net and joint rosette diagrams. The approximate 126 degree trend of the TAS04 tunnel is marked as a black line. One main orientation set can be seen, 1 m: 123/69. N refers to magnetic north.*

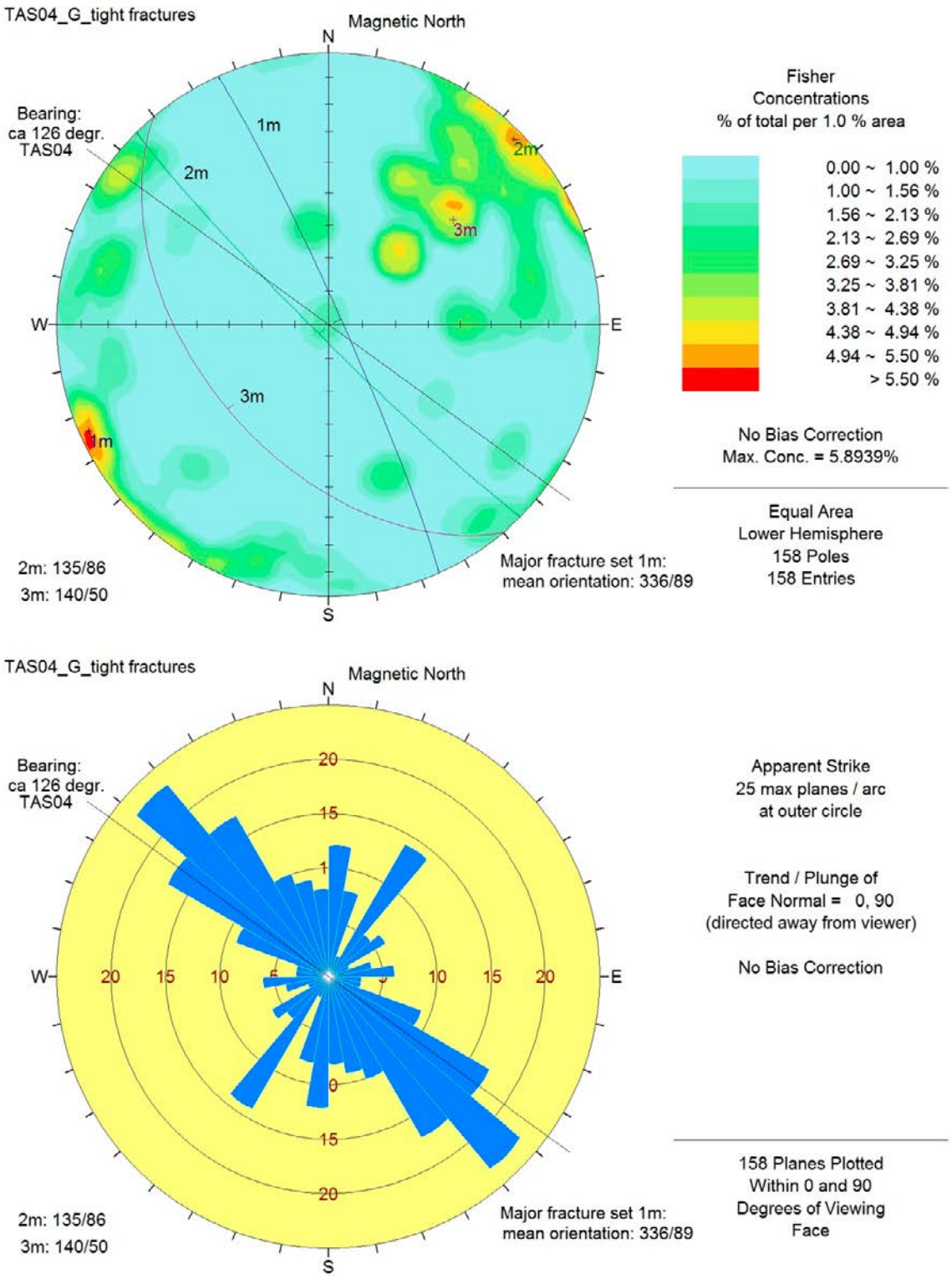

Figure 6-5. *Orientation of RoCS-mapped tight fractures from the floor in TAS04 presented in Schmidt net and joint rosette diagrams. The approximate 126 degres trend of the TAS04 tunnel is marked as a black line. Three main orientation sets can be seen, 1 m: 336/89 and two somewhat less prominent, 2 m: 135/86 and 3 m: 140/50. N refers to magnetic north.*

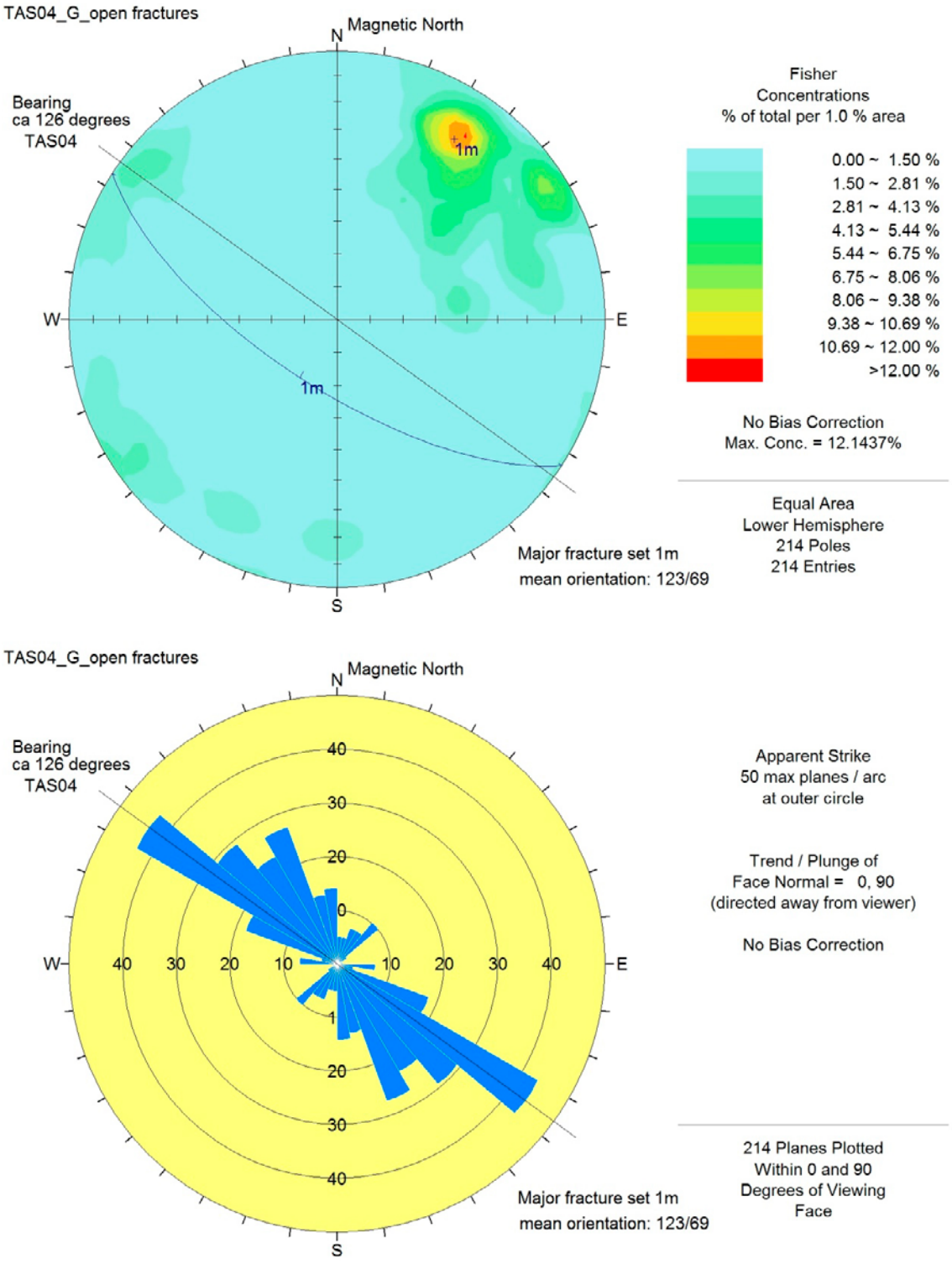

Figure 6-6. *Orientation of RoCS-mapped open fractures from the floor in TAS04 presented in Schmidt net and joint rosette diagrams. The approximate 126 degree trend of the TAS04 tunnel is marked as a black line. One main orientation set can be seen, 1 m: 123/69. N refers to magnetic north.*

The locations of the mapped fractures in the floor of the TAS04 tunnel are shown in Figure 6-7.

Core logging of the short boreholes shows only a few fresh fractures in the upper part of 12 of the boreholes. Most of these fractures are probably blast-induced. The holes with broken (open) fresh fractures are randomly distributed over the studied area. Almost all boreholes show broken (open) natural fractures, as well as unbroken (tight) ones. It is uncertain whether the interpreted broken

(open) fractures were natural open fractures or if they were broken (opened) by drilling and core handling (drill induced). Broken fractures without mineral fillings can in general be interpreted as possible EDZ.

In the boreholes, a division of the fine-to-medium-grained granite into two types based on difference in colour, red versus lighter red, seems plausible. This division is very diffuse on the surface of the tunnel floor, so no mapping of a contact between the two types could be done. Another observation connected to the colouring of the fine-to-medium-grained granite is that the number of fractures seems to be higher in the red granite boreholes when compared to the light-red granite. One possible explanation for the colour difference between the two rock types is the number of fractures, i.e. the higher number of fractures leads to a slightly stronger red colouring of the rock type. The higher number of fractures in the red fine-to-medium-grained granite is therefore the cause of the redder colour and the light red fine-to-medium-grained granite is only lighter because of fewer fractures. The red colouring seems to be the result of hydrothermal alteration (Drake and Tullborg 2004, Eliasson 1993).

A table showing the various types of fractures can be found in Appendix 4. An example from part of borehole K04033G03 is shown in Table 6-2.

Table 6-2. Part of a larger Excel sheet showing results from the Boremap mapping of one of the boreholes in the floor of tunnel TAS04. Broken fractures = Open fractures. Unbroken fractures = Tight fractures. Drill-induced = Fractures without fracture filling that are assumed to be the result of drilling and/or core handling, usually because of lack of fracture filling and good fitting of core bits. The drill-induced fracture with the designation uptake is the bottom fracture of the core (usually from where the core was broken at the end of the borehole). Mineral 1/Operational and Mineral 2/Roughness; before the slash is the mineral filling 1 and 2 in broken and unbroken fractures and after the slash is the type of core breakage and appearance of drill-induced fracture. See also Appendix 4.

ID	Borehole	Sec. Up	Sec. Low	Packer depth	Obs. ID	Mineral 1 / Operational	Mineral 2 / Roughness	Min. 3	Min. 4
8	K04033G03	0.011	0.011	0–0.1	Drill-induced	Break	Irregular		
8	K04033G03	0.033	0.033	0–0.1	Drill-induced	Break	Irregular		
8	K04033G03	0.065	0.065	0–0.1	Unbroken fracture	Calcite	Quartz	Epid.	Oxid. walls
8	K04033G03	0.110	0.110	0.1–0.2	Broken fracture	Chlorite	Calcite	Oxid. walls	
8	K04033G03	0.120	0.120	0.1–0.2	Unbroken fracture	Epidote	Calcite	Chl.	
8	K04033G03	0.162	0.162	0.1–0.2	Drill-induced	Break	Irregular		
8	K04033G03	0.185	0.185	0.1–0.2	Unbroken fracture	Calcite	Oxidized walls		
8	K04033G03	0.220	0.220	0.2–0.4	Drill-induced	Break	Irregular		
8	K04033G03	0.295	0.295	0.2–0.4	Drill-induced	Break	Irregular		
8	K04033G03	0.388	0.388	0.2–0.4	Drill-induced	Break	Irregular		
8	K04033G03	0.662	0.662	0.6–2	Unbroken fracture	Quartz	Chlorite		
8	K04033G03	0.970	0.970	0.6–2	Broken fracture	Calcite	Laumontite		
8	K04033G03	1.220	1.220	0.6–2	Unbroken fracture	Quartz	Calcite		
8	K04033G03	1.300	1.300	0.6–2	Broken fracture	Chlorite	Calcite		
8	K04033G03	1.345	1.345	0.6–2	Unbroken fracture	Epidote	Quartz	Chl.	Calc.
8	K04033G03	1.345	1.345	0.6–2	Drill-induced	Break	Irregular		
8	K04033G03	1.662	1.662	0.6–2	Drill-induced	Break	Irregular		
8	K04033G03	1.853	1.853	0.6–2	Broken fracture	Laumontite			
8	K04033G03	2.017	2.017	0.6–2	Drill-induced	Uptake	Undulating		

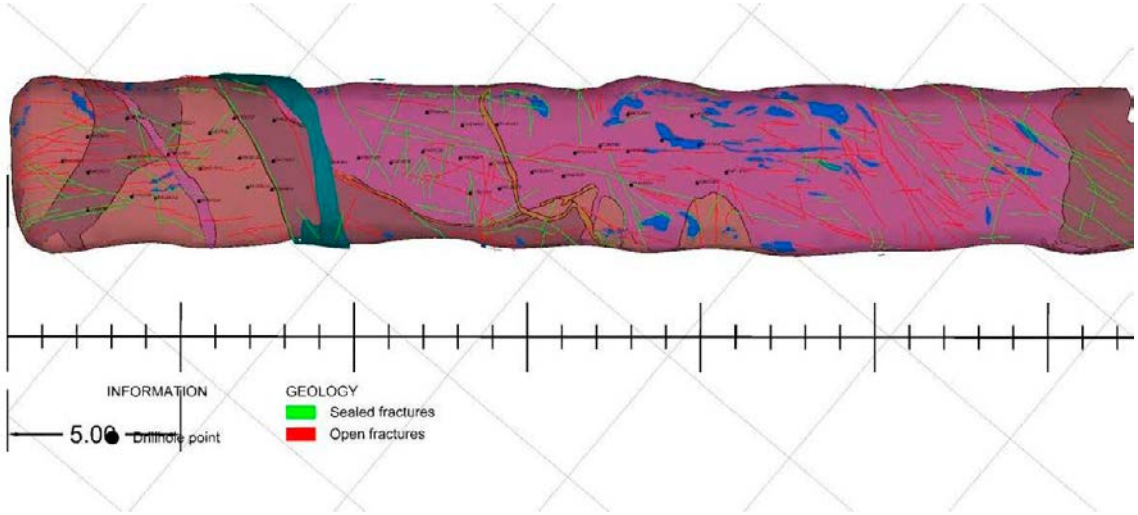

Figure 6-7. *Map of fractures and rock types in the floor of TAS04. The tunnel length from the centre of TASP is approximately 4.3–37.5 m. Boreholes are located between approximately 15 and 37.5 m. A deformation zone with orientation approximately 190/85 (strike is in magnetic North and dip is to the West) is lokated between approximately 28 m in the left wall and 31 m in the right wall and is shown as a green coloured band projected from the 3D mapping of the walls and roof of the tunnel. Sealed fractures = tight fractures and blue areas indicate smooth fracture surfaces.*

6.2.3 Fracture visualization

The mapped fractures from the floor of the TAS04 tunnel were then visualized in 3D from their manual strike and dip measurements. The results from fractures that come close to, or intersect, the boreholes in the floor are shown in Figure 6-8.

The density of mapped fractures, both open and tight, varies between rock types, see Table 6-3. The fractures belong to the rock type that includes most of their visible length. The fractures seem to intersect most rock contacts with two exceptions: no mapped fractures intersect the deformation zone and no open fractures intersect the thin pegmatite dyke between boreholes K04023G03 and K04023G02 on the one hand and K04023G01 on the other hand (see Figure 6-7 and Appendix 5).

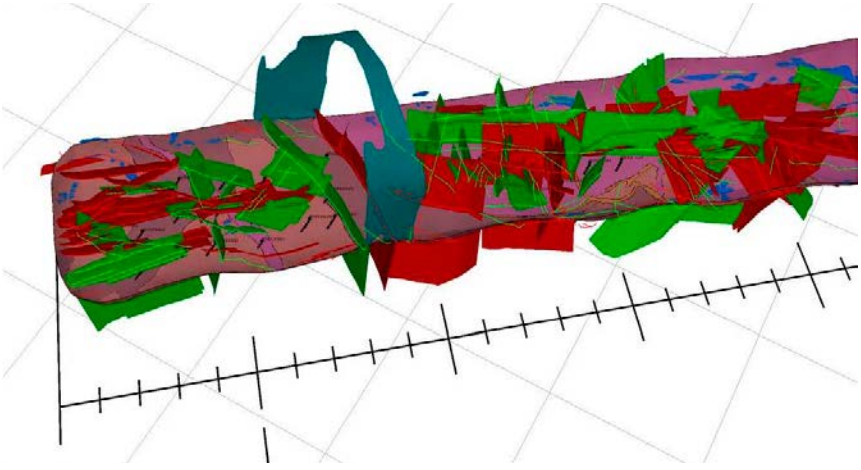

Figure 6-8. *A 3D map of mapped fractures, shear zone and rock types in the floor of the TAS04 tunnel from approximately 15 to 37.5 m is shown. Only the shear zone is shown from the tunnel mapping of the walls and roof of TAS04 here. The total tunnel length from the centre of the TASP tunnel is approximately 4.3–37.5 m. Boreholes are located between approximately 16 and 35 m. A deformation zone with orientation approximately 190/85 (strike is in magnetic North and dip is to the West) is located between approximately 28 m in the left wall and 31 m in the right wall and is shown as a green coloured band. Tight fractures are shown in green, open fractues in red and blue areas indicate smooth fracture surfaces.*

Table 6-3. Table showing the fracture distribution in the RoCS-mapped rock types on the floor of TAS04. The Rock ID is taken from the RoCS mapping of the floor in TAS04.

Rock type	Rock ID	Area (m^2)	Number of fractures	%	Fractures/m^2
511058 Fine-grained granite	B2	98	302	71	3.1
501037 Äspö diorite	B0	41.2	96	22	2.3
501056 Ävrö granodiorite	B1	33.5	29	7	0.9
501061 Pegmatite	B4	1.04			
501061 Pegmatite	B5	0.68			
511058 Fine-grained granite	B3	1.87			
Total		**176.32**	**427**	**100**	**2.4**

In general the fine-to-medium-grained granite is more brittle than both the Äspö diorite and Ävrö granodiorite. The granite often contains a large number of short chlorite-filled fractures that are usually tight (unbroken), but the surface activity of cleaning the tunnel floor several times caused considerable amounts of small broken-up rock pieces to loosen from the floor, see Figure 6-9.

Associating the modelled fractures from the RoCS mapping with the mapped fractures from the Boremap mapping is not simple for two reasons: one is the difference in mapping scale and the other the lack of orientation (strike) in the borehole mapping.

The difference in mapping scale is that in the RoCS mapping, the visible fracture traces need to be at least 1 m in length, while every visible fracture is mapped in the core. The Boremap-mapped fractures are not orientated because the boreholes were too short to be photographed with the BIPS system, so only a simple borehole camera was used. While this simple borehole camera is better than no image from the boreholes, it has limitations. It has one camera lens which faces down and one which faces to the side, allowing some orientation, but the camera is handheld and has a cable that measures depth in dm. The camera was in general held so that it filmed through the downward lens on the way down and through the side lens while going up, and the rod was held roughly so that the side lens faced the bottom of the tunnel (direction approximately 125 degrees). The orientation of the fractures in the cores is therefore limited to the angle of the fracture that intersects the core (the so-called alpha angle). In addition, it should be mentioned that if an attempt is made associate modelled fractures from the RoCS mapping with a nearby borehole, the orientation of the fracture is an average, measured with a compass in the field.

Figure 6-9. *Enlargement from an RoCS-mapping photograph from the floor of TAS04 at approximately 19 m showing the fractured fine-to-medium-grained granite with the broken-up smaller pieces (some are indicated by the white arrows). The red circle is the coordinate point G16, measured with total station as an orientation for the 3D model (coordinates in ÄSPÖ96: X: 2429,588, Y: 7351,559, Z: –409,107).*

Some of the modelled fractures are shown with probable counterparts in the boreholes in Appendix 6, using the photographs of the tunnel floor at each borehole site (Appendix 7), the core photographs (Appendix 8), the Boremap mapping (Appendix 4), the modelled RoCS mapping (Appendix 6 and the actual 3D-modell, see Figure 6-8) and to some extent the DVD films from the simple borehole camera.

6.3 Groundwater conditions

6.3.1 Hydraulic pressure in the area

The pressure of groundwater was monitored throughout the excavation period as a means to ensure that drawdown did not exceed the requirements for the excavation project. The requirement was to not cause a drawdown of hydraulic head exceeding 50 m, see Olofsson et al. (2014). The location of the observational borehole KA2050A is shown in Figure 6-10 and the drawdown due to excavations at the 410 m level within the Äspö expansion project is shown in Figure 6-11. The pressure head stabilized a couple of months after the construction works were completed at a far-field pressure head of 2,430 kPa.

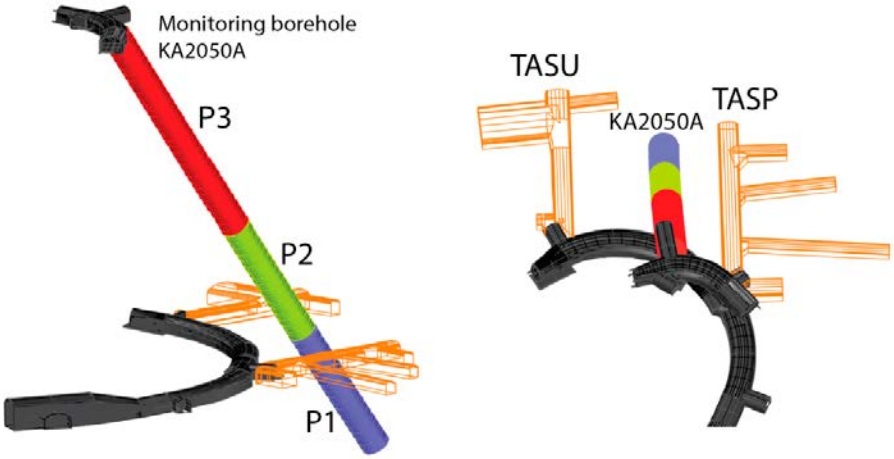

Figure 6-10. *Location of the borehole KA2050A. The borehole was drilled from the 350 m level and positioned between the TASU and TASP tunnels. The borehole had three packed-off sections for monitoring of groundwater pressure.*

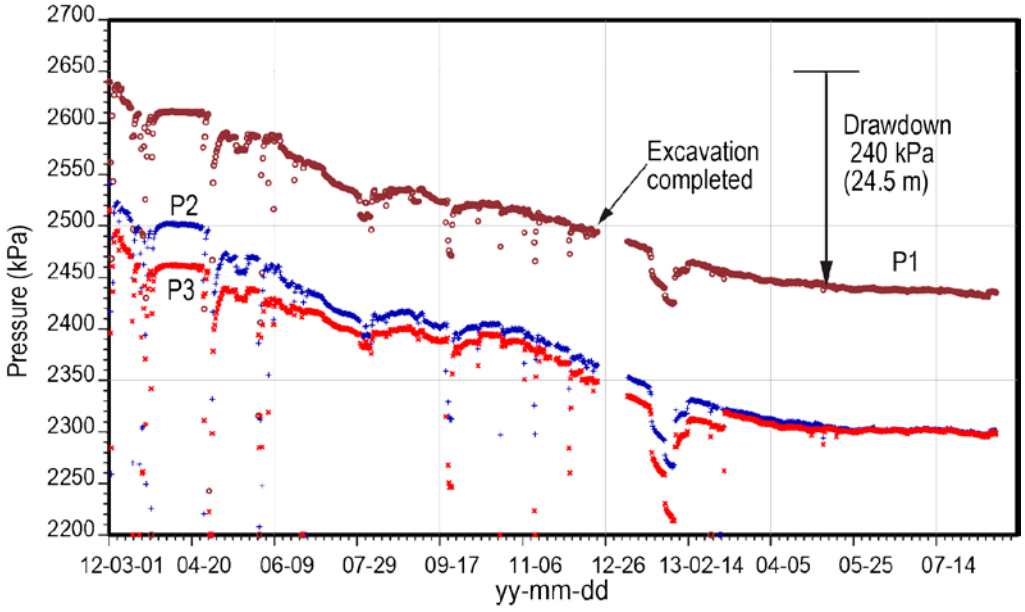

Figure 6-11. *Drawdown observations in KA2050A in the three piezometers P1 (brown), P2 (blue) and P3 (red). The drop in pressure at the end of 2012 is related to rock bolting after completion of the excavations.*

During the measurement period, a sub-horizontal borehole was drilled in a tunnel located 60 m from the test area in TAS04 tunnel. Drilling caused responses in some observation sections. Pressure responses in the observation sections were observed most clearly in some relatively tight boreholes with high in situ pore pressures (formation pressures). The observed pressure disturbances due to drilling were relatively small compared with the pressure responses from the injection tests and have a very limited impact on the evaluated steady-state results.

6.3.2 In situ pore pressures and kriging interpolation

In the evaluations of the injection tests, pore pressures (formation pressures) were calculated from the measured pressure before the injection phase, from the pulse tests before injection and from the recovery phase after injection. An analysis has been done using the formation pressure evaluated during the injection tests and creating a 3D kriging interpolation with this type of data. As the injection tests lasted from mid-November 2013 to mid-February 2014, the determinations were done at different times. The advantage of these estimates is that they have been done for all injection sections along the boreholes, i.e. even in the lower parts of the boreholes, which do not have such good hydraulic contact with the tunnel floor. The disadvantage is that the estimates may be uncertain, especially in sections with low transmissivities. The interpreted formation pressure distribution underneath the tunnel floor is shown in Figure 6-12, which shows different slices of the resulting kriging interpolation.

There are about 35 sections that have an estimated formation pressure equal to or higher than 100 kPa, relative to the atmospheric pressure in the current level, which is shown in Figure 6-13. In most of the holes, the formation pressure increases with depth. This increase is not uniform but intermittent, and one section near the tunnel front shows a lower formation pressure that continues with depth. If this is compared with the lithological map of the tunnel, this section can be seen to correspond to a deformation zone. The highest estimated pressure in a section is 865 kPa, which is not visible in the selected views. There are another 8 sections in which pressures are estimated to be equal to or higher than 250 kPa, relative to the atmospheric pressure.

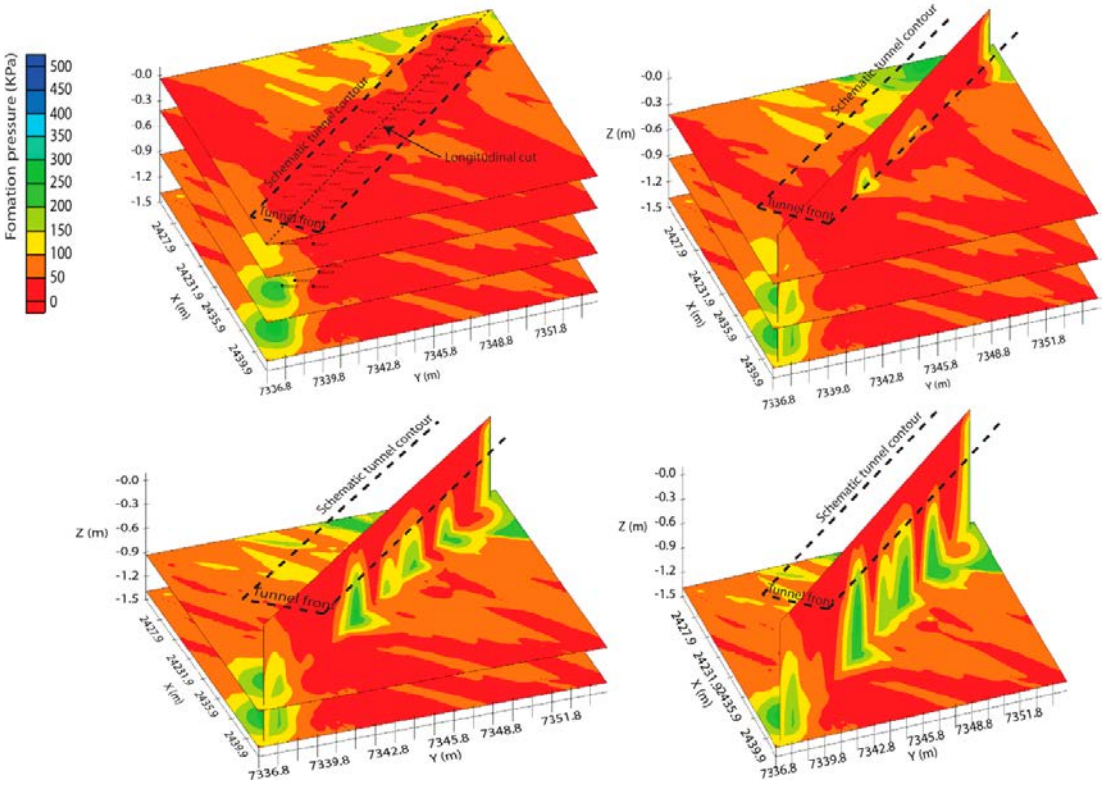

Figure 6-12. *3D kriging interpolation of the estimated formation pressure values obtained from the single-hole injection tests conducted at TAS04. Subfigures 1, 2, 3 and 4 shows the interpolated 3D volume composed of several horizontal slices. The tunnel boundaries and front are indicated in all figures. The legend shows the formation pressure in kPa.*

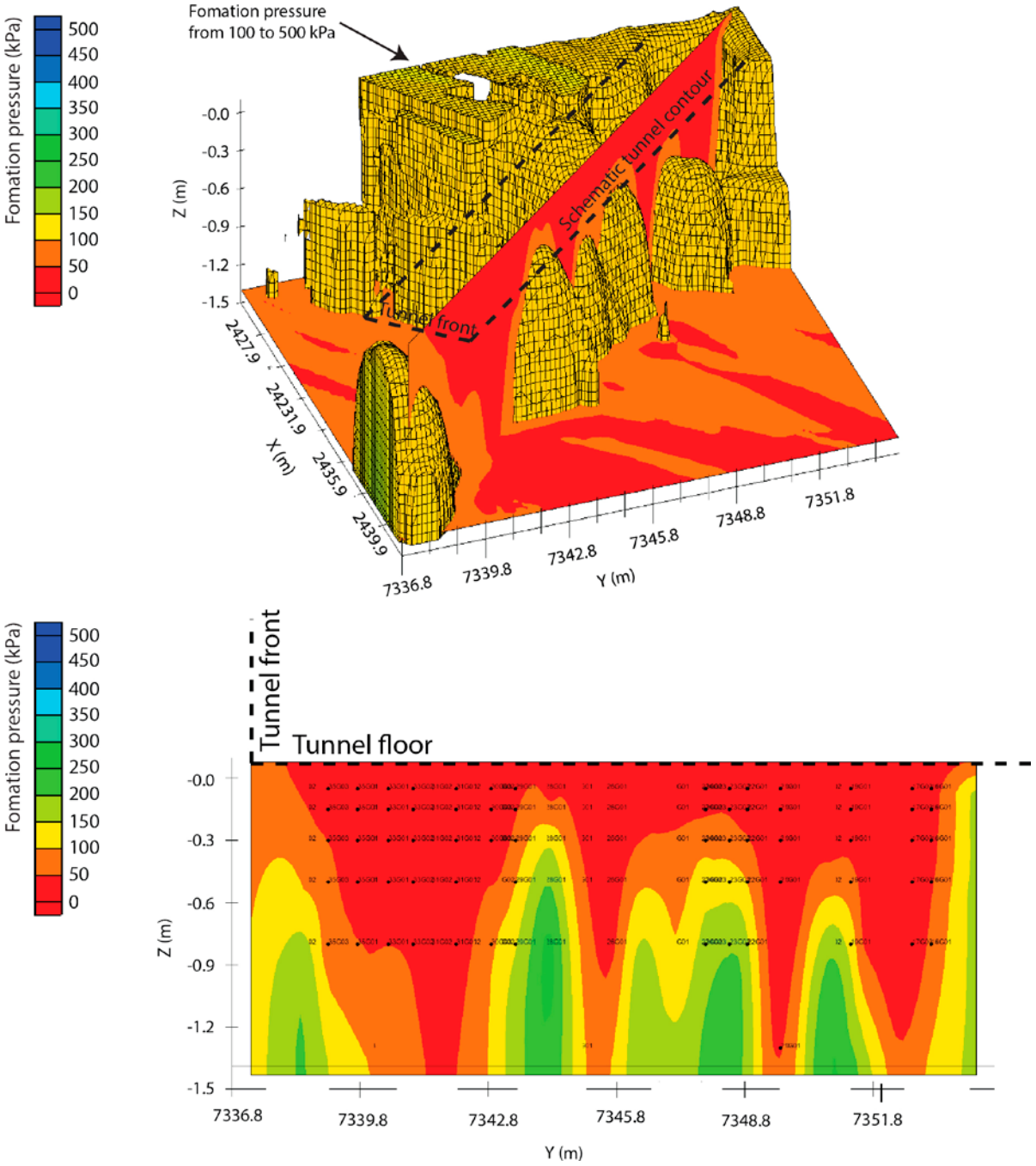

Figure 6-13. *View in perspective and longitudinal cut of the 3D kriging interpolation of the estimated formation pressure values obtained from the single-hole injection tests conducted at TAS04. The filled volume in the perspective view represents a pressure > 100 kPa. The legend shows the formation pressure in kPa.*

6.3.3 Groundwater inflow

The inflow to the investigation area can be divided into water coming from the roof, walls and floor and water coming out of the holes before the packers are installed. The total inflow to the 20 m long test section was collected by pumping in seven pump ponds, see Figure 6-14. The water levels in the ponds were kept constant and the pump flow from each pond could be calculated against time. The mean total inflow was 0.54 L/min as an average over three days.

A visible flow of water could be observed from 8 of the 42 boreholes in the floor before the packers were installed. The total inflow detected at the 7 pump locations in Figure 6-14 was reduced by 0.08 L/min after packer installation. It should be noted that no grouting was carried out in TAS04.

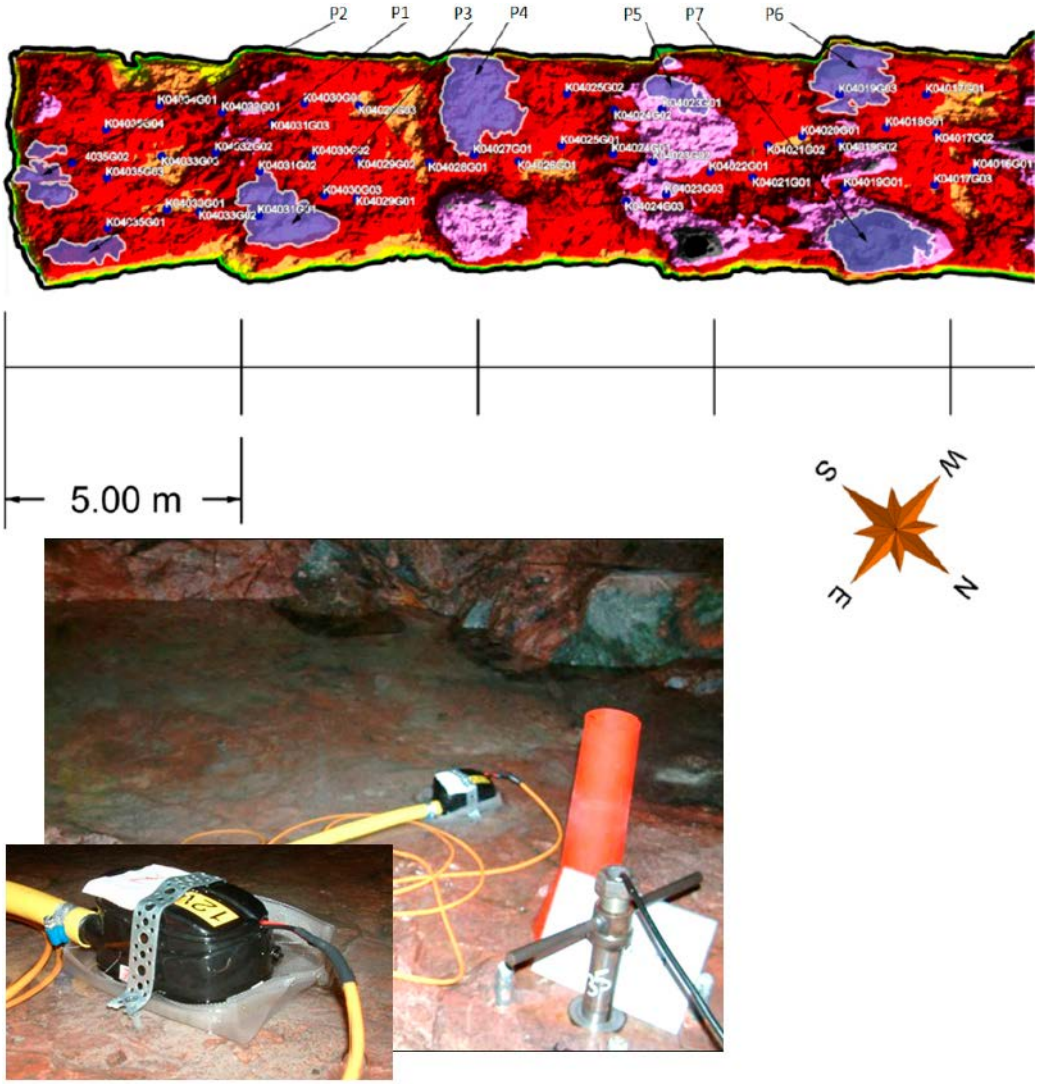

Figure 6-14. *Top: Location of depressions where ponds of water with free water table surfaces were created by the inflowing water. Small pumps were used to maintain a constant water table, permitting a precise reading to be obtained of the inflow to the test area.*

6.4 Rock mechanical conditions

6.4.1 Mechanical properties of rock

The bedrock at the Äspö HRL consists of diorite intersected by granitic and pegmatitic dykes. Typical mechanical properties for the investigation area are given in Table 6-4.

Table 6-4. Intact rock mechanical parameters derived from laboratory tests on core samples of Äspö diorite.

Parameter	Mean	Range
Uniaxial compressive strength [MPa]	211	187–244
Crack initiation stress [MPa]	121	80–160
Young's modulus [GPa]	76	69–79
Poisson's ratio	0.25	0.21–0.28
Indirect tensile strength [MPa]	14.9	12.9–15.9
Friction angle, intact rock [°]	49	
Cohesion, intact rock [MPa]	31	
Density [kg{m^3]	2,750	2,740–2,800

As mentioned above, the fracturing consists of three major sets: two steeply dipping sets oriented NW and NO and one gently dipping set. The NW trending set is the most dominant water-bearing fracture set on the Äspö HRL site.

6.4.2 State of stress

The in situ stress state is described by, among others, Christiansson and Jansson (2003). They tested three different methods for stress measurements in two orthogonal boreholes at the 450 m level. The major horizontal stress was estimated to be 24 ± 5 MPa, probably in the lower range at the 410 m level. The orientation of the major horizontal stress is NW–SE, nearly parallel to the dominant water-bearing fracture set and TAS04. Christiansson and Jansson (2003) reported the vertical component to be in the range of 15–20 MPa and the minor horizontal component to be close to the gravitational stress, 10–13 MPa. There are however other indications that the minor horizontal stress and the vertical component are quite similar, around 11–13 MPa at the 420–450 m level.

The expected stress conditions have been assessed using a simplified 2D elastic model with 10 MPa as the vertical and horizontal stress components perpendicular to the tunnel. Young's Modulus was assumed to be 55 MPa. The maximum stress on the boundary of the tunnel floor is roughly 9 MPa, and the maximum vertical displacement in the floor is estimated to be less than 1 mm. The response to tunnelling in the rock mass under the floor of the tunnel is probably just elastic. However, it is possible that natural or blast-induced fractures close beneath the central part of the floor might open up due to the small heave. The stress concentrations in the corners of the model are merely an artefact of the simplified tunnel geometry.

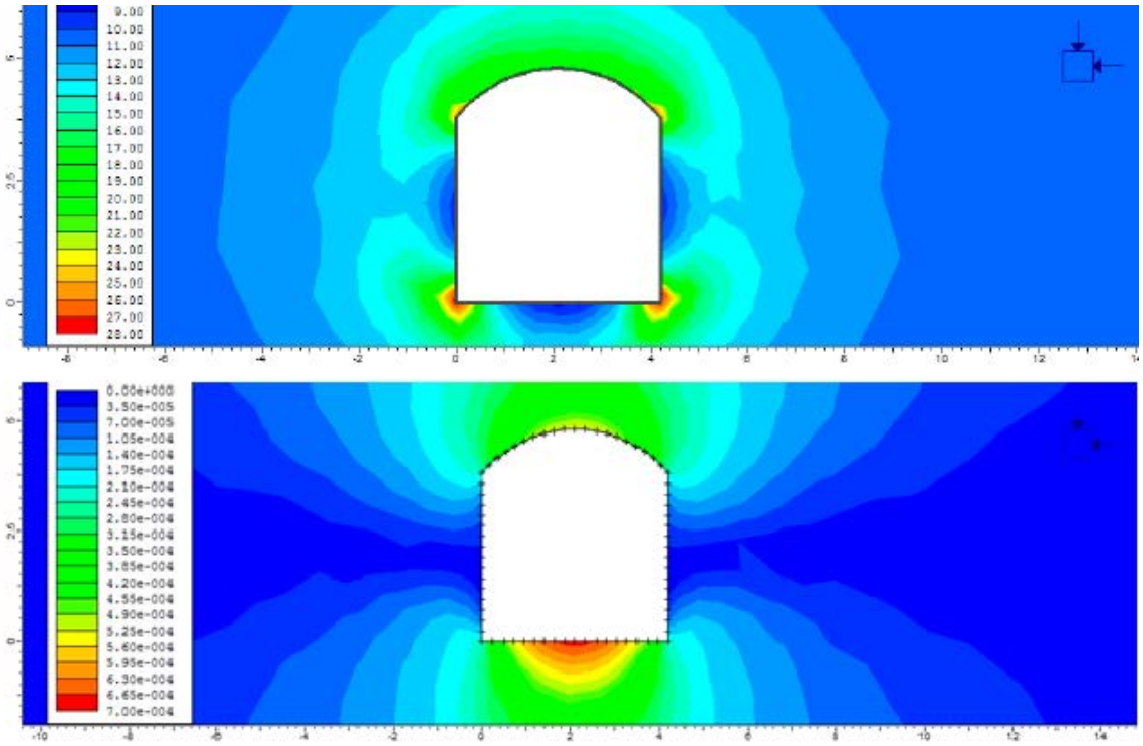

Figure 6-15. *Estimated stress concentration in MPa around the TAS04 tunnel (top) and vertical displacement in metres.*

7 Geophysical investigations

7.1 Methods

As a part of the quality control of the excavation works, Ground Penetrating Radar GPR measurements were conducted in TAS04. The tunnel floor is most important for the long-term performance of a future repository and was therefore the only surface that was investigated.

The GPR survey on the tunnel floor of TAS04 was performed using a high-frequency, shielded, ground-coupled 1.5 GHz bandwidth antennae. The equipment used was GSSI's (Geophysical Survey Systems, Inc.) SIR-3000 GPR system. The data was collected by positioning the antennae against the cleaned and dried tunnel floor and ensuring best possible contact. Recording of the data was triggered by a calibrated line encoder with 1 cm point interval. The measurement was performed in lines parallel to the tunnel with an increment of 10 cm covering the whole width of the tunnel. The antennae were positioned on measurement lines using a laser liner, which ensures correct lateral positioning. The tunnel was measured in two parts at two different times. The first part covered the tunnel lengths 7–21 m (width 4.0 m) and was performed before drilling of the holes for hydraulic measurements. This first measurement consisted of 41 parallel lines. The second part, which was performed after drilling of the holes, covered the tunnel lengths 21–36 m (end of tunnel) and consisted of 39 parallel lines (width 3.8 m), see Figure 7-1 and Figure 7-2

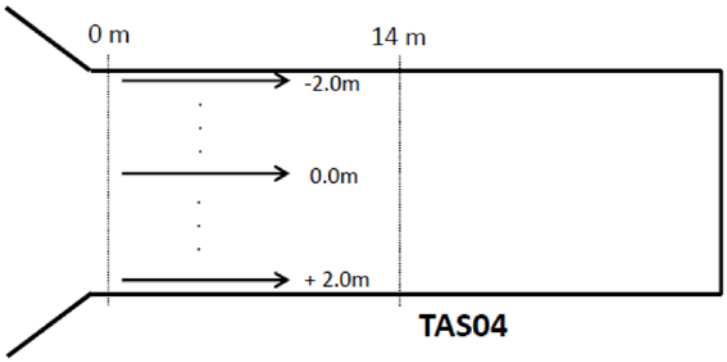

Figure 7-1. *Layout of the GPR survey. Part 1 covered tunnel lengths 7–21 m and part 2 the rest of the tunnel. The line increment was 10 cm resulting in 41 and 39 lines, respectively.*

Figure 7-2. *GPR measurements at the TAS04 tunnel floor.*

The GPR method is based on electromagnetic wave field reflections. In operation, the GPR antenna transmits an electromagnetic pulse which is affected by the electrical properties of the media. The signal penetrates, reflects or bends from electrical boundaries. When reflected, the signal comes back to the antenna and a GPR image is formed. With the high radar frequency used, strong signal attenuation limits depth penetration, which under these conditions is max. 1 m.

The effect of excavation on the rock mass is studied by GPR image analysis. Images may display single cracks and fractured areas. Many of the fractures are small in size and not in a favourable direction to be detected by GPR as interpretable reflection or diffraction. In a GPR image (radargram), the reflections are caused by contrast in the material properties, e.g. conductivity and dielectric permittivity. In fractures these properties include water content, clay content, and content of electrically conductive minerals such as pyrite, pyrrhotite and graphite. The zone of influence around a fracture (conjugate or splay cracks) will also contribute to the results. All reflections are not necessarily caused by fractures, and any discontinuity where there is a contrast in electrical properties could cause a reflection. Lithological contacts and foliation are examples of such discontinuities. Thus, fresh fractures with small hydraulic aperture may occasionally be difficult to detect with GPR due to low contrast in electrical properties.

Interpretation of distinct reflectors from each measurement line was done by selecting reflectors that could be followed in more than 4 parallel lines. This gives a 30 cm "cut-off". No migration was done before selection and no geometry correction for the selected reflectors was done, which means that the locations and slopes of the reflectors are not corrected for, but must be considered as apparent. For reflectors close to horizontal these errors are not significant, but for more inclined ones the errors are larger and must be considered when performing integrated analysis with other results. An average value for wave velocity was used (dielectric permittivity 6 gives a velocity of 0.12 m/ns), providing a good estimate of depth for reflectors with few percentage errors. Reflector interpretation was done for the tunnel section where boreholes were drilled, range 15–36 m.

Excavation also has an effect on the rock material at the granular level, and loosening of the grain boundaries caused by excavation has been noted. These defects cannot be seen in the GPR images directly as anomalies, reflectors or diffractions. Information on these features is conveyed by GPR frequency content.

The increase in porosity of the rock at the tunnel surfaces due to increased number of fractures and loosening of grain boundaries reduces electrical resistivity, which affects the GPR signal. At high GPR frequencies the resistivity is highly dispersive (depending on the frequency), i.e. when resistivity decreases, attenuation increases more at higher frequencies than at lower frequencies. This fact is used when investigating the EDZ using GPR by computing the GPR EDZ frequency response for a finite block in a moving window. The response is integrated from the amplitude spectrum at a selected frequency range (Kantia et al. 2010). The selected frequency range determines the resolution and depth in the GPR EDZ response. In this case a broad window of 1,500–5,000 MHz was selected in order to get responses from both the mineral grain level and larger fractures, but also to ensure an adequate depth range. This result is affected by all discontinuities where the electrical properties differ and does not distinguish between natural and mechanical features, but can be used to evaluate whether there are an increased number of anomalies in some parts compared with unaltered rock, which would indicate the extent of the EDZ.

The GPR EDZ data can be displayed as profiles (vertical sections) indicating EDZ depth variation along the line (Figure 7-3). For presentations it is necessary to limit the GPR EDZ response with a threshold value. A statistical approach ~~is~~ can be used to determine this value by calculating e.g. median + standard deviation ~~utilizing~~ from data collected previously at the site or the threshold value can be derived utilizing reference information. The statistical approach requires lot of measurements using same antennae and settings in same conditions and geological environment in order to become applicable. In this case the threshold value was selected using results from borehole mapping and from hydraulic measurements to get a best fit with observed features. The threshold value of 100 gave the best fit with the reference information, and this value was used in the final presentation. By combining all the results from several lines, a topographical map can be produced where different colours indicate different depth ranges for the calculated GPR EDZ response. This allows the areas of a potential EDZ to be extracted from the GPR data, see Figure 7-4.

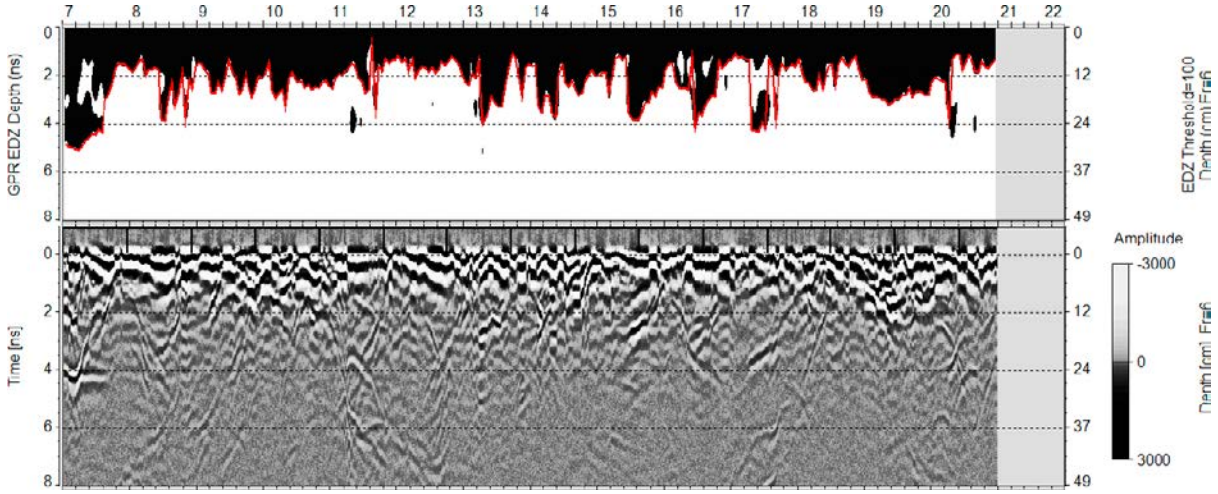

Figure 7-3. *A 2D GPR EDZ output on top of original GPR data, profile measured at the centre line in TAS04 range 7–21 m.*

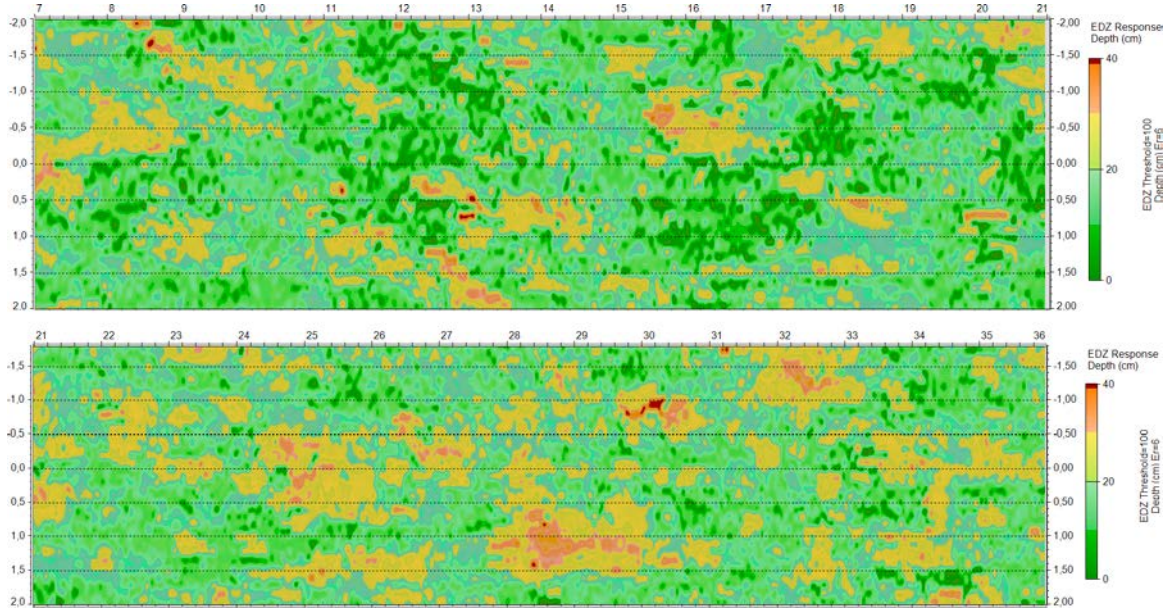

Figure 7-4. *GPR EDZ response output from TAS04 as topographical maps. The upper figure presents the results from range 7–21 m and the lower figure from range 21–36 m.*

7.2 Results

Generally, the GPR EDZ data collected from TAS04 is of good quality, not only in terms of the EDZ analysis but also with respect to the GPR images. The resistive rock is optimal for GPR analysis due to relatively low attenuation. Cracks and fractured areas can be spotted as far as 1 m below the surface. The GPR EDZ method outputs reveal areas where the EDZ penetrates deeper than on average. These areas provide valuable information in evaluation of excavation quality and general rock damage level. Interpreted distinct reflectors also provide an indication of EDZ formation close to the tunnel surface, as well as the presence on larger structures, whether natural or excavation-induced.

Figure 7-5 shows results from the GPR EDZ response calculation made using RoadDoctor software as a topographical map together with interpreted reflectors seen as shadows under the coloured map. The reflectors are not planar, are located at different depths and are inclined. In many locations there are also reflectors on top of each other (see 3D view in Figure 7-6). The map shows good correlation between areas where the depth extent of the GPR EDZ response is greater and where there are interpreted reflectors.

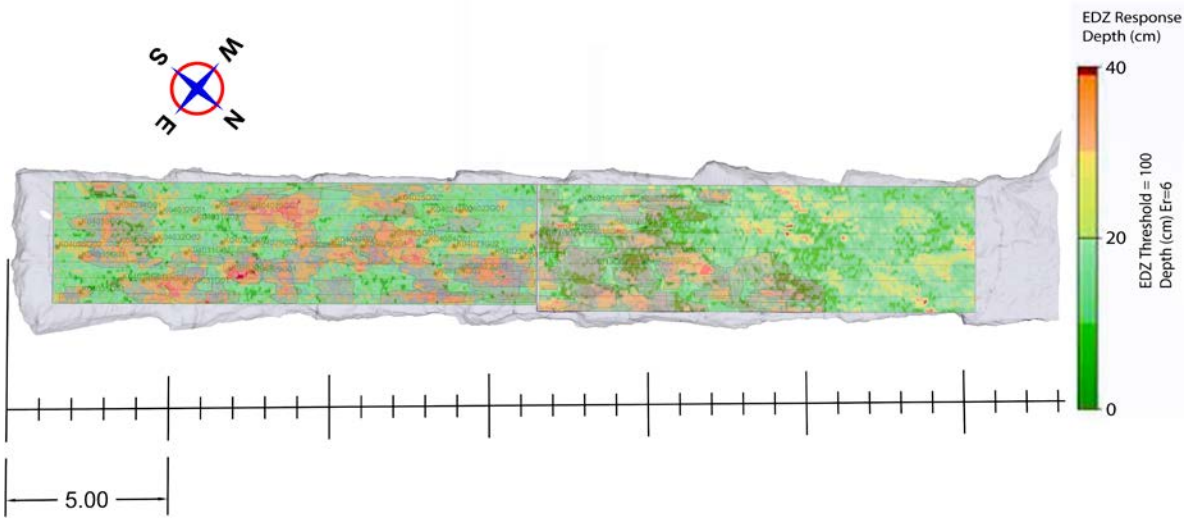

Figure 7-5. *GPR EDZ response output from TAS04 as topographical map shown at real locations in the tunnel. The colour scale is the same as in Figure 7-4 Interpreted reflectors are shown as brown "shadows" in a plan view.*

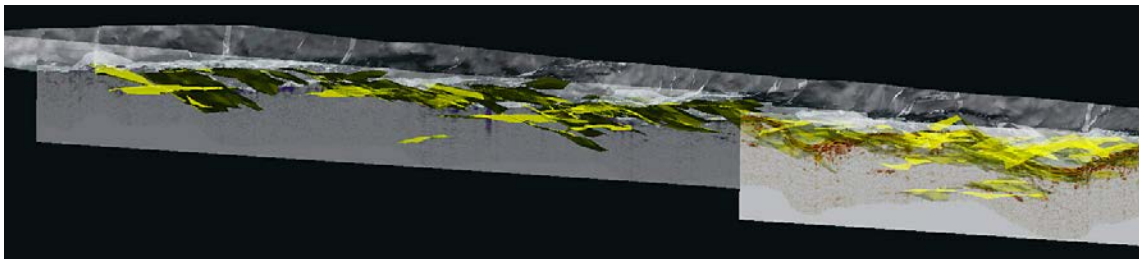

Figure 7-6. *A 3D view of interpreted reflectors. In the background are the outermost radar profiles.*

From the 3D model (partly shown in Figure 7-6), where all results in this study are included, it is possible to determine the orientation (strike and apparent dip) of the reflectors, and the results can also be used to study reflector length variation or reflector density variation (see below). The full 3D model is shown in Appendix 2. The model shows that most of the interpreted reflectors are sub-horizontal, and the apparent dip varies from 0 to a maximum of approximately 40 degrees in some cases. The GPR method has limitations in detecting fractures in a larger angle (45–60 degrees) to the surface where the measurements are carried out.

The total number of interpreted reflectors is 130. The horizontal length of the reflectors varies between 0.1 and 3.8 m in the direction parallel to the tunnel and between 0.1 and 2.0 m in the perpendicular direction. Reflector lengths shorter than the "cut-off" of 0.3 m are explained by the fact that in some cases a reflector is selected if it is visible in one direction, but only in a limited range in the other direction. For example, some reflectors that are visible in the outermost measurement lines are long along the line but not visible in many parallel lines. This could mean that the reflector ends and continues outside the tunnel. The distribution of maximum horizontal lengths for each reflector along and across the tunnel is shown in Figure 7-7. The average reflector length horizontally along the tunnel is 0.91 m and across the tunnel 0.61 m.

Figure 7-8 shows the number of 1 m long reflectors and the tunnel width section for every 1 m tunnel interval. The first part of the tunnel is dominated by fine-grained granite (up to tunnel length ~ 26 m), which is more brittle than Äspö diorite or Ävrö granodiorite. This is also visible in the figure with a higher reflector frequency in the first part of the tunnel. One exception is the tunnel length interval 21–24 m, where the reflector frequency is lowest, even though a round end occurs in that interval. Otherwise the round ends show a larger number of reflectors than other areas. The low number at the end of the tunnel is due to the fact that the lines ended 0.5 m before the tunnel face, leaving most of the end outside (bottom charge location) of the last round.

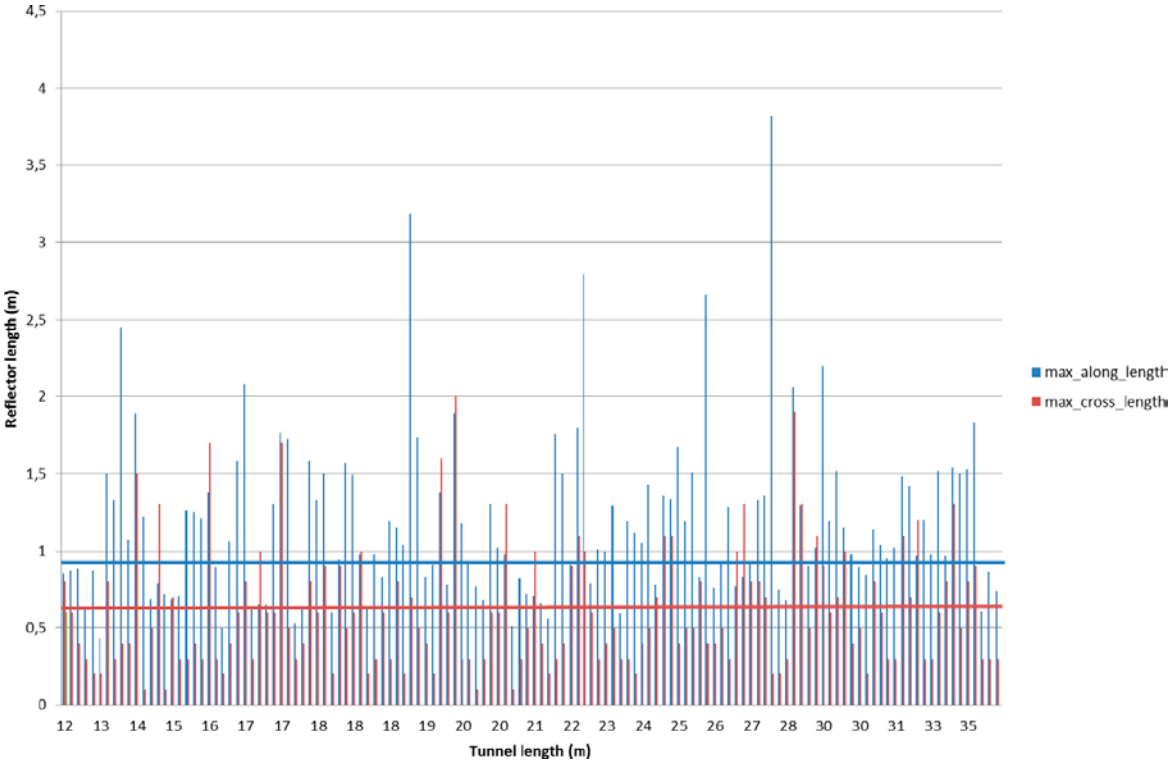

Figure 7-7. *Distribution of maximum horizontal lengths for each reflector along and across the tunnel. The horizontal lines show the mean horizontal lengths in the different directions.*

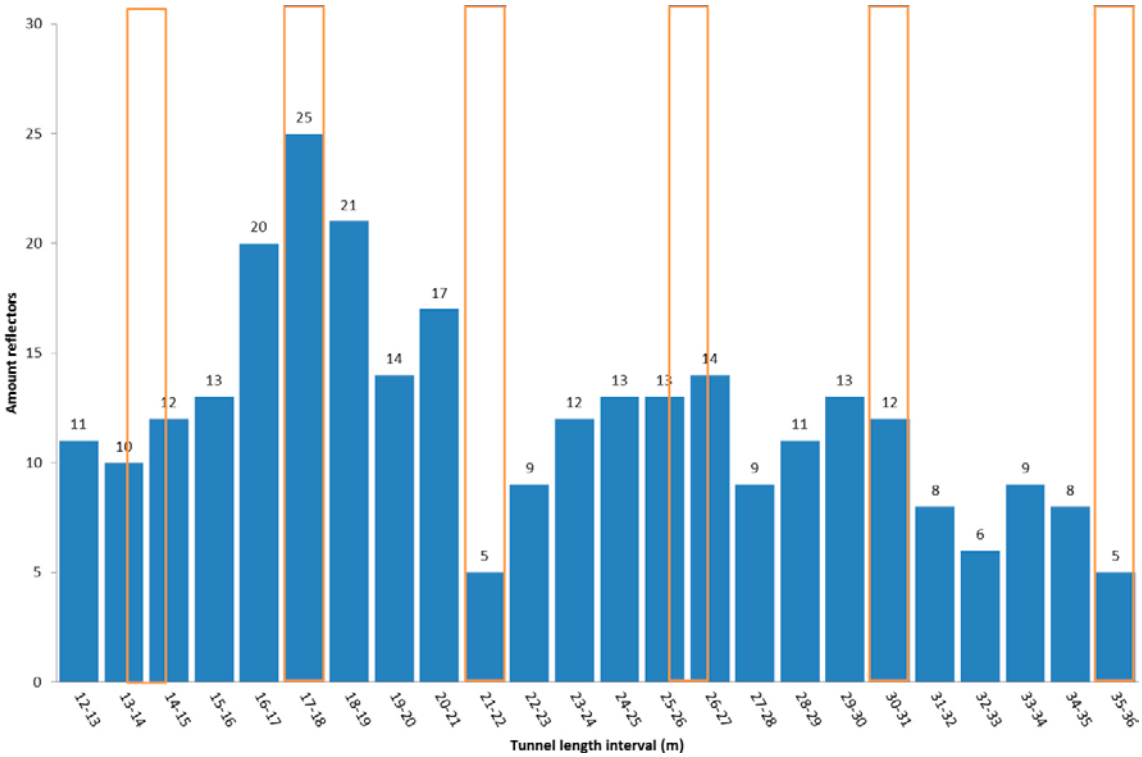

Figure 7-8. *Number of 1 m long reflectors and the tunnel width section for every 1 m tunnel interval. Yellow rectangles indicate locations of the round ends.*

In this study, depth penetration is almost 1 m at best using GPR, with a variation between 0.6 and 1 m, and the resolution (vertical) is around 6 cm. Usually, the first wavelength is masked by the direct wave and surface reflections, which means that results down to a range of 0.06–0.08 m cannot be reliably interpreted. Detectability (how small structures can theoretically be detected) is calculated from the wavelength as a function of depth. In this study, detectability varies between 6 and 30 cm (depth range 0.05–1 m), which means that in the deeper parts of the studied object a feature has to be at least 30 cm in diameter in order to be detected as a reflector, if the electrical contrast is great enough and the orientation of the structure is favourable for reflection.

The depth determination for reflectors is based on the radar wave velocity (travel time) in the media, which is governed by its dielectric properties. The average value of wave velocity that was used (0.12 m/ns) gives a good estimate of depth for reflectors with few percentage errors. Another source of error is the true location of inclined reflectors. In the case of inclined structures, the reflection from each source point comes from the direction normal to the structure. This means that the true location and inclination of inclined reflectors are not correct. The error is greater for more inclined reflectors.

One issue that must be kept in mind when looking at the radar results is the fact that there were holes drilled in the floor when the second part of the tunnel was measured. This gives always a GPR anomaly at the location of each hole, which may lead to false interpretations. Furthermore, when the measurements were performed the antennae had to be lifted a few centimetres up from the surface at each hole, which means that at those locations the reflector depths are not correct. This also causes ringing in the signal (signal bounces between rock surface and antennae) which results in errors in the data. This can be seen in Figure 7-5, where the GPR EDZ topography map indicates a deeper response at each borehole location at tunnel chainage 21–36 m. These false anomalies in the data were taken into account and treated as artefacts in the reflector interpretations and in the analyses of the GPR EDZ results.

It can also be noted that the GPR EDZ response topographical maps for the different tunnel sections (see, Figure 7-4) differ slightly from each other (the mean value for chainage 7–21 is 15 cm and for chainage 21–36 m 17.5 cm). This is partly due to different conditions during the measurements. The tunnel floor was probably more saturated during measurements in the second part of tunnel, which is evident in the results.

8 Hydraulic tests

As stated in the background to this EDZ project, the hydraulic testing has focused on transmissivity and flow connectivity in the context of characterization, without considering specific flow modelling issues. Since the assessment of long-term safety is based on saturated conditions, the testing and analysis methods do not include unsaturated situations, even though the tunnels and niches are open and in atmospheric contact.

In the development of an appropriate hydraulic test method, several aspects have been considered, e.g. choice of test location, equipment robustness, equipment mobility, measurement resolution, initial and boundary conditions of testing, confinement, hydro-mechanical couplings and test durations.

Furthermore, for the evaluation and interpretation of test responses in terms of flow and pressure changes, it has been essential to consider boundary conditions, heterogeneity, anisotropy (hydraulic and structural), spatial variability and scale dependence. Different practical aspects and their implications for test analysis are highlighted in Appendix 9.

8.1 Evaluation methods

Groundwater flows in hard rock through a network of fractures, whose ability to conduct water is dependent on their aperture variability and connectivity. Fracture flow often exhibits considerable variation, and proper evaluation of the hydraulic properties of the rock is not an easy task. In practice, simplified calculation formulas are used in many test evaluation methods. These formulas are usually based on the assumption that the rock constitutes a homogeneous and isotropic continuum on the scale of the measurement, where scale is associated with the length of the test section L_i [m]. As the assumptions of homogeneity and isotropy are never fulfilled in hard rock and the scale of the measurement is dependent on test duration and boundary conditions, the evaluated value of the transmissivity of the test section is only an equivalent value, T_{eq} [m^2/s], based on a formula. For the same reason, the ratio T_{eq}/L_i is only a way to calculate an equivalent hydraulic conductivity of the same test section, K_{eq} [m/s]. It is important to note that in the case of sequential adjacent test sections in the same borehole where $L = \Sigma L_i$ we often find that:

$$T_{eq,L} \cong \sum_{i=1}^{n} T_{eq,i}$$

whereas

$$K_{eq,L} < \sum_{i=1}^{n} K_{eq,i}$$

because

$$\left(\sum_{i=1}^{n} T_{eq,i} \right) / \sum_{i=1}^{n} L_i < \left(\sum_{i=1}^{n} T_{eq,i} / L_i \right)$$

Hydraulic conductivity is a point property. The sum of point properties is trivially larger than any average of these point properties.

In this study it has not been possible to determine the transmissivity of single fractures beneath the tunnel floor in the depth range of a potential EDZ. Therefore, the study has focused on measuring flow in short vertical boreholes, which in turn are divided into several shorter test sections by means of packers. Different hydraulic evaluation methods have been used in the study. In the interest of a better understanding of the methodology used and the results obtained, the following is noted:

- An approximate value of the test section's conductivity can be derived from the specific hydraulic capacity $Q/\Delta h_p$ (m^3/s/m), where Q (m^3/s) is the flow rate and h_p is the pressure head (m).

- Transmissivity data in this report are assumed to represent the hydraulic conditions of the rock adjacent to the each test section. (In more traditional cases the evaluation methodology usually considers the whole sequence of water-bearing strata surrounding the test.).
- Hydraulic conductivity values, when used in this report, should be considered as equivalent porous medium values for the fractured medium. The section-specific hydraulic conductivity values are based on the test section transmissivity determinations divided by the test section length.

8.1.1 Steady-state hydraulic tests

In order to ensure saturated conditions near the tunnel floor, a positive hydraulic boundary condition was maintained at the floor by means of a constant water level above or close to the tunnel floor and with the aid of pumps in the ponds. The injection or packer tests that have been used in this project were performed in uncased short boreholes in order to permit interpretation of a section transmissivity of individual layers by isolating them with the aid of packers. Even though the concept can be disputed, the method is widely used for approximately estimating the hydraulic characteristics of fractured rock (see e.g. Singhal and Gupta 1999 or Gustafson 2012).

In injection tests, the measured variables – flow, Q, and pressure head change, Δh – are considered to be representative of an overall magnitude that applies to the immediate surroundings of the borehole. If Q and Δh are constant over time, steady-state conditions prevail. In the international literature there are several derivations for determining hydraulic conductivity or section transmissivity according to injection tests. Different conceptual models suggest different equations. Conventional evaluation methods assume that the length of the test section, L, is great compared with the diameter of the borehole, $2 \cdot r_w$, and that the flow conditions in the vicinity of the borehole are two-dimensional, i.e. cylindrical.

Due to the existence of positive boundary conditions as well as the very short packer intervals (slimness in project r_w/L varies from 0.027 to 0.38), a sensitivity analysis was carried out in order to suggest a suitable determination method for the steady-state injection tests (see Appendix 10). It was concluded from the analysis that the specific capacity, S_c, where $S_c = Q/\Delta h_p$, provides a conservative approach for the section transmissivity values, i.e. $Q/\Delta h_p > T$, considering all treated concepts. If a positive boundary condition is involved in the determination of section transmissivities (denominated T_{LOE} in the sensitivity analysis), comparatively lower values will be obtained in relation to Moye's formula (Moye 1967). Moye's formula actually assumes $r_w/L < 0.019$ in order to take into account radial flow at the borehole wall and a spherical pressure head boundary at a distance of $r = L/2$.

In order to treat boundary condition uncertainties, the section transmissivities from the injection tests have mainly been evaluated using Moye's formula, see Equation 8-1:

$$T_{Moye} = \frac{1}{2\pi}\left(1+\ln\frac{L}{2r_w}\right)\frac{Q}{\Delta h} \qquad \text{Equation 8-1}$$

where:

L = Length of test section [m]

Q = Injection flow rate at the end of the test period (shut-in) [m^3/s]

Δh = Pressure head change [m]

r_w = Radius of borehole [m]

Tunnel floors are more or less damaged, depending on the excavation method used. Some zones such as those where bottom charges have been used are expected to have a high fracture frequency, while in other zones, such as those where column charges have been used, only single existing fractures may occur. The number of conductive fractures affects the interpretation results with respect to the boundary conditions as well as the sealed-off test lengths (Sven Follin, personal communication, December 2014). Another simplified sensitivity analysis has therefore been carried out (see Appendix 32) to study how testing interval length affects the interpretation of section transmissivity, T_{Moye} and hydraulic conductivity. Since the test section length in the interpretations is an indirect measure of the boundary condition in the equations used in our evaluation, and if only single fractures are tested, section transmissivities in relative terms may be overestimated by a factor of about 3 and hydraulic conductivities may be underestimated by a factor of about 3, if the test section length is changed from 0.1 m to 1.0 m. This is an essential aspect to be aware of when comparing the results of transmissivity interpretations and hydraulic conductivity estimates.

8.1.2 Transient hydraulic tests and interference (cross-hole) tests

The transient evaluations have been done using the software Aqtesolv V4.50.002, which contains a library of different evaluation models. The tests were carried out in fractured rock, but the models regard the rock as an equivalent porous medium. This means, for example, that the injected flow is assumed to be distributed uniformly in all directions from the injection section (space filling). This assumption is, however, rarely fulfilled in fractured hard rock.

The transient evaluations of the injection tests have been done both for selected injection sections and observation sections. For the injection sections, separate evaluations have first been done of the injection and recovery periods, assuming constant head change, Δh, in the injection section. The evaluation of the injection period is based on the ratio $dh/Q(t)$ where $Q(t)$ is the measured flow rate with time (t), while the evaluation of the recovery period is based on the measured pressure recovery after the end of the injection phase.

Subsequently, transient evaluations were done of the entire pressure sequence including both injection period and recovery period, with the measured varying flow rate as an inner boundary condition. The estimation of the storage coefficient has been based on the 3D (spherical) distance between the midpoints of the injection and observation sections.

In the transient evaluation of the responses the skin factor was assumed to be zero, both for the injection sections and for the observation sections. The corresponding storage coefficient in the injection and observation sections was estimated based on this assumption. Wellbore storage, WBS, is treated in Aqtesolv as the initial source of water discharged from a well with a finite diameter that was stored in the well casing. The wellbore storage coefficient, C, is calculated as $C = \pi\, r(c)^2/\rho\, g$ in $[m^3/Pa]$ units, where the radius, r(c), is treated as the radius of a fictive standpipe connected to the test section. For further information about WBS, see Appendix 11.

As stated above, many tests in the tunnel floor may quite possibly have been affected by a leakage point at some distance from the seal of the borehole extender or from the uppermost parts of the seal sections of the packer. A numerical modelling approach was therefore used for a sensitivity analysis, see Appendix 12. The numerical modelling approach treated transient conditions. The simulations with the alternative model have been done in an exploratory manner and should be seen as examples of more advanced analysis for cases with significant floor leakage. It was concluded that given the amount of additional evaluation effort required, the transmissivity evaluation according to Moye's equation could still be accepted as a robust measure. These examples with alternative interpretations could, at this point, instead serve to illustrate some pitfalls in interpretation of test results.

8.1.3 Connectivity along the tunnel floor

Different evaluation activities have been carried out to determine hydraulic connectivity along the tunnel floor or beneath the floor, see Figure 8-1. The pressure responses from the injection tests were analyzed in qualitative ways. Another option for interpreting connectivity conditions has been to assess the variability of the specific capacities or section transmissivities along the tunnel floor.

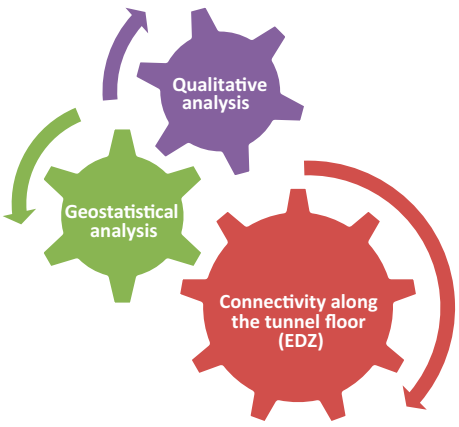

Figure 8-1. *Approach used to evaluate connectivity along or beneath the tunnel floor (EDZ).*

This has been done by means of semi-variogram analysis and kriging. The kriging has been carried out in 2D for each test interval. Furthermore, depth dependence between different layers in the floor has been assessed according to specific capacity values.

8.2 Hydraulic test set-up

The equipment for the hydraulic tests was designed to perform measurements in short holes drilled in tunnels. The equipment was developed to meet the following specifications:

- it must be capable of measuring transmissivities between $5 \cdot 10^{-10}$ and $5 \cdot 10^{-7}$ m^2/s at an assumed pressure disturbance of 500 kPa,measurements along the drilled holes must be made from the borehole opening (tunnel floor),
- it must be possible to display numeric values and produce simple graphs with selected parameters versus time,
- a measurement must include both an injection and a recovery phase, and
- the measurements will be evaluated mainly by stationary methods, but some tests may be evaluated in transient mode.

The equipment used was developed and tested at Geosigma's workshop in Uppsala and field-tested at the Äspö HRL at a depth of around 355 m. Additional specifications are presented in Appendix 14.

8.2.1 Equipment

The injection test equipment consists of:

- a data collection and control system mounted on a carriage,
- packer systems for an active hole and an observation hole, and
- a borehole extender permitting sectional hydraulic tests directly from the rock surface.

The data acquisition and control system is connected to the packers via hydraulic tubes. The measurement principle is based on the fact that a pressure tank with water is pressurized to a predetermined pressure using nitrogen gas. The water flow is measured by an accurate mass flow meter. Flow rates can be measured in two different flow directions, but pressure regulation works only for injection tests. The pressure in the borehole sections is measured by pressure sensors connected to the measuring sections by a separate tube. This tube is also used to vent the injection sections and hydraulic tubes, see Figure 8-2 and Figure 8-3.

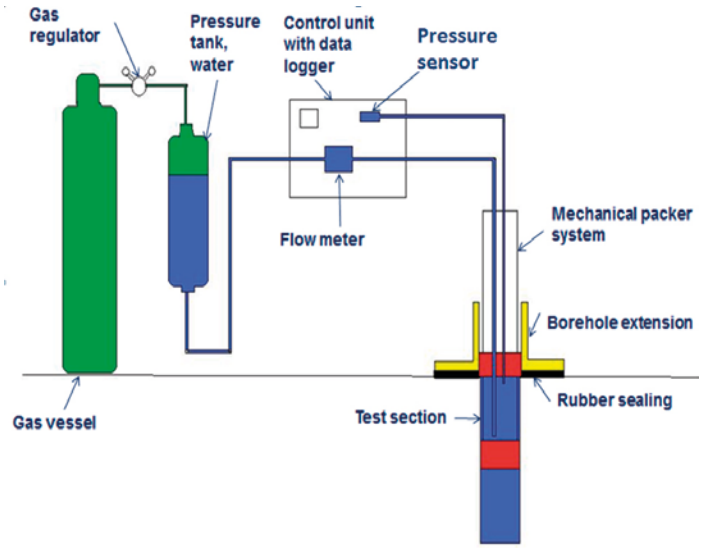

Figure 8-2. *Schematic illustration of the measuring equipment.*

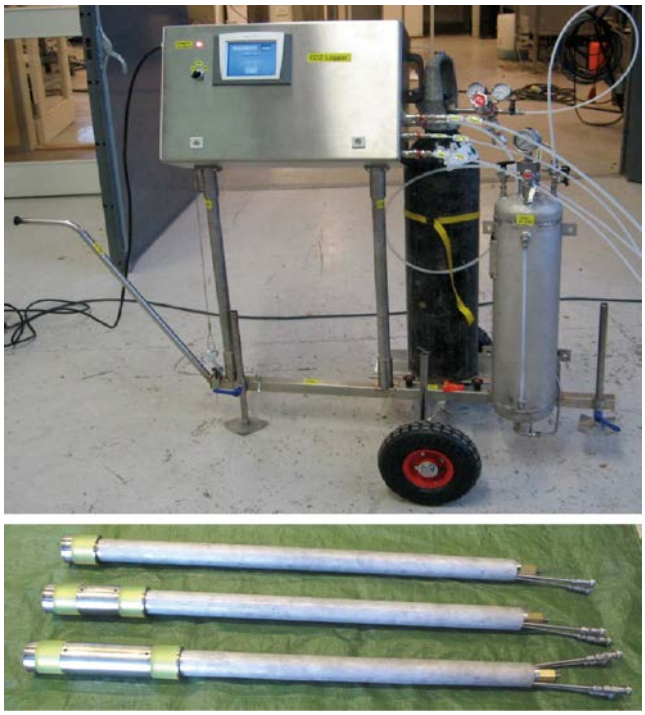

Figure 8-3. *Control unit, pressure tank and gas vessel mounted on a transport carriage (upper picture). Packer system for section lengths 10 and 20 cm and for single-hole packer measurements (lower picture).*

The instrumentation cabinet consists of:

- PLC with touch screen,
- data logger with exchangeable memory card for data storage,
- flow sensor (range: 1 to 1,800 mL/min),
- three pressure sensors (active section, observation section, pressure tank),
- pressure sensor for air pressure (range 0 to 6,000 kPa), and
- temperature sensor for surrounding air.

All pressure sensors in the boreholes are mounted in the instrumentation cabinet and connected to the packers by tubes with quick connectors. During the injection tests two types of mechanical packers were used, where the sealing length of the packers is 50 mm:

- a double packer system with a section length of 10 cm, and
- a double packer system with a section length of 20 cm, which also could be used for a single packer test to the borehole bottom without taking the system out of the hole.

For measurements from the top of the hole a special borehole extender has been developed and mounted above every tested hole. To obtain a good seal against the rock, the area around hole was flattened and smoothed to a diameter of 300 mm. A rubber seal was inserted between the flattened surface of the rock and the extender, see Figure 8-4. A more detailed account of the equipment and the specifications is provided in Appendix 14.

The range of the flow meter is estimated to be between 1 and 1,800 mL/min), where different packer intervals and different injection pressures will entail different lower and upper limits for the transmissivity evaluations. The range of the section transmissivities according to Moye's formula is estimated to be between $1.4 \cdot 10^{-10}$ and $3.7 \cdot 10^{-6}$ m^2/s. More information regarding resolution and measurement limits is presented in Appendix 13.

Figure 8-4. *Flattened area around a borehole (at left); borehole extender in place and fastened to the flattened area (at right).*

8.2.2 Monitoring system

Packers and pressure transmitters in observation holes

All mechanical packers for pressure monitoring were specially designed so that the pressure sensor membrane assembly is expected to be under the water surface in all the boreholes. The packer's rubber seal was installed adjacent to the borehole opening. The outer diameter of a non-expanded packer is 73.5 mm and the sealing length is 10 cm, see Figure 8-5. The pressure transmitters are of type Druck PTX 1830-3642 abs with a pressure range of 0 to 600 kPa.

The calibration constants for the transmitters included in the Hydro Monitoring System, HMS (see paragraph below), were the constants obtained on delivery of the sensors.

Before the packers were installed and after they were taken out of the boreholes, the pressure transducers were checked against air pressure. The pressure reference for the tests was a calibrated Paulin barometer.

Before the packers were installed, 40 of the 42 pressure sensors showed a deviation not more than ± 1 kPa from the reference sensor. One showed a pressure difference of –1.5 kPa and the other +1.2 kPa relative to the reference sensor. Pressure values for all sensors are presented in Appendix 15. These pressure deviations are small and therefore have no bearing on the pressure analysis, since the measurements are primarily used to analyze pressure responses during the injection tests and then relate them to the values of the pressure before the pressure disturbance. One pressure sensor in borehole K4035G02 broke during the measurement period and was replaced by a new sensor.

After installation, 38 of the 41 pressure sensors showed a deviation not more than ± 1 kPa from the reference sensor. Two pressure sensors showed pressure deviations of +1.5 kPa and +2.5 kPa from the reference sensor and one –1.5kPa. Pressure values for all sensors are presented in Appendix 15. There are small deviations between the pressures measured before and after the injection tests, ≤ 1 kPa for 38 of the 41 sensors.

Hydro Monitoring System (HMS) at Äspö HRL

The 42 pressure sensors in the observation holes and the seven pumps controlling the water level in the tested tunnel were connected to the SKB data acquisition system, HMS, which also supplied the pumps with electricity (see Figure 8-6). SKB's acquisition system (HMS) permits continuous collection of data from sensors in boreholes in the Äspö HRL as well as from boreholes located on the surface. Data is typically collected via a peripheral logger that is in contact with a central computer. This computer can be accessed by internal and external users and usually displays readings almost instantaneously when measurements are made.

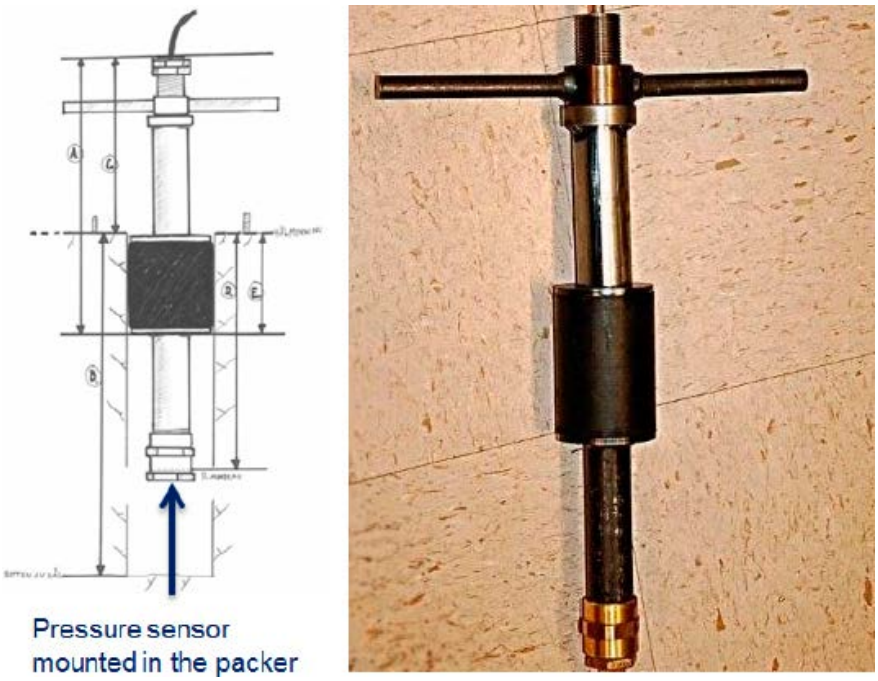

Figure 8-5. *Sketch and photo of the mechanical packer used for monitoring. The distance D between the top of hole and the pressure sensor diaphragm is usually 195 mm.*

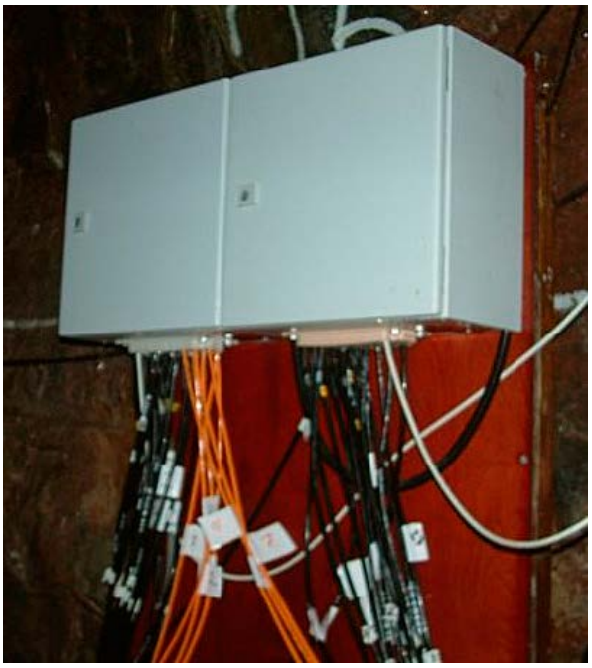

Figure 8-6. *Boxes in the TASS tunnel with data logger communication system to the host computer. The logger has also local data storage.*

8.2.3 Hydraulic boundary conditions

To create a positive hydraulic boundary and saturated conditions in the tested tunnel and thus facilitate the evaluation of the test results, all fractures in the tunnel floor should preferably be submerged before testing. For practical reasons, it was not convenient to submerge the entire tunnel floor. Therefore, seven pumps were installed in the lowest depressions in the test area to control the water levels in nearby fractures and boreholes (see Figure 6-14 in Chapter 6).

Pump ponds were selected to:

- ensure fully saturated conditions in the tunnel floor while permitting the “leakage” points in the tunnel floor to be seen during the injection tests in the higher-lying parts of the tunnel floor,
- calculate the leakage from the walls, roof and floor of the tunnel to different areas of the test site,
- indicate via measured pump flows any major leakage to the ponds during the injection tests, and
- create local positive hydraulic boundaries for the injection tests.

Flows were calculated from recorded times between start and stop of the pumps included in the HMS system and measured pump flows for the separate pumps. The water level was controlled by pumps with a built-in level control. The water level in the ponds was regulated so that it was about 3–5 cm below the collar of the nearest boreholes. It should be noted that any flux of water leaving the test site via ventilation was not determined.

8.2.4 Injection pressure

There was some risk that measurements made near the tunnel floor could cause jacking or elastic deformations in the fractures if the injection pressures were too high. Furthermore, the selected injection pressure should be high enough in relation to the error of the hydraulic formation pressure so that it has a minimal effect on the evaluation of the test. However, injection pressures must not be so high that turbulent flow is obtained. In our test set-up, it has been estimated that laminar flow in single fractures occurs if the mean aperture does not exceed 0.3 mm, i.e. fracture transmissivities are lower than $T = 3 \cdot 10^{-5}$ m^2/s (Zimmerman and Bodvarson 1996, Gustafson 2012).

In order to determine the over-pressure that could be used in the injection tests, initial measurements were made of the deformations in selected sections with different injection pressures. Nine sections were selected based on geological information concerning the fractures in the boreholes. During the measurements, the regular injection equipment was connected to special equipment for measuring deformations, see Figure 8-7 (a further description is provided in Appendix 16).

In addition, evaluation of flow regimes due to deformations in fractures was also done (see Appendix 17). The results are from evaluated injection tests in over-pressure steps up to about 500 kPa. The deformation measurements from the nine sections and the hydraulic evaluations indicated no jacking and minimal elastic deformations. The elastic deformation has only a marginal effect on the evaluated steady-state transmissivity values. Based on the results of the measurements, the over-pressure used in relation to the hydraulic formation pressure was about 200 kPa for sections 0.00 to 0.10 m and 0.10 to 0.20 m and about 500 kPa for the deeper sections.

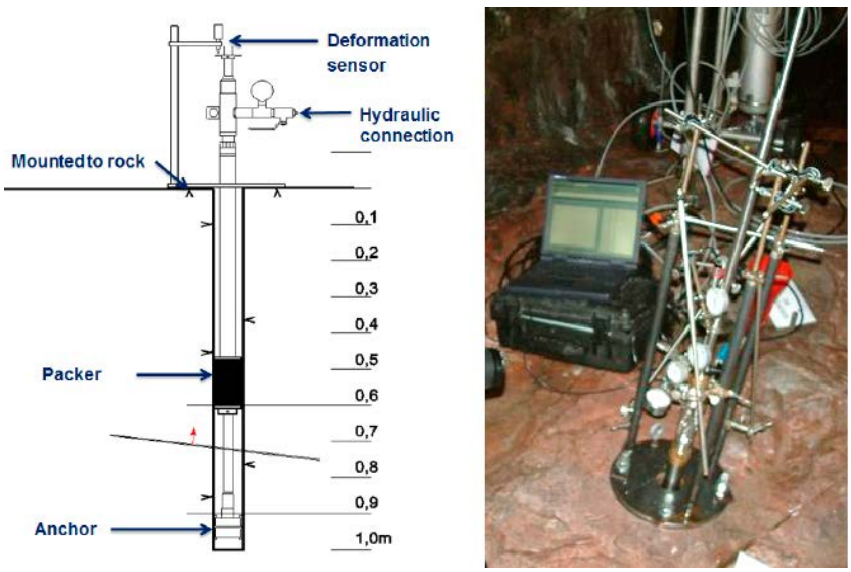

Figure 8-7. *Equipment for “mechanical” measurements of deformations in rocks at different hydraulic pressures.*

8.2.5 Test procedure

The measurements were made with the following section lengths:

- 10 cm between 0.0 and 0.10 m, and 0.10 and 0.20 m along the borehole,
- 20 cm between 0.20 and 0.40 m, and 0.40 and 0.60 m along the borehole,
- 40 cm between 0.60 m and the bottom of the borehole in one-metre boreholes, and
- 1.40 m between 0.60 m and the bottom of the borehole in two-metre boreholes (4 boreholes in total).

The reason that section lengths were increased with depth was that the measurement time could be optimized according to the expected depth of the damage produced by the blasting procedure.

Before the start of the injection tests an estimate of the formation pressure was made as follows:

- measured pressure before injection,
- short pulse test,
- information on pressures in the sections surrounding the measurement section, and
- pressure measurements in the hole during monitoring.

The test sequence for an injection test has been as follows:

- the packer system was expanded in the desired section,
- tubes (injection tube and pressure measurement tube) were vented,
- flow out of the section was measured for about 5 minutes (optional),
- the formation pressure was recorded for about 10 minutes after which a short pulse test was performed,
- the formation pressure was estimated based on the information presented above,
- the pressure disturbance was calculated based on the estimated formation pressure,
- the pressure disturbance in the active section continued for about 20 minutes (flow phase), provided the flow rate was above 1 mL/ min, and
- pressure recovery continued for about 20 minutes (fall-off phase).

Further information regarding choice of testing time is provided in Appendix 18.

8.3 Data handling

The data collected during the tests have been handled and stored in comprehensive protocols, (see Appendix 19 for further information). Documentations of all 210 injection test are presented in Appendix 20. Not only have measurement data been handled, data on hydraulic communication between the injection sections and communication to the tunnel floor (leakage points) have been documented, see Appendixes 21, 22 and 23. Figure 8-8 to Figure 8-12 show examples of the documentation of the injection tests.

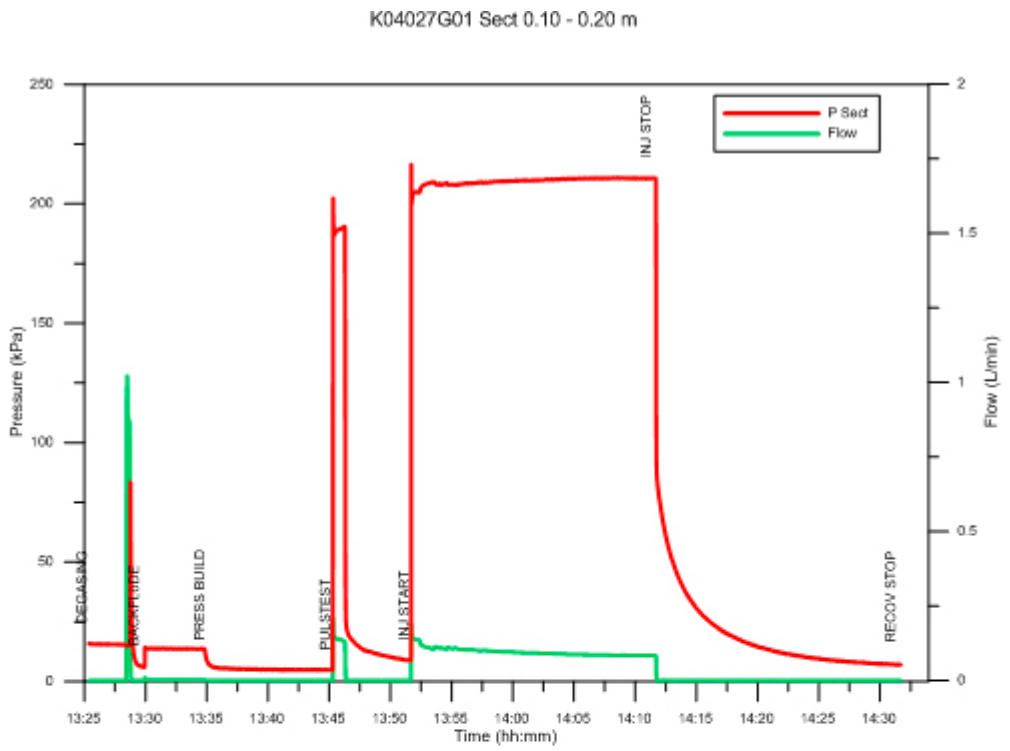

Pressure = Absolute pressure – Air pressure + Difference in altitude between the pressure transmitter and the middle of section (converted to pressure).

Injection start: 2013-12-10 13:51:40	Injection stop: 2013-12-10 14:11:40
Assumed formation pressure before injection start: 9 kPa	Evaluated formation pressure: 7 kPa
Difference in altitude between the pressure transmitter and the middle of section: 1.3 m	Position of leakage and photos on leakage (Y/N): Y
Comments: There was a leakage flow of approximately 0.1 /min coming up from the bottom of a large puddle close to the borehole.	

Section length (m)	Injection pressure* (kPa)	Flow** (L/min)	Specific capacity (m^2/s)	Transmissivity$_M$ (m^2/s)	Hydraulic conductivity$_M$ (m/s)
0.10	204	0.084	6.73E-08	1.37E-08	1.37E-07

*Mean pressure at the end of the injection phase

** Mean flow at the at the end of the injection

Figure 8-8. *Reporting protocol of measurements and estimated hydraulic parameters. Hydraulic conductivity and transmissivity have an index M, which shows that the calculations were done with Moye's equation.*

Figure 8-9. *Core images where the measured section is marked with two red lines.*

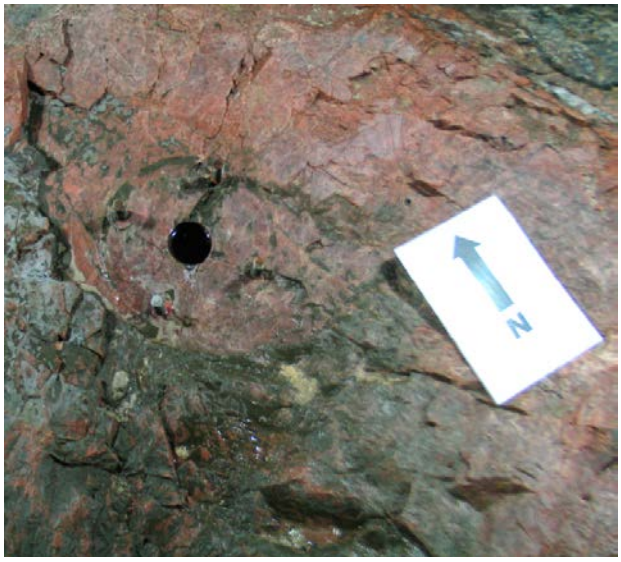

Figure 8-10. *Flattened surface on top of the borehole.*

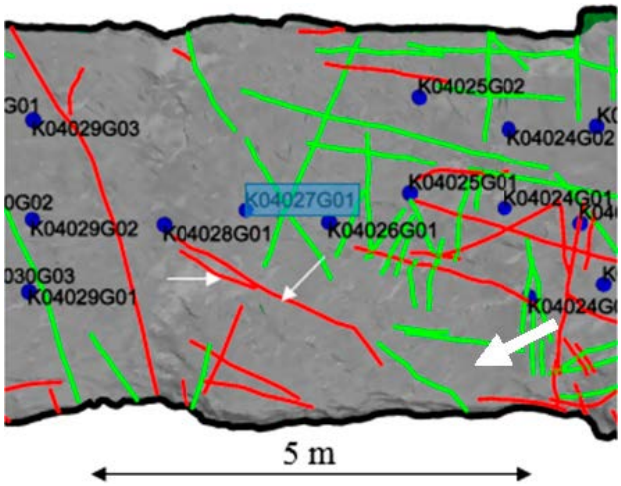

Figure 8-11. *Markers of leakage points represented by arrows on the figure. The green lines indicate filled fractures and the red lines open or partially open fractures.*

Figure 8-12. *Markers of leakage points (arrows) in the pond. The leakage points were discovered due to air bubbles coming up from the bottom of the pond. The distance between the two leakage points was 1 m. The total flow was estimated to be 0.1 L/min. The picture is taken from the inside of the tunnel.*

8.4 Injection tests – steady-state analysis and results

The steady-state analysis focused on section transmissivities determined using Moye's formula. Hydraulic conductivities and specific capacities were also determined and are presented in tables in Appendices 24, 25, 26. The interpreted transmissivity as well as measured specific capacity results versus borehole depth are shown in Figure 8-13. The estimated results are grouped according to different characteristic pressure responses during the injection tests.

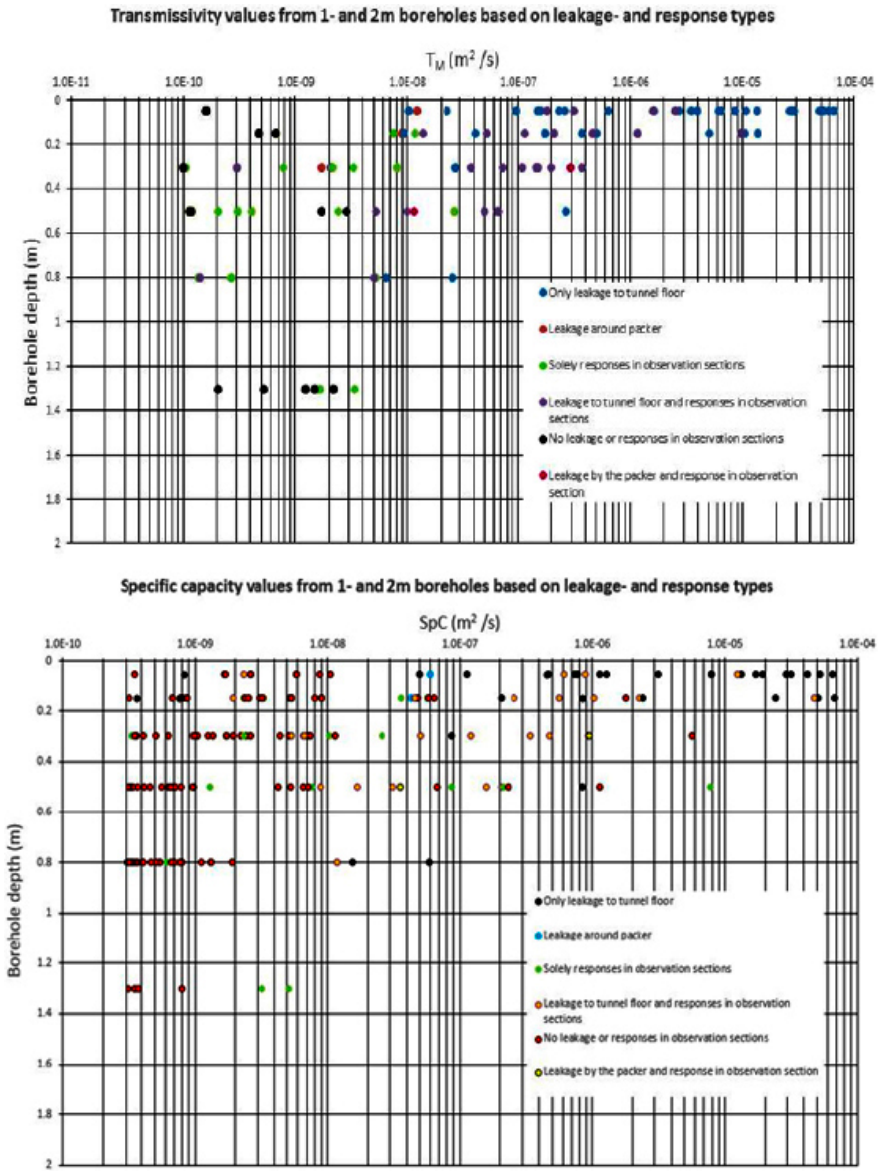

Figure 8-13. *Estimated transmissivities and specific capacities for each section in all boreholes versus borehole depth. According to Section 8.1.1 and Appendix 32, section transmissivities at depths below 0.2 and in relative terms may be overestimated by a factor of about 2–3 compared with the more superficial layers.*

The responses represent:

- **Solely leakage to tunnel floor**: The estimated transmissivities may be affected by observed outflow (leakage) on the tunnel floor. The leakage may be observed in fractures on the tunnel floor or in fractures located at the seal between the borehole extender and the rock surface.
- **Leakage around packers:** The estimated transmissivities may be affected by leakage in the rock around the packer. (The values are uncertain)
- **Solely responses in observation borehole sections:** Estimated transmissivities of injection borehole sections with hydraulic connections to surrounding observation borehole sections.
- **Leakage to tunnel floor and responses in observation borehole sections.** The estimated transmissivities may be affected by observed outflow (leakage) on the tunnel floor. The sections are hydraulically connected with surrounding borehole sections
- **No leakage or no responses in observation borehole sections.** Estimated transmissivities of injection sections with no hydraulic connections to surrounding observation borehole sections and no leakage to the tunnel floor.
- **Leakage around the packers and responses in observation borehole sections.** The estimated transmissivities may be affected by rock leakage around the packers. The sections are hydraulically connected with surrounding borehole sections. (The values are uncertain)

Figure 8-13 shows that the estimated transmissivity is high in the uppermost sections, which are often hydraulically connected with the tunnel floor. The values decrease with depth. Relatively high transmissivities were estimated for sections down to the section 0.40 to 0.60 m.

8.5 Transient analysis – single-hole and interference tests

In the transient evaluation, the data fit has been done according to different evaluation models to deduce which conceptual model is most representative and shows the best agreement with the test data. All evaluations are presented in Appendix 27.

First, transient evaluations of the flow and recovery periods based on constant head tests were done for selected tests. Second, transient evaluations based on the entire pressure sequence during the flow and recovery periods were done based on variable flow rate tests. Evaluations according to two different types of hydraulic models were done for the selected test sections, both injection sections and corresponding observation borehole sections. Evaluations based on Barker's Generalised Radial Flow, GRF, model (Barker 1988) according to the concept implemented in Aqtesolv were done first, after which evaluations based on a leaky flow model, usually Moench, were done, since 3D flow was estimated for nearly all test sections from the previous GRF analysis. However, for two tests a pseudo radial flow (1.5D flow) transiting to an apparent no-flow boundary was indicated, see Appendix 27.

The following designations have been used for the estimated transmissivity presented in the tables below:

- specific capacity, S_c, is calculated as the final flow rate, Q, divided by the injection head, Δh, assuming steady-state conditions,
- T_M = Transmissivity of the injection section according to Moye's equation assuming steady-state conditions and a spherical boundary condition (see Section 8.1.1),
- T_{LOE} = Transmissivity of the injection section according to Lars O. Ericssons equation assuming steady-state conditions and a positive boundary condition (see Appendix 10),
- T_{THI} = Estimated transmissivity of the injection section from transient evaluation of the entire test period (injection period and recovery period),
- T_{TIK} = Estimated transmissivity of the injection section from transient evaluation of the injection period, based on model for constant head tests,
- T_{TAK} = Estimated transmissivity of the injection section from transient evaluation of the recovery period, based on model for constant head tests, and
- T_{THO} = Estimated transmissivity of the observation section from transient evaluation of the entire test period (injection period and recovery period).

The transient analysis of seven selected injection tests is presented in Table 8-1. For comparison, the results determined according to T_M and T_{LOE} as well as the specific capacity values are also presented. It is concluded that the transient interpretation, e.g. T_{THI}, gives results similar to those of the steady-state determination, see also Figure 8-14.

Table 8-1. Results and estimated transmissivity of the injection sections according to different methods

Borehole section	Leakage	Responding sections	Specific capacity (m^2/s)	T_M (m^2/s)	T_{LOE} (m^2/s)	T_{THI} (m^2/s)	T_{TIK} (m^2/s)	T_{TAK} (m^2/s)
17G02 0.40–0.60	L*	4 R**	2.1 E–7	6.6 E–8	4.8 E–8	6.6 E–8	9.0 E–8	7.3E–8
17G03 0.40–0.60	L*	1 R**	1.6 E–7	4.9 E–8	3.6 E–8	1.3 E–7	1.4 E–7	1.1E–7
18G01 0.10–0.20	L*	2 R**	1.0 E–6	2.1 E–7	1.3 E–7	6.9 E–8	8.3 E–7	6.2E–8
20G01 0.10–0.20	–	1 R**	3.7 E–8	7.4 E–9	4.9 E–9	1.8 E–8	4.8 E–8	6.7E–9
21G02 0.20–0.40	L*	2 R**	6.1 E–7	1.9 E–7	1.4 E–7	2.5 E–7	4.4 E–7	2.5 E–7
33G02 0.40–0.60	–	1 R**	6.5 E–10	2.0 E–10	1.5 E–10	3.2 E–10	–	1.4 E–10
16G01 0.10–0.20	L*	–	5.0 E–6	5.0 E–7	3.2 E–7	2.7 E–7	–	1.5 E–7
29G03 0.10–0.20	L*	–	1.0 E–4	1.0 E–5	6.8 E–6	1.2 E–5	3.5 E–5	–

L* = Leakage from fracture/fractures.

The number before R** denotes the number of pressure responding sections.

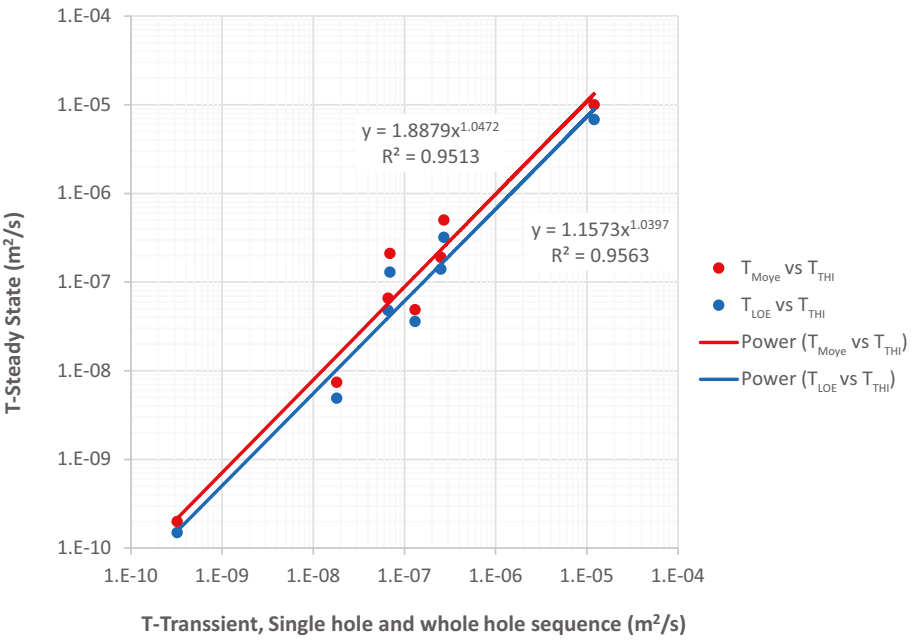

Figure 8-14. *Steady-state determinations according to Moye, T_M, give similar results as determinations according to the transient approach, which involves the whole testing sequence, T_{THI}. Section transmissivities according to a steady-state interpretation and assuming a positive hydraulic boundary, T_{LOE}, show slightly lower values than T_M.*

Transient evaluations of interference tests according to responses in observation sections (six injection sections, some with outflow in fractures at the tunnel floor, and nine observation holes) are presented in Table 8-2. Estimated transmissivities, T_{THO}, and storativities (storage coefficients), S, from observation sections are shown. The same table also presents the corresponding estimated transmissivities of the injection sections.

In addition to transmissivities and storage coefficients, transient evaluation of the responses in the observation sections provide an indication of the flow dimension and the hydraulic boundaries, see Appendix 27. In seven of the nine evaluated tests, the estimated transmissivities from the observation sections were higher than those from the corresponding injection sections. Four of the interference tests showed relatively high discrepancies and higher values compared with the single-hole interpretations, see Figure 8-15. This discrepancy is most likely due to heterogeneities in the rock, which means that the flow is not uniformly distributed in all directions from the injection section.

Transient interpretation shows a correlation between the storage coefficient values and the transmissivities calculated from the observation holes, see Figure 8-16. The variation in data is most probably caused by heterogeneities in the rock and the boundary conditions. The storage coefficient indicates the degree of confinement of the tested groundwater aquifer conditions. Higher values indicate more unconfined conditions with more potential connections between the test section and the atmospheric conditions at the tunnel floor.

Table 8-2. Interpreted transmissivities, T_{THO}, and storage coefficients, S, according to transient responses in observation holes/sections. For the sake of comparison, single-hole transient determinations, T_{THI} are also presented in the table.

Injection holes and sections	Leakage	Observation holes and sections	T_{THO} (m^2/s)	Storage coefficient (S)	Hydraulic diffusivity T_{THO}/S	T_{THI} (m^2/s)
17G02 0.40–0.60	L*	16G01 0.10–1 m	2.7 E–8	1.5 E–4	1.8 E–4	6.6 E–8
17G02 0.40–0.60	L*	17G01 0.10–2 m	5.0 E–6	1.0 E–3	5.0 E–3	6.6 E–8
17G02 0.40–0.60	L*	17G03 0.10–1 m	3.4 E–6	1.2 E–3	2.8 E–3	6.6 E–8
17G02 0.40–0.60	L*	18G01 0.10–1 m	7.9 E–5	1.7 E–4	4.6 E–1	6.6 E–8
17G03 0.40–0.60	L*	17G02 0.10–2 m	2.1 E–7	2.8 E–4	1.8 E–1	1.3 E–7
18G01 0.10–0.20	L*	17G01 0.10–2 m	1.7 E–7	1.2 E–6	1.4 E–1	6.9 E–8
20G01 0.10–0.20		21G02 0.10–2 m	1.3 E–6	3.2 E–5	3.8 E–3	1.8 E–8
21G02 0.20–0.40	L*	20G01 0.10–1 m	7.5 E–8	2.0 E–5	3.8 E–3	2.5 E–7
33G02 0.40–0.60		33G01 0.10–1 m	7.7 E–10	3.0 E–6	2.6 E–4	3.1 E–10

L* = Leakage from fracture/fractures.

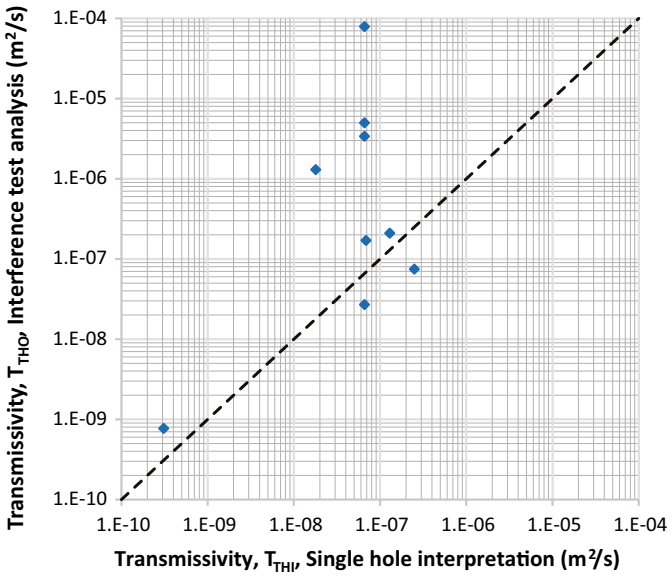

Figure 8-15. *Comparison between transmissivity values determined in transient mode from interference test evaluation, T_{THO}, and corresponding transmissivity evaluation from single holes, T_{THI}.*

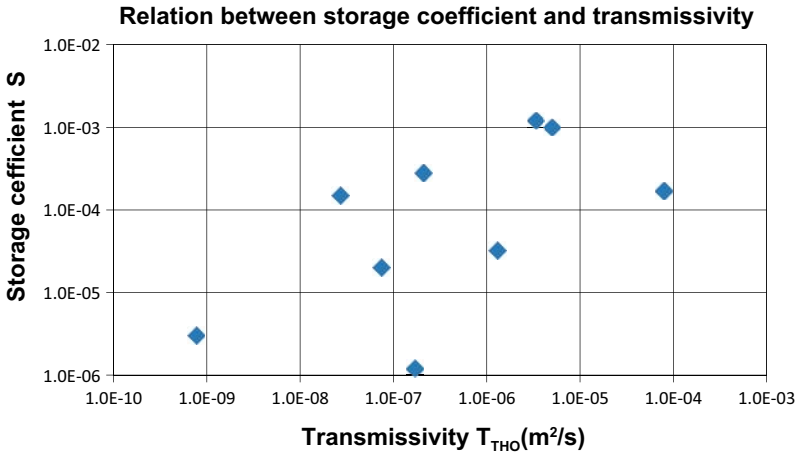

Figure 8-16. *Relationship between storage coefficient and transmissivity.*

8.6 Connectivity analysis regarding pressure disturbances in observation holes and leakage to the tunnel floor

Pressure disturbances in observation holes were analyzed during the injection tests, seeSection 8.5. There may be several reasons for pressure disturbances in observation sections:

- installation/re-installation of monitoring packers in observation boreholes,
- Installation/re-installation of injection packers in the injection hole,
- Pulse test in the injection section, and
- Injection and recovery period in the injection section.

Installation and re-installation of packers, as well as the other events mentioned above, were noted in an activity log with a time resolution of around 1 second and entered into a data file, see Appendix 19 and Appendix 28. The packer installations/re-installations and the responses were compiled in a Excel sheet which included about 1,000 potential qualitative assessments of responses during the 210 injection tests. The Excel sheet is presented in Appendix 23. A subset of the Excel sheet is shown in Figure 8-17.

				Borehole	K04016G01		K04017G01		K04017G02		K0417G03		K04018G01	
				P (kPa, rel)	≤10		≤10		≤10		≤10		≤10	
				Kacc (m/s)	5.59E-07		1.65E-07		3.74E-08		9.71E-08		2.35E-07	
Borehole	Section (m)	K_M (m/s)	Leakage		INJ	IM	INJ	MI	INJ	IM	INJ	IM	INJ	IM
K04016G01		MM					RMO,IMO		RMO,IMO		RMO,IMO		RMO,IMO	
K04016G01	0.00-0.10	6.42E-06	2				O	IO,RO	O	IO,RO	O	IO,RO	O	IO,RO
K04016G01	0.10-0.20	4.95E-06	3				O	IO,RO	O	IO,RO	O	IO,RO	O	IO,RO
K04016G01	0.20-0.40	1.11E-08	1				O	IO,RO	O	IO,RO	O	IO,RO	O	IO,RO
K04016G01	0.40-0.60	1.01E-09	1				O	IO,RO	T	I?,R?	O	IO,RO	O	IO,RO
K04016G01	0.60-1.00	1.23E-08	3				O	IO,RO	PIF (15 kPa)	I,R	PIF (2kPa)	IO,RO	O	IO,RO
K04017G01		MM			RMO,IMO				RMO,IMO		RMO,IMO		RMO,IMO	
K04017G01	0.00 0.10	5.14E-04	2		O	IO,RO			O	IO,RO	O	IO,RO	O	IO,RO
K04017G01	0.10 0.20	1.70E-06	3		O	IO,RO			O	IO,RO	O	IO,RO	O	IO,RO
K04017G01	0.20-0.40	7.17E-07	3		O	IO,RO			O	IO,RO	O	IO,RO	PIF (18 kPa)	IO,RO
K04017G01	0.40-0.60	5.77E-10	1		O	IO,RO			O	IO,RO	O	IO,RO	O	IO,RO
K04017G01	0.60-2.00	3.71E-10	1		O	IO,RO			O	IO,RO	O	IO,RO	O	IO,RO
K04017G02		MM			RMO,IMO		RME,IME				RMO,IMO		RMO,IMO	
K04017G02	0.00-0.10	1.55E-09			O	IO,RO	E	IE,RE			O	IO,RO	O	IO,RO
K04017G02	0.10-0.20	4.67E-09	1		O	IO,RO	E	IE,RE			O	IO,RO	O	IO,RO
K04017G02	0.20-0.40	1.05E-08	1		O	IO,RO	E	IE,RE			IF (0.4 kPa)	IO,RO	O	IO,RO
K04017G02	0.40-0.60	3.31E 07	1		PIF (1.4 kPa	IO,RO	PIF (0.3 kPa	IO,RO			PIF (3 kPa)	IO,RO	PIF (0.4 kPa	IO,RO
K04017G02	0.60-2.00	5.43E-09	3		O	IO,RO	E	IE,RE			O	IO,RO	O	IO,RO
K04017G03		MM	1		RMO,IMO		RMO,IMO		RMO,IMO				RMO,IMO	
K04017G03	0.00-0.10	9.51E-07	3		O	IO,RO	O	IO,RO	O	IO,RO			O	IO,RO
K04017G03	0.10 0.20	1.38E 09	1		O	IO,RO	O	IO,RO	O	IO,RO			O	IO,RO
K04017G03	0.20-0.40	1.88E-07	3		O	IO,RO	O	IO,RO	PIF (16 kPa)	IO,RO			O	IO,RO
K04017G03	0.40-0.60	2.46E-07	3		O	IO,RO	O	IO,RO	PIF (24 kPa)	IO,RO			O	IO,RO
K04017G03	0.60-1.00	1.39E-09	1		O	IO,RO	O	IO,RO	O	IO,RO			O	IO,RO

Figure 8-17. *Part of the Excel sheet showing the results of the analysis of the pressure responses.*

For qualitative assessments based on the individual measurements, the following definitions have been used in the Excel sheet according to the daily plots:

IM: Installation of monitoring packer (highlighted in orange in the Excel sheet)

IMO: Installation of monitoring packer (no responses)

RM: Re-installation of monitoring packer (highlighted in orange in the Excel sheet)

RMO: Re-installation of monitoring packer (no responses)

I: Installation of injection packer (highlighted in orange in the Excel sheet)

IO: Installation of injection packer (no responses)

R: Re-installation of injection packer (highlighted in orange in the Excel sheet)

RO: Re-installation of injection packers (no responses)

PIF: Very clear responses during pulse test, injection and recovery period (marked with red colour in Excel sheet with the numerical value of pressure response in kPa):

IF: Clear response during the injection and recovery period (marked with green colour in Excel sheet with numerical value of pressure response in kPa)

T: Possible response (highlighted in blue in the Excel sheet)

O: No Response

E: Distorted data, due either to high noise level in the measurements or data affected by other activities in neighbouring tunnels.

Thus, by means of section-specific injection tests, hydraulic connections may be revealed with the surrounding observation sections and with the tunnel floor. A packer was installed in the uppermost part of the observation holes in all injection tests, which means that the observation sections have a length of 0.9 m (one-metre holes) or 1.9 m (two-metre holes). The hydraulic connections with the tunnel floor have been subdivided into: 1) Flows out of the fractures found in the tunnel floor, 2) Flows out of the edge of the sealfor the borehole extender and along fractures below the sealing unit, and 3) Flows around the upper packer and then through the borehole up to the tunnel floor.

The distribution of pressure responses and leakage points is presented and discussed in Appendix 29. Table 8-3 shows the number of injection sections in different depth intervals from which pressure responses were obtained in the observation sections. In addition, the number of observation sections in combination with some type of connection with the tunnel floor is reported. In the table, those ten injection sections in which the pressure responses in the observation sections were classified as “probable” are excluded. In one of the holes, none of the injection sections had no hydraulic communication with either the surrounding observation sections or the tunnel floor.

Table 8-3. The number of injection sections versus depths from which pressure responses were obtained in observation sections and from which flows were obtained on the tunnel floor.

	0.00–0.10 m	0.10–0.20 m	0.20–0.40 m	0.40–0.60 m	0.60 m to borehole bottom
Number of injection sections from which only responses in observation holes occurred	0	2	2	5	4
Number of injection sections with only responses in observation holes and leakage in fractures to tunnel floor	1	7	8	5	1
Number of injection sections with only responses in observation holes and leakage through the seal for the borehole extender	2	0	0	0	0
Number of injection sections with only responses in observation holes and leakage around packers.	0	0	1	1	0
Total	3	9	11	11	5

The number of injection sections that are hydraulically connected with the observation sections is 22, see Appendix 28. The results presented above do not take into account the number of observation sections connected with each injection section. In the database, the maximum number of observation sections that one injection section is in hydraulic contact with is four. The maximum number of observation sections that have pressure responses caused by injection is 58, see Appendix 28. Because the presentation includes hydraulic responses in observation sections caused by injection tests, the number of connecting paths in which hydraulic connections were obtained is less than the number of pressure responses, since many of the paths are tested in two directions.

In addition to the qualitative evaluation of observation-hole responses, compilations have been made of pressure disturbances for the test area. A proxy parameter called the Pressure Disturbance Index (PDI) has been introduced. Since the pressure disturbances in the test sections may differ greatly depending on transmissivity, the relative pressure response has been used in the calculation of the PDI. The PDI has been calculated according to the following equation:

$PDI = (dP_{obs}/dP_{inj}) \cdot d$

where:

dP_{inj} = Pressure disturbance in the injection section (kPa)

dP_{obs} = Pressure response in the observation section (kPa)

d = Distance between the midpoints of the injection section and observation section (m)

Figure 8-18 shows the PDI values plotted against midpoints of the injection sections for the whole area. There are more points in the graphs than the number of injection sections, since individual injection sections may be in hydraulic contact with several observation sections. Since the PDI varies widely, the PDI values have been plotted on a logarithmic scale.

From Figure 8-18 it can be seen that the number of injection sections, within different intervals with associated pressure responses in observation boreholes, are distributed as follows:

- Interval 0.0–0.1 m – 3 sections,
- Interval 0.1–0.2 m – 13 sections,
- Interval 0.2–0.4 m – 18 sections,
- Interval 0.4–0.6 m – 15 sections,
- Interval 0.6–1 m – 5 sections, and
- Interval 0.6–2 m – 4 sections.

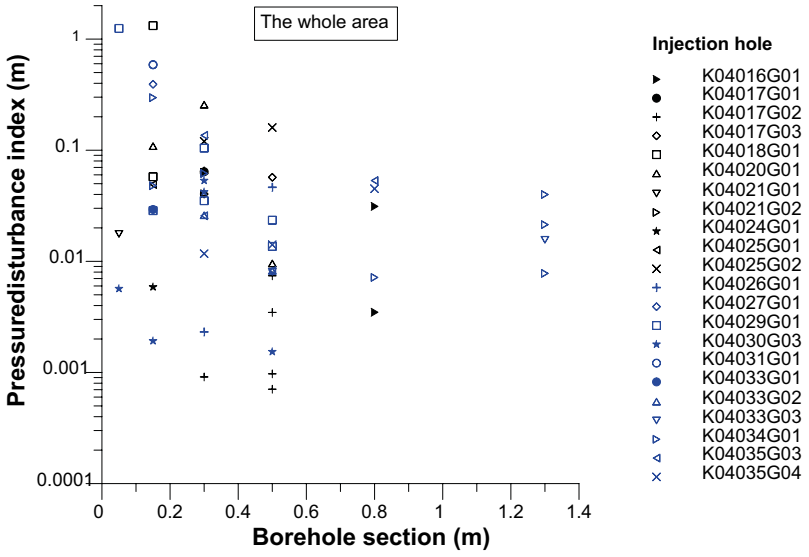

Figure 8-18. *Diagram of the Pressure Disturbance Index (PDI) in the responding borehole sections versus the midpoint of the injection sections. Results from the whole test area.*

The PDI shows a significant decreasing trend versus depth if the uppermost section (0.0–0.1 m) is excluded. This section has many leakage points via fractures under the seal on the borehole extender and to other superficial fractures in the tunnel floor. Thus, the pressure response from these sections is generally small. One getsthe impression, however, that that PDI decreases with depth to about 0.5 m (middle section). The few values below 0.5 m show a more constant PDI. The pressure responses above have not been subdivided into different fracture types.

A separate evaluation has been carried out regarding flows from injection test sections to the tunnel floor only. The results are summarized in Table 8-4. The table confirms many leakage points in the floor from the shallowest packer interval.

In Figure 8-19 the observed hydraulic connections in the actual rock volume are presented in a horizontal view and in a vertical view.

In the horizontal view the hydraulic connections between holes are plotted as lines with arrows indicating the direction of flow during the injection tests. Hydraulic connections between sections are marked with coloured lines and arrows. The colours of the lines are based on a division into classes of the relative pressure responses, see legend in Figure 8-19. In some cases there are two arrows with opposite directions on the same line, which means that the injection test has detected communication in two directions.

Leakage to the tunnel floor is indicated by a black line with a blue dot for the leakage point. However, no leakage is indicated in the figure at the edge of the borehole extender seal. Since the figure is a 2D representation of a 3D model, all connections from lower sections are covered by the connections (lines and arrows) from the uppermost sections.

In the vertical view of Figure 8-19, the transmissivities in the injection sections are indicated by different colours according to the legend. The hydraulic connections between the injection and observation sections are illustrated by lines with arrows according to the above description. A line representing a connection runs from the injection section to the midpoint of an observation section. This means that the line does not need to go to the “correct inflow spot” in the observation hole.

Table 8-4. Number of injection sections which only have flows up to the tunnel floor, see Appendix 22.

	0.00–0.10 m	0.10–0.20 m	0.20–0.40 m	0.40–0.60 m	0.60 m to borehole bottom
Number of sections with only leakage in the borehole extender	20	1	1	0	0
Number of sections with only leakage in fractures to the tunnel floor	4	6	0	0	0
Number of sections with only leakage around packers	1	1	1	0	0
Number of sections with only leakage in the borehole extender and in fractures to the tunnel floor	5	1	0	0	2
Number of sections with only leakage in fractures to the tunnel floor	0	0	0	1	0
Number of sections with only leakage in the borehole extender and around packers to the tunnel floor	0	0	0	0	0
Number of sections with only leakage in fractures and only leakage around packers to the tunnel floor	0	0	0	0	0
Total	**30**	**9**	**2**	**1**	**2**

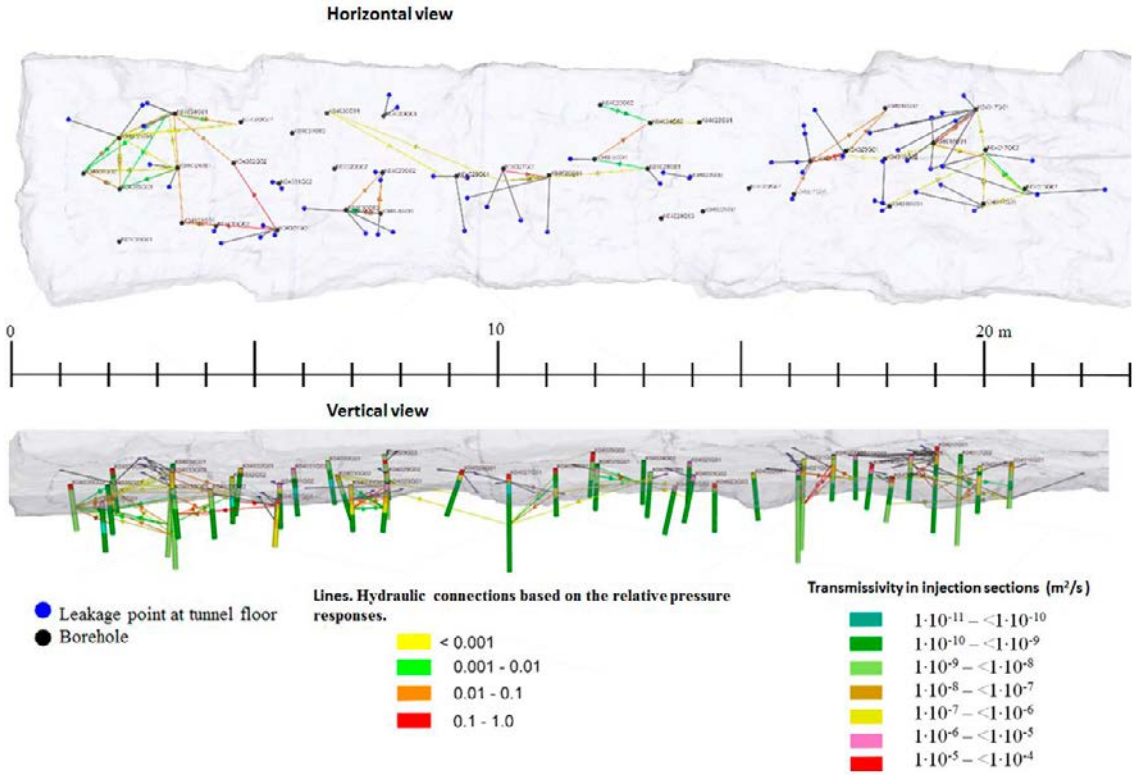

Figure 8-19. *Horizontal and vertical views with hydraulic connections along the test area. The transmissivities in the injection sections are marked by different colours based on a division into transmissivity classes. Hydraulic connections between sections are marked by coloured lines and arrows showing the direction of the responses. The lines are based on a division into classes of the relative pressure responses. Leakage to the tunnel floor is marked by black lines and blue dots.*

To summarize, the evaluation of the pressure responses in observation holes and the analysis of leakage to the tunnel floor give the following results:

- The shallowest tests, 0 to 0.10 m, show a high frequency of leakage paths to the tunnel floor in the immediate surroundings of the test section.
- In the interval 0.10 to 0.60 m, some of injection sections are hydraulically connected with adjacent boreholes. However, the frequency of connections decreases with depth.
- For sections below 0.6 m, the PDI estimates showed similar results, i.e. the frequency of connections decreases with depth.
- The longest hydraulic connections between two boreholes are about three metres, as estimated from a single test.
- If the length calculations are based on measurements in several injection tests in neighbouring holes, the total connecting length can be about seven metres. However, no pressure responses from one single test were registered for this entire length.

The following aspects may be considered regarding uncertainties in the methodology for evaluation of pressure responses:

- Pressure disturbances in observation sections have sometimes been detected down to 0.5 kPa, but generally the lower detection limit is around 1–2 kPa.
- Injection sections with low injection pressure caused by heavy leakage to the tunnel floor offer fewer opportunities for detecting pressure responses in the surrounding holes, although potential connections may exist.
- Observation sections have a length of 0.9 m (one-metre holes) or 1.9 m (two-metre holes). This means that fractures may be short-circuited along the borehole, which complicates the analysis.

8.7 Connectivity conditions according to kriging of section transmissivities

This section presents a geostatistical interpolation of the data obtained from all the single-hole injection tests conducted in the studied tunnel TAS04 in order to analyze the correlation structure of transmissive conditions in the rock mass close to the tunnel floor, "the EDZ".

8.7.1 Section transmissivity distribution

Thanks to an essentially horizontal tunnel floor and the use of identical types of injection tests (packer tests) at different intervals in each borehole, statistical distributions can be obtained, where data are pooled and analyzed in various ways. The data can be used to build a database that is representative of the rock mass being studied. Figure 8-20 shows experimental section transmissivity distributions for all results at the same level in each borehole using Moye's equation (Equation 8-1) (42 measured values in each layer, 5 layers at different depth intervals). Figure 8-20 shows that there is a spread of data over several orders of magnitude.

In order to treat scale effects of different test boundaries/test lengths, Figure 8-21 shows a comparison of the experimental cumulative distribution functions (CDFs) of the base-10 log specific capacities for each section and their fitted log-normal distributions. This figure also shows that the deeper the section the smaller the spread in the data, which could indicate less impact or effect of the blasting works. On the other hand, blasting damages in confined rock volumes in the tunnel floor could contribute to hydraulic homogenization, which is further discussed in9.5. Differences in the variability results could to some extent be due to the differences in the length of the section intervals (two sections with 10 cm length, two with 20 cm length and one with 40 cm length). Longer intervals tend to homogenize the media.

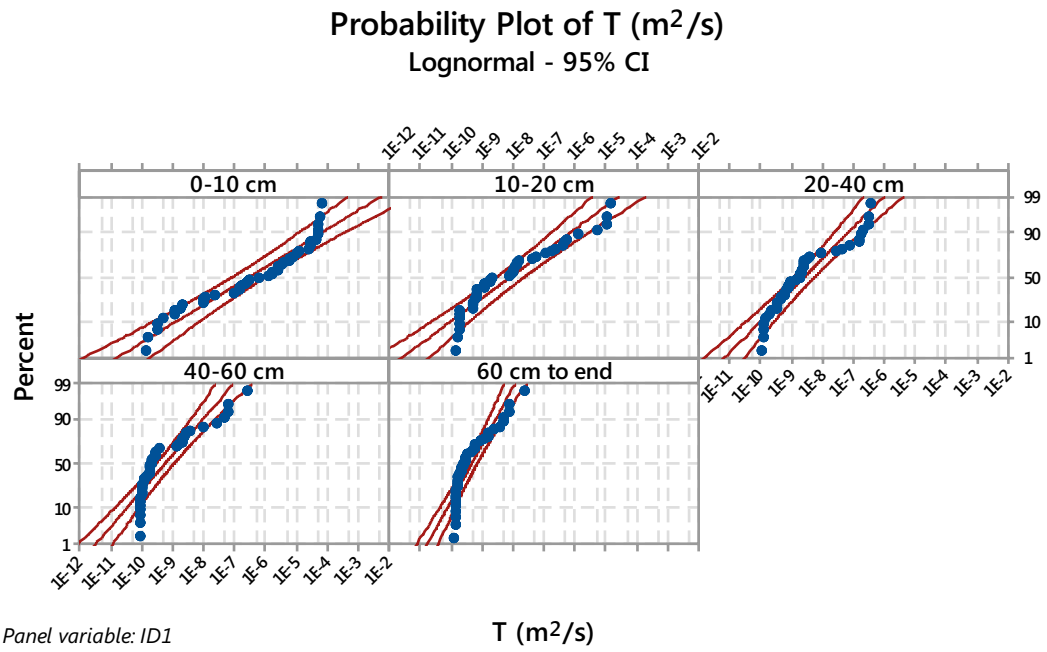

Figure 8-20. *Probability plot of the section transmissivity values obtained from tests conducted in all different sections. The lines show the 95% confidence interval.*

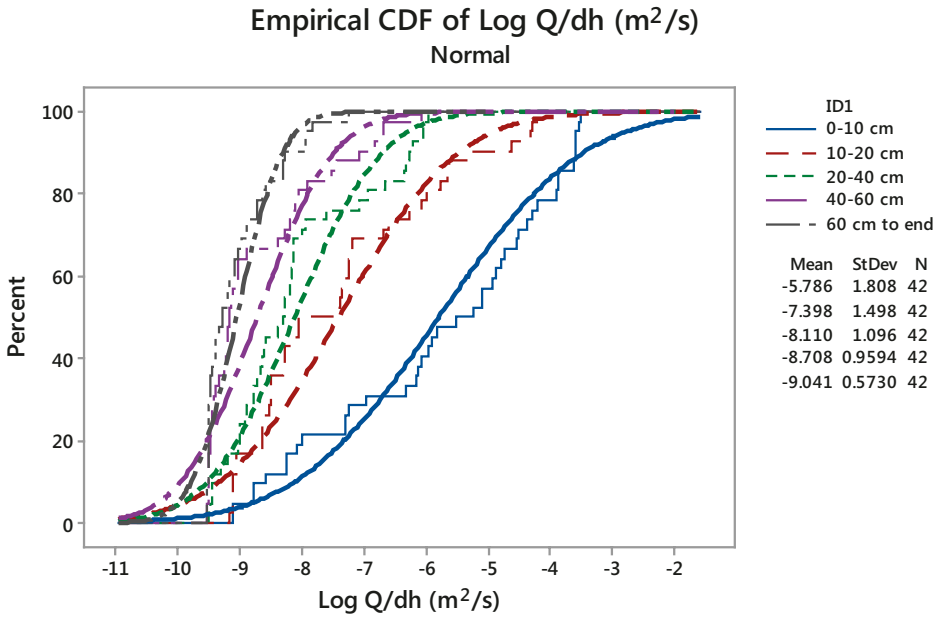

Figure 8-21. *Empirical cumulative distribution function of the base-10 log-specific capacities for each section and their fitted log-normal distributions.*

8.7.2 Rate of transmissivity change (variogram function)

In this study, all the single-hole injection test results from the different layers were used to obtain a section transmissivity variogram in 2D for every tested section. The omni-directional variograms obtained, which average behaviour over all directions, were further analyzed in order to investigate whether the data showed a "geometric anisotropy" in the omni-directional experimental variograms. Thus, their direction was changed until the best fit was observed, while the tolerance was kept at 30. Once the direction was changed, a slight difference in the length scale was observed. Figure 8-22a and Figure 8-22b show, for example, the resulting spherical model variograms which reproduce the best experimental variograms for sections 0.0 to 0.1 m and 0.4 to 0.6 m. The rest of these results are shown in Appendix 30. The fitting results are used to interpret the correlation length, which is around 2.4 m from 0 to 10 cm depth, see Figure 8-22a. As shown in Appendix 30, the correlation lengths of sections 10 to 20 cm and 20 to 40 cm are less than 2 m. These estimated connectivity lengths could also be the result of a large open fracture (sub-horizontal) that came into contact with and connects different observation boreholes.

Figure 8-22b shows the resulting variogram in the 0.40 to 0.60 m section and it shows a shorter correlation length, around 1.4 m. The correlation length of the last section, 0.60 m to the bottom of the borehole, shows a similar result of around 1.4 m. All these results could indicate that the connectivity in the rock mass from around 0.40 m and below represents the base connectivity of the rock mass, while from 0.0 to 0.40 m it represents a connectivity in which the rock has been altered substantially by the blasting works. It can be also observed that the correlation length from 0.40 m and below is slightly larger than the distance between adjacent observation boreholes, indicating that the test setup provides a good picture of the connectivity of the rock mass even if no alteration occurred.

Using the fitted variogram models shown in Figure 8-22 and used in the variogram analysis, a comparison of the kriging results between 0.0 to 0.10 cm and 0.40 to 0.60 m is shown in Figure 8-23. This comparison gives the impression that section 0.0 to 0.10 m, with transmissivity areas of 10^{-4} m^2/s, is more transmissive than section 0.40 to 0.60 m, with transmissivity areas of 10^{-7} m^2/s. On the other hand, both figures show areas with low transmissivity, 10^{-8} m^2/s and 10^{-9} m^2/s. This is also apparent in the rest of the tested sections shown in Figure 8-23 and Appendix 31. The characteristic size of these transmissive and less transmissive areas is approximately 2 to 7 m. They are asymmetric with their *shortest length* in the axial direction parallel to the blasting direction of the tunnel.

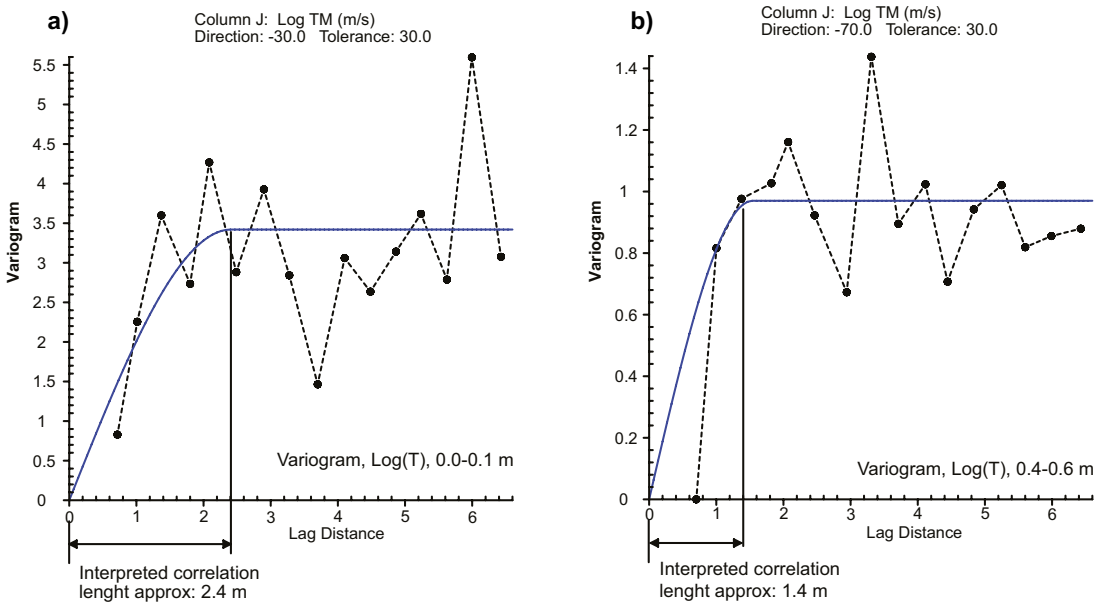

Figure 8-22. *Variogram of the base-10 log transmissivity values obtained from injection tests conducted in TAS04. The dots are the experimental variogram and the curve is the fitted model (spherical). The arrows shows the interpreted correlation length: (a) 0.0 to 0.10 m section; (b) 0.40 to 0.60 m section.*

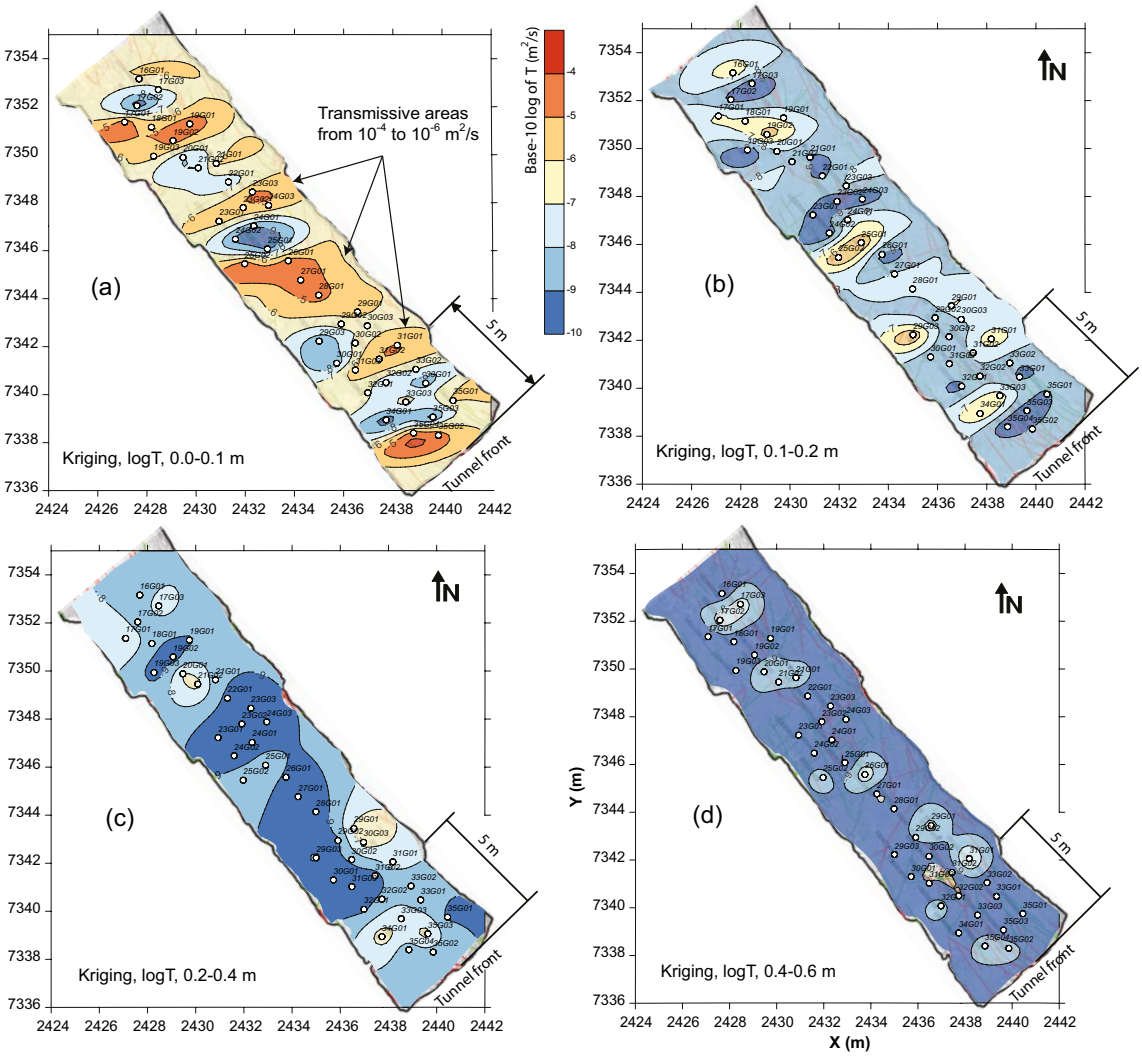

Figure 8-23. *Interpolation by kriging of the base-10 log transmissivity values obtained from injection tests conducted at TAS04. The dots represent the locations of the boreholes and the scale the base-10 log transmissivity: (a) 0.0 to 0.10 m section; (b) 0.10 to 0.20 m section; (c) 0.20 to 0.40 m section; and (d) 0.40 to 0.60 m section.*

Furthermore, comparisons of all tested sections (see Appendix 31) show that sections 0.0 to 0.10 m and 0.10 to 0.20 m are more transmissive, or show more transmissive areas, than sections 0.40 to 0.60 m and 0.60 m to the bottom of the borehole. Section 0.20 to 0.40 m seems to show a transition zone between them, where few highly transmissive areas are present and a more background transmissivity is observed. This change in the transmissivity fields with depth corroborates quite well the observation that there is some kind of alteration in the rock mass within the depth range 0.0 to 0.40 m. This alteration could be caused by the presence of more fractures, the opening of existing fractures due to the blasting or the fact that some of the fractures are connected with the tunnel floor, creating a shortcut and giving a higher transmissivity result. Either way, this analysis shows that the alteration of the rock mass ends at around 0.40 m depth, it is not continuous along the tunnel floor and that the highly transmissive areas, when present, are no longer than 7 m.

8.7.3 Connectivity conditions indicated by the geostatistical analysis

The section transmissivity and specific capacity distributions show that:

- There is a spread of data over several orders of magnitude in the sections/layers closest to the tunnel. Some distributions show that the deeper the section, the smaller the spread of the data and the less conductive the rock mass it is.

This indicates a lessening impact or effect of the blasting with depth down to the section 0.40 to 0.60 m. The increase in section length could somehow enhance the difference in the variability of the transmissive properties.

The variogram analysis shows:

- That the connectivity range decreases with depth. Section 0.0 to 0.10 m shows a correlation length of around 2 m, sections 0.10 to 0.20 cm and 0.20 to 0.40 cm less than 2 m and 0.40 to 0.60 m and 0.60 to the bottom of the borehole around 1 m.

Using the fitted variogram models, a kriging interpolation was done. The comparison gives the impression that section 0.0 to 0.10 m, with transmissivity areas of 10^{-4} m^2/s, is more transmissive than section 0.40 to 0.60 m, with transmissivity areas of 10^{-7} m^2/s. On the other hand both figures show areas with low transmissivity, 10^{-8} m^2/s and 10^{-9} m^2/s. This is also apparent in the rest of the tested sections and implies that:

- The characteristic size of transmissive and less transmissive areas is approximately 2 to 7 m. They are asymmetric and non-continuous in the axial tunnel direction with their *shortest length* in the axial direction, i.e. parallel to the blast hole direction.

Furthermore, a comparison of all tested section shows:

- That sections 0.0 to 0.10 cm and 0.10 to 0.20 cm are more transmissive, or show more transmissive areas, than sections 0.40 to 0.60 and 0.60 to the bottom of the borehole. Section 0.20 to 0.40 m seems to represent a transition zone between them.

This change in the transmissivity fields with depth corroborates quite well the observation that there is some kind of alteration in the rock mass within the depth range 0 to 40 cm.

Finally a combination of the blasting design and the kriging results shows:

- That the most transmissive areas are located around the bottom charge area of the blasting rounds, where most damage is expected to occur, and that the axial connectivity is not continuous but exhibits an intermittent/periodic behaviour.

This corroborates the results found by Ericsson et al. (2009), who concluded that the EDZ is composed of microfractures with an extent of 25 cm to 35 cm from the wall of the studied tunnel at Äspö and that the axial connectivity is not constant but shows zonation behaviour around the tunnel contour. This behaviour is further discussed in Section 9.5.

8.8 Transmissivity averaging along the tunnel floor

If the flow regime is assumed to be uniform along a prospective EDZ in a tunnel floor, it is possible to average a transmissive property based on local measurements. The arithmetic mean is usually applied in cases where the local measurements represent test volumes (blocks) in parallel. In the case of test volumes in series, the averaged transmissive property is represented by the harmonic mean (see e.g. de Marsily 1986).

Simple calculations of the averaged transmissivities at the test site give the following results, as shown in Table 8-5. The tunnel has been divided into 20 transects with widths 0.87–1.31 m along the floor. The transects have been assigned representative arithmetic means (occasionally only one value is available). Then the harmonic mean transmissivities have been calculated for the investigated floor in the tunnel section. The calculations have only been done for a depth interval where indications of EDZ (max. 0.6 m) were possible according to previous interpretations. The table shows that if the uppermost 10 or 20 cm are removed from the floor, the transmissivity will be drastically reduced along the tunnel, see Appendix 33.

Table 8-5. Averaged transmissivity, T_{Moye}, along a 20 m tunnel section at the test site TAS04. Averaging has been carried out for different test intervals, 0–0.6 m, 0.1–0.6 m, 0.2–0.6 m and 0.4–0.6 m in order to show the effect of blasting damage.

Test sections Depth interval (m)	Harmonic mean T_{Moye}, (m^2/s)
0.0–0.6	2.5 E–07
0.1–0.6	1.4 E–08
0.2–0.6	1.3 E–09
0.4–0.6	3.6 E–10

9 Integrated analysis

9.1 Blast design versus as-built

Based on the documentation and experience from the excavation of TAS04, it is possible to conclude that high charging precision was achieved. The logger data from the bottom holes in TAS04 indicates that evaluated charge concentrations are generally in the upper range of the tolerances or exceed the tolerances for the bottom holes. Charging data for individual holes indicate, however, that the tolerances were exceeded only to a limited extent. The deviations in geometry could be explained by a combination of drilling deviation and water-filled holes leading to a larger burden and insufficient decoupling. This could lead to extended blast damage in some areas. Alternatively, the uneven geometry of the blasted surface in the floor of TAS04 suggests that there could have been an accumulation of emulsion in the bottom part of the hole, i.e. in practice a longer bottom charge and an uncharged part of the column charge, since half pipes are missing for the most part at the end of the blast round. This explanation is considered to be less likely, since the bottom holes were string-charged.

9.2 Blasting versus rock types

There are no obvious effects of various rock types on the blasting results. The main difference between the rock types in the TAS04 tunnel is the relative difference in hardness between the diorites (Äspö diorite and Ävrö granodiorite) and the fine-to-medium-grained granite. The fine-to-medium-grained granite is more brittle. Just walking on the brittle rock resulted in considerable amounts of small broken-up rock pieces that needed to be cleaned out before photographing and/or geological mapping of the floor, see Figure 6-9 in Section 6.2.3.

9.3 Blasting versus fracturing

Degree of fracturing and fracture orientation have an impact on drilling precision, since percussion drilling for blast holes tends to be influenced and guided by the occurrence of fracturing in the rock. The dense occurrence of sub-vertical fractures parallel to the TAS04 tunnel in the fine-grained granite (see Figure 9-1, left) was the limiting site condition for the field works presented in this report (see also Figure 6-2).

9.4 Blasting versus geophysics

The GPR results seem to have little or no direct correlation with the blasting. Figure 9-2 shows a comparison between the GPR EDZ response depth map and blasting hole information (charge concentration in bottom holes, see Section 5.3). A weak correlation with the bottom charge locations and the GPR EDZ response is noticeable, but the strongest anomalies are usually caused by larger structures that are interpreted to be natural and not caused by blasting.

In some cases there is an indication that at the locations where the hole is over-charged there is an increase in the depth of the GPR EDZ response (circled by yellow in the figure). The GPR EDZ response is probably governed by geological structures that also often control the formation of EDZ fractures (Olsson et al. 2009). In the case of holes where the charge concentration is within design limits, one explanation for the GPR EDZ anomaly besides the geological one could be the achieved drilling accuracy. This cannot be verified because in the case of most of the blasting holes the realized locations were not surveyed.

Figure 9-1. *Examples of the influence of fractures on the drilling of perimeter holes in the floor. Left: Round No 3, just in front of the test area. The fine-grained granite is heavily fractured, with sub-vertical fractures aligned parallel to the tunnel. Right: Round No 8, massive diorite. Both photos are taken along the tunnel axis.*

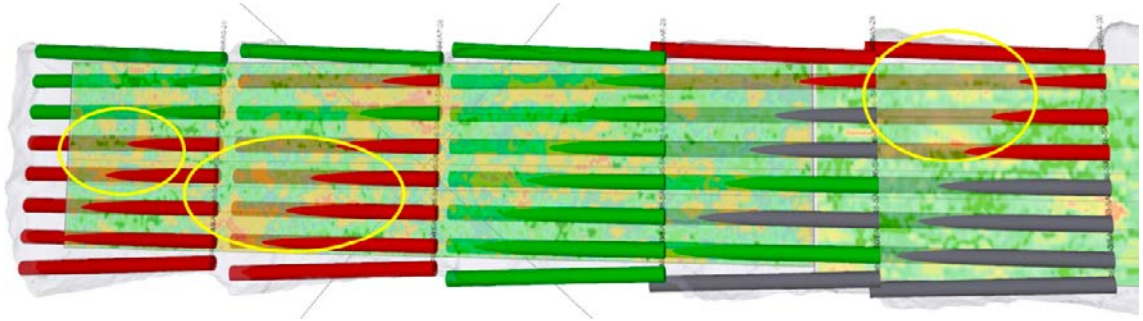

Figure 9-2. *GPR EDZ response depth map shown together with evaluated charge concentration in tunnel floor blast holes. Green and red boreholes: concentrations of explosives within and exceeding the design value, respectively (kg/m). Grey boreholes: not able to evaluate.*

9.5 Blasting versus hydrogeology

9.5.1 Correlation between test sections located in the bottom charge areas and depth beneath the tunnel floor

Figure 9-3 shows an overview of the blast hole locations in the tunnel floor (horizontal boreholes) and the location of the drilled boreholes used for the hydraulic testing (vertical boreholes) that are closest to end of blast rounds, i.e. bottom charge holes. Note that only boreholes (14 out of 42 boreholes) that were close to the bottom charge are illustrated in Figure 9-3. Table 9-1 presents these 14 boreholes and their designation for further analysis.

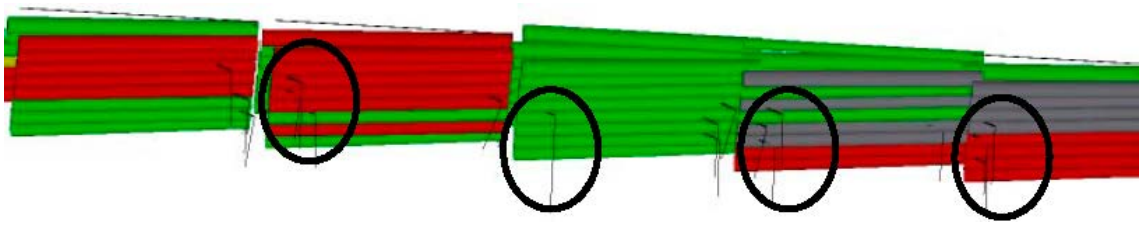

Figure 9-3. *All boreholes that are considered to be close to the end of the blast rounds. Boreholes considered to be close to the bottom charge in each blasting round are circled.*

Table 9-1. 14 boreholes considered to be closest to the bottom charge areas, see Figure 9-3.

Borehole (1 m)	Borehole (2 m)
K04018G01	K04027G01
K04019G01	
K04019G02	
K04019G03	
K04022G01	
K04023G01	
K04023G02	
K04023G03	
K04026G01	
K04031G01	
K04031G02	
K04031G03	
K04035G01	

Figure 9-4 shows section transmissivity values, T_M, and specific capacity values versus depth for boreholes near the end of blast rounds where the bottom charge is expected to cause most damage to the rock and for boreholes within column charge areas. The figure shows that highly transmissive fractures, blast-induced or natural, do not exist below 0.4 m depth. Following the classification of bottom charge and column charge in Table 9-1, Figure 9-4 shows that the frequency of higher section transmissivity values (10^{-6}–10^{-4} m^2/s) or specific capacity values (in the uppermost part 0–0.10 m) is higher for the boreholes in the bottom charge area (1.8 kg/m) compared with the column charge area (0.5 kg/m). In the 0–0.10 interval, the percentage of sections with very high transmissivity, i.e. $T_M > 10^{-6}$ m^2/s, and belonging to the bottom charge class is much higher (91%) compared with the proportion of the sections in the column charge class (22%). At deeper levels the two areas do not exhibit such an obvious contrast in transmissive properties.

Using the specific capacities, $S_C = Q/dh$, i.e. "raw data" from each test in every single borehole section, a section-by-section correlation plot can be obtained where the data gathered from different sections are compared to determine the strength of the correlation (relationship) between such sections. Figure 9-5a, b, c, and d present a comparison between the specific capacities obtained at different depth intervals below 0.10 m and the test results in the uppermost section, 0.0–0.10 m, of the holes and within the interpreted bottom charge areas. The graphs may illustrate a possible dependence between deeper strata and the most affected/damaged layer at the floor. The resulting graphs show that Figure 9-5a shows more points close to a 1:1 line. This means that in the case of the boreholes located in the bottom charge areas there could be a better correlation between the results obtained between 0.0–0.10 m and 0.10–0.20 m than with the rest of the borehole sections where the permeability contrast is more evident.

Using the specific capacities from all the single borehole tests in the column charge areas, Figure 9-6 is obtained. The resulting graphs show that *F*igure 9-6a shows more points around a 1:1 line, but the points are more scattered and the permeability contrast is not well expressed.

In general, all diagrams in Figure 9-5 and Figure 9-6 show that the specific capacity is much higher (several orders of magnitude) close to the tunnel floor, but the occurrence of these higher values is more frequent for the bottom charge areas compared with the column charge areas.

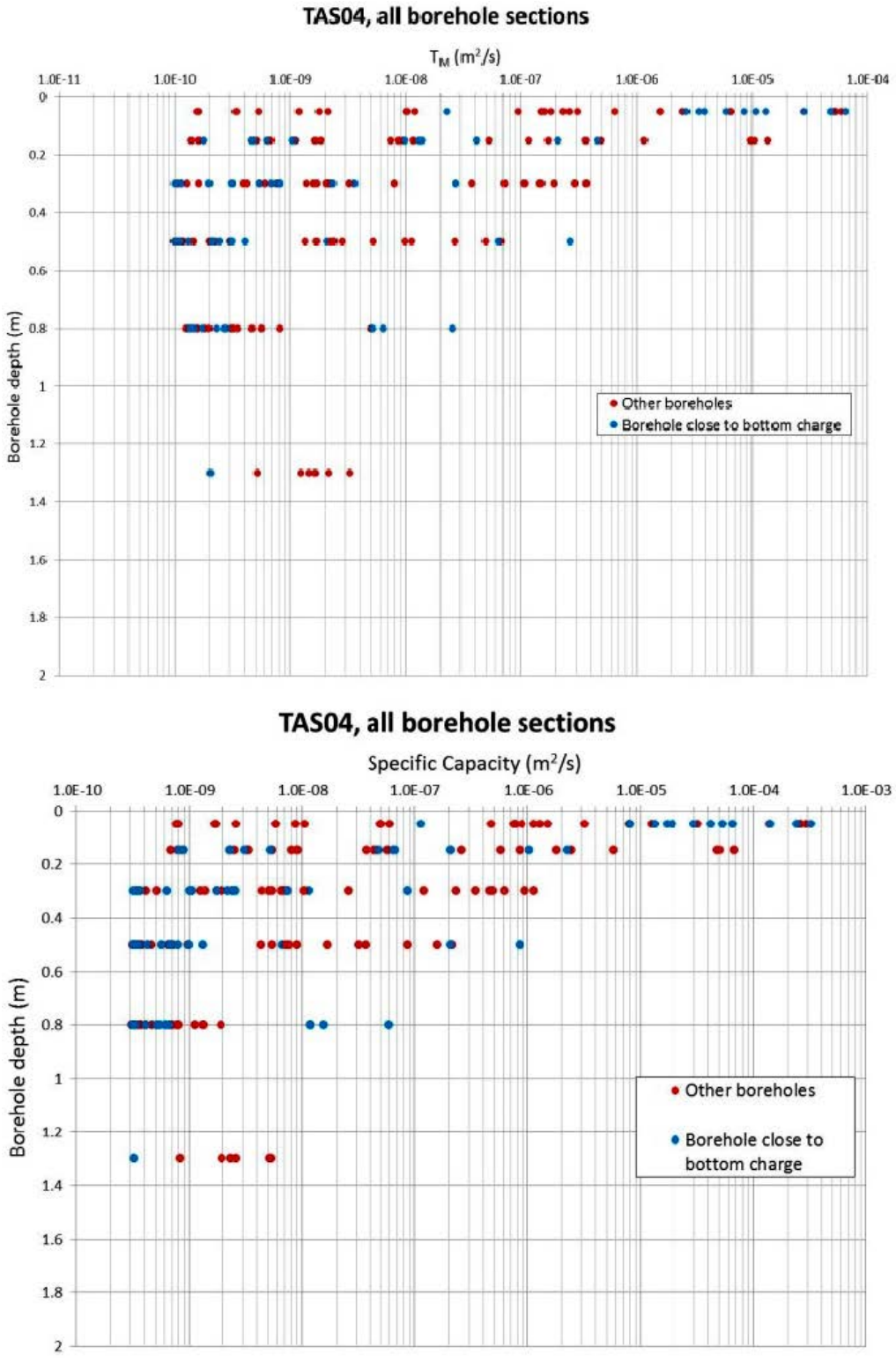

Figure 9-4. *Section transmissivity values, T_M, and specific capacity values versus depth for boreholes near the end of blast rounds with bottom charge holes (blue), and for holes within the column charge area (red).*

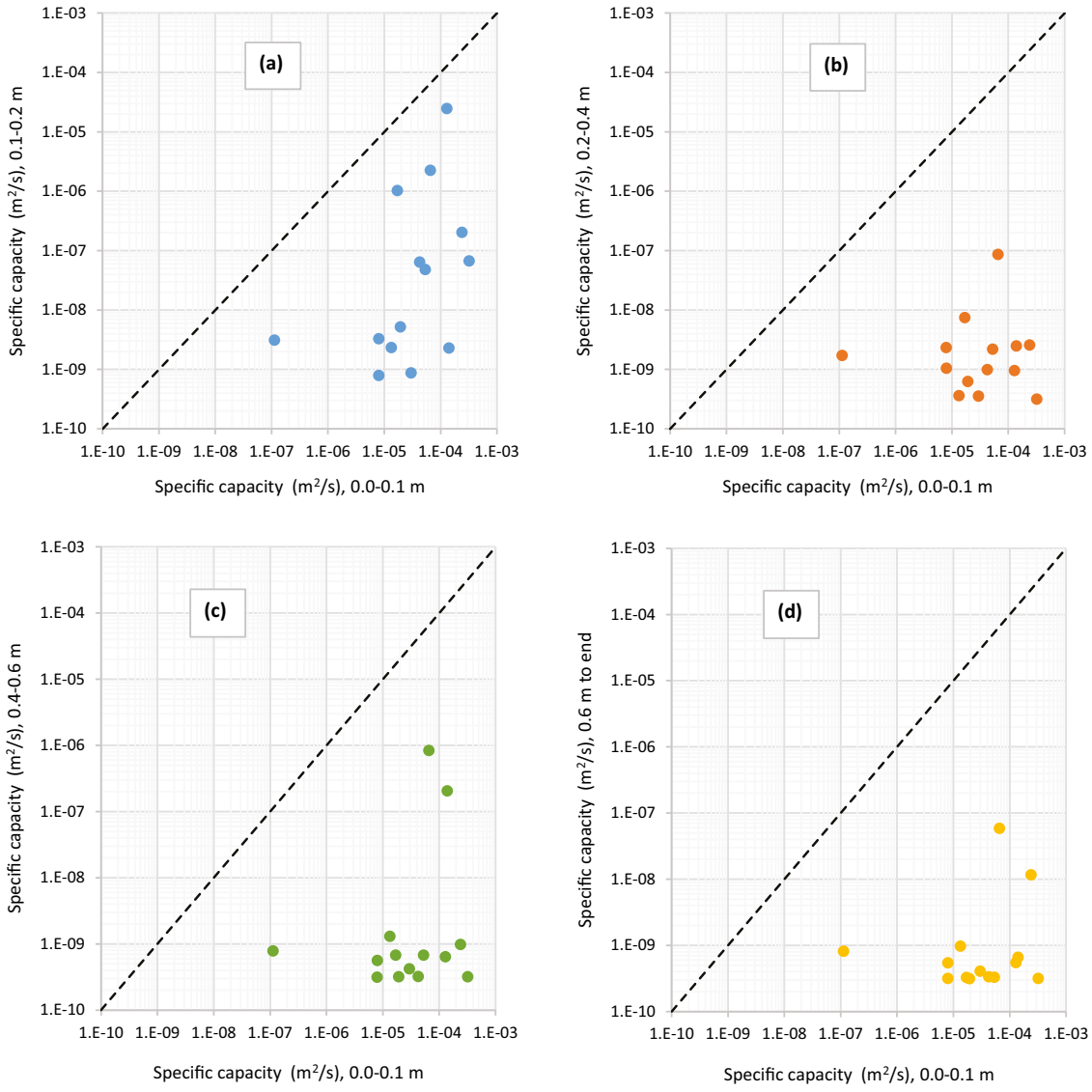

Figure 9-5. *Cross-correlation between the results obtained in different test sections below 0.1 m and the uppermost part, 0.0 –0.1 m. In these cases the boreholes are close to the bottom charge area.*

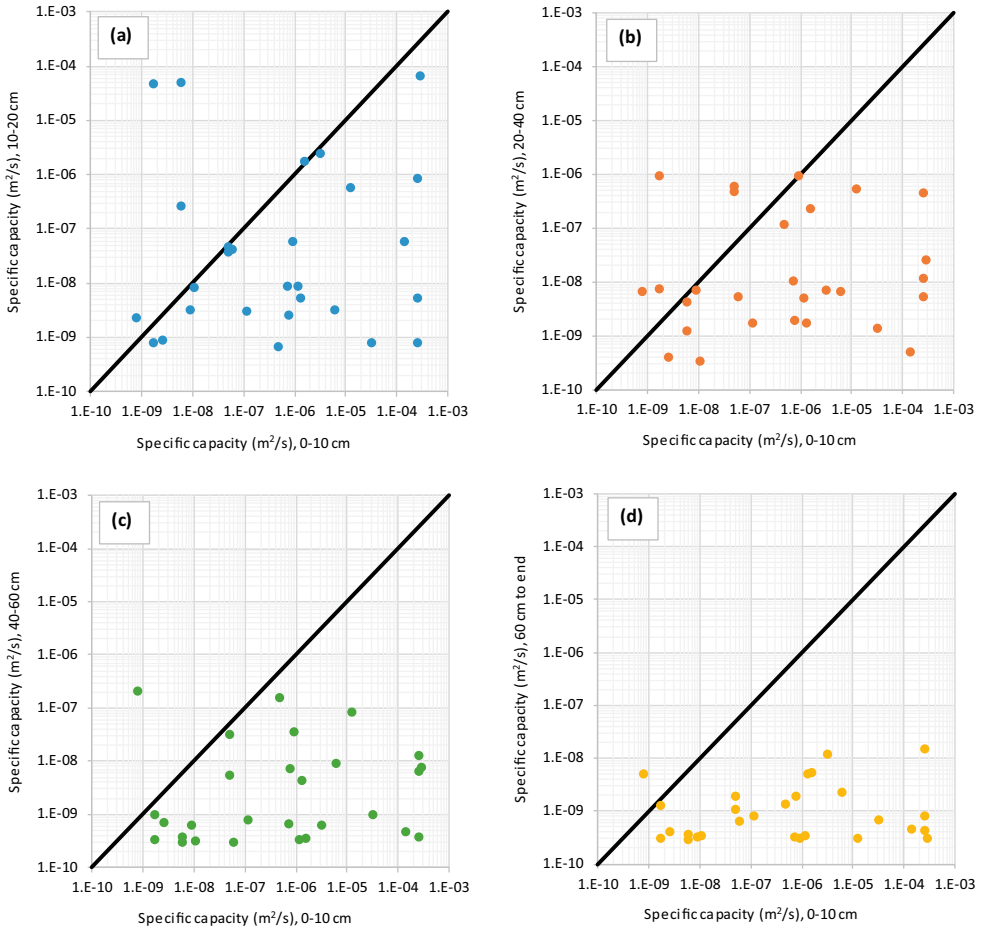

Figure 9-6. *Cross-correlation between the results obtained at 0.0 to 0.10 m and the column charge areas.*

An additional assessment of the confidence in permeability differences and depth dependence was performed as a simplified significance analysis. The analysis assumed the calculated section transmissivity values. Furthermore, the transmissivity values were assumed to follow a log-normal distribution. Figure 9-7 shows that the log-normal mean values for bottom charge areas are significantly (confidence level of 95%) higher than the values for the column charge areas at the uppermost level 0.0–0.1 m. At deeper levels, the discrepancies between the two charging classifications are not so obvious.

A simple way to indicate this behaviour was by comparing rock matrix hydraulic conductivity values from a drill core localized in the bottom charge zone with values from a drill core from the column charge zone, see Figure 9-7. The determination of hydraulic conductivity was done in a specially designed permeameter in the geo-laboratory at the Department of Civil and Environmental Engineering, Chalmers University of Technology (see Ericsson et al. 2009). The results in Figure 9-8 indicate comparatively higher matrix conductivity values in the bottom charge area down to approximately 0.50 m. A similar indication of zonation was also found for matrix porosity behaviour when a few samples from a bottom charge area were compared with samples from a column charge area, see Figure 9-9. The bottom charge area show higher porosity values near the tunnel floor compared with the column charge area.

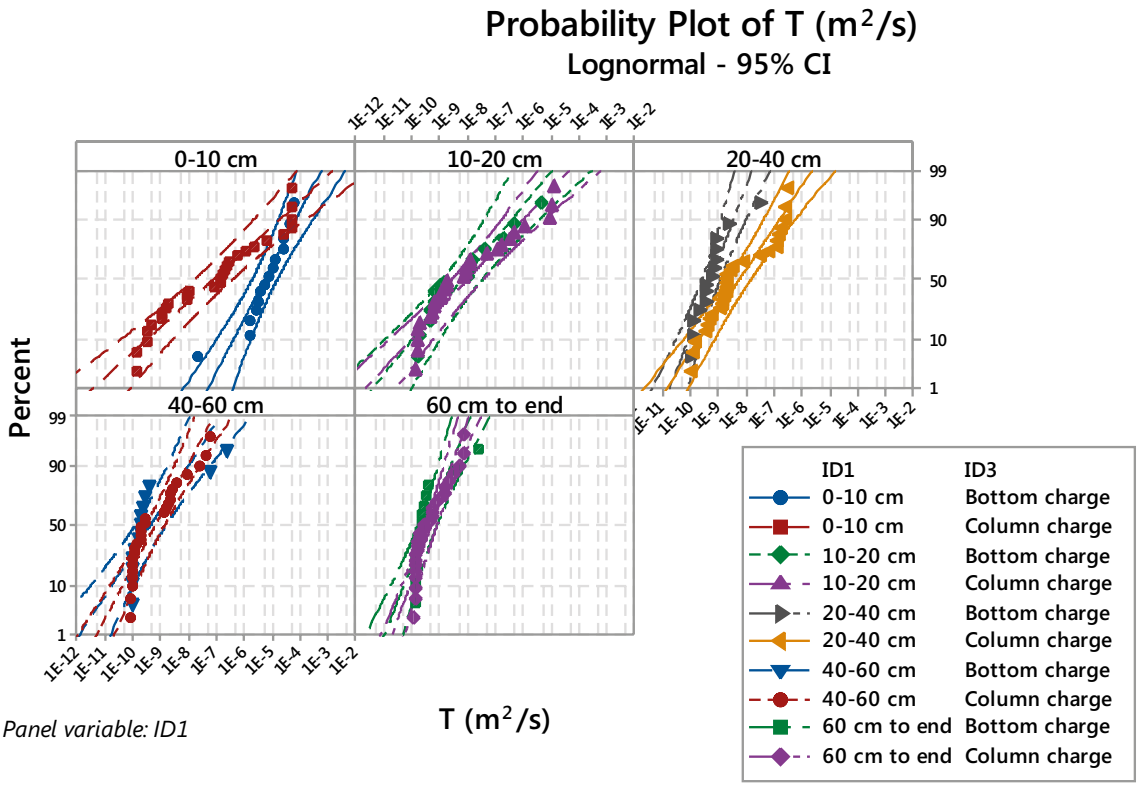

Figure 9-7. *Probability plots of the interpreted transmissivity values obtained from tests conducted in different sections with bottom charge areas and column charge areas, respectively. The lines show the 95% confidence interval.*

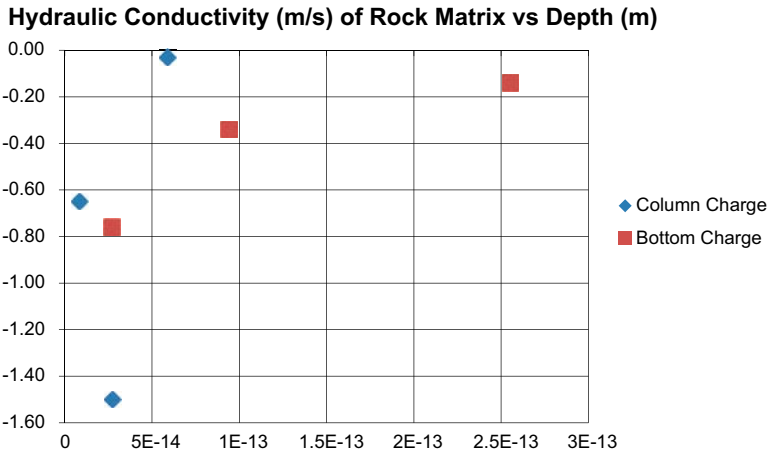

Figure 9-8. *Rock matrix hydraulic conductivity values from a dril core located in the bottom charge zone (Core K0423G03) compared with with a drill core from a column charge zone (Core K04021G02); Sample sizes: diameter 62 mm, thickness 10 mm.*

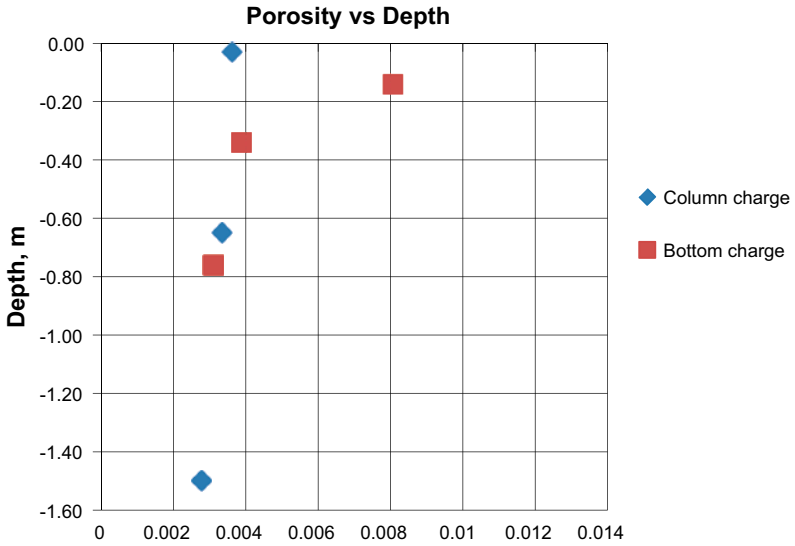

Figure 9-9. *Rock matrix porosity values vs. depth. Data from hole K04021G02 represent the column charge area while data from hole K04023G03 represent the bottom charge area in the tunnel floor.*

9.5.2 Zonation of transmissive conditions according to blasting impact

According to the results in the previous Section 9.5.1, the EDZ should be more visible close to the end of the blasting boreholes (bottom charge areas) and these sections of the tunnel floor should be more transmissive. These areas should show a greater spread in the section transmissivity distributions and a slightly wider connectivity range.

Figure 9-10 shows the blast rounds with the possible bottom charge zones and kriging interpolation results of the base-10 transmissivity values. The contour of the tunnel floor is also shown. The visual arrangement shows a clear correlation of the blasting effects and provides a deeper understanding of the heterogeneity and connectivity of the study site. Figure 9-10 shows that the most transmissive areas are located around the bottom charge zones, where most damage is expected to occur, and that the less transmissive areas are in between. The kriging results are indicative for a conceptual model where axial connectivity with regard to permeability is not continuous but shows intermittent behaviour. This verifies the results found by Ericsson et al. (2009), who concluded that the EDZ is indirectly indicated by microfractures with an extent of 25 cm to 35 cm from the wall of the studied tunnel at Äspö and that axial connectivity is not constant but shows intermittent behaviour around the tunnel contour.

9.5.3 Influence of blasting on shallow, transmissive fractures

It is well documented that blast-induced fracturing tends to form fractures sub-parallel to the tunnel contour, see Figure 9-11 and Figure 9-12. This is expected based on one of the main principles of blast design: the energy used shall be sufficient to create the intended opening. The consequence – that over-use of explosives causes damage to the tunnel contour with the risk of increased need of support – was first observed by Sjöberg et al. (1977).

The leakage to the tunnel floor was observed during the injection tests. All observed leakages are shown in Figure 8-19. The transmissivities of these leakages are shown in Figure 8-13. The transmissivity distribution with depth for these tests is also shown in Figure 9-19. There is a decreasing trend with depth of both the number of tests that leaked to the tunnel floor and their transmissivity.

It is not possible to correlate the leakage from individual tests to discrete fractures. But it is likely that the blast-induced fractures have a great impact on the dense occurrence of highly transmissive fractures/leakage points in the first few decimetres beneath the tunnel floor. These fractures are probably rather short (see Figure 9-11 and Figure 9-12) and must terminate at the tunnel contour, since they originate primarily from the perimeter blast holes. The limited extent of blast-induced fractures may also be a reason for the poor connectivity along the investigated area. The connectivity between induced fractures as well as between induced and natural fractures seems to be limited.

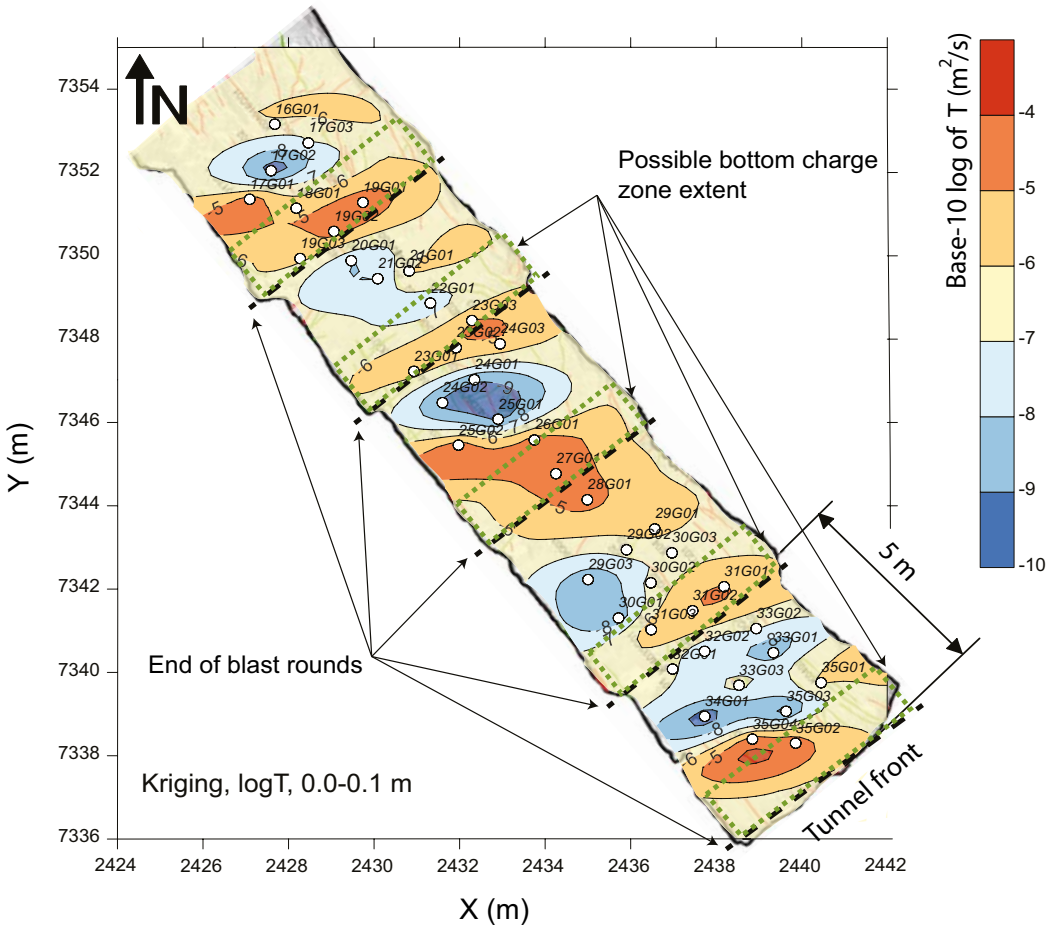

Figure 9-10. *Combined illustration of the kriging interpolation of the base-10 transmissivity values and the areas for possible bottom charge zones locations (dotted green lines).*

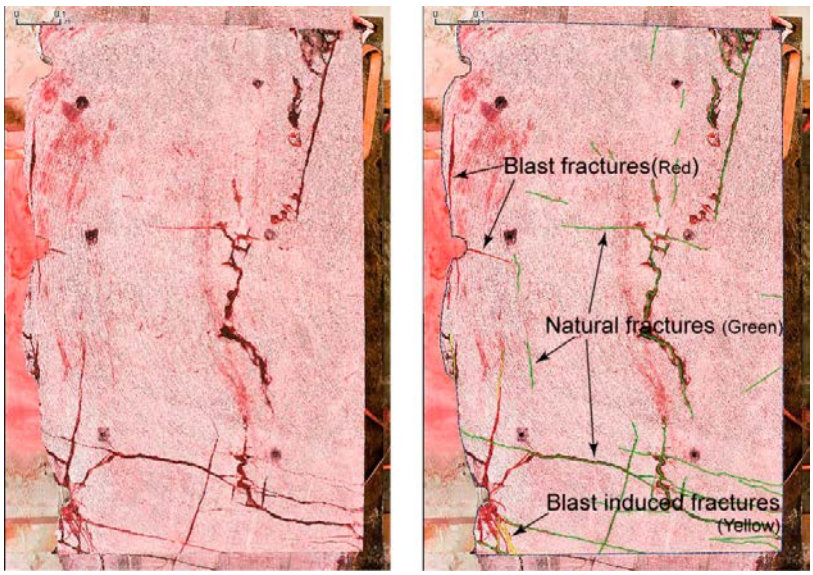

Figure 9-11. *A cross-cut in a tunnel wall at the Äspö HRL. An 8 m long section of a tunnel wall was cut down and sliced up into 76 slabs (Olsson et al. 2009). The fracturing was investigated by means of a penetrating dye, causing the red colour. Left: all fractures are shown dark red lines. Right: colour code for natural fractures (green), "blast fractures" originating from the perimeter holes on the left side of the samples (red) and other fresh fractures assumed to be blast-induced (yellow). Note that the tunnel contour (left side of the sample) is formed by blasting, i.e. it is a set of "blast fractures".*

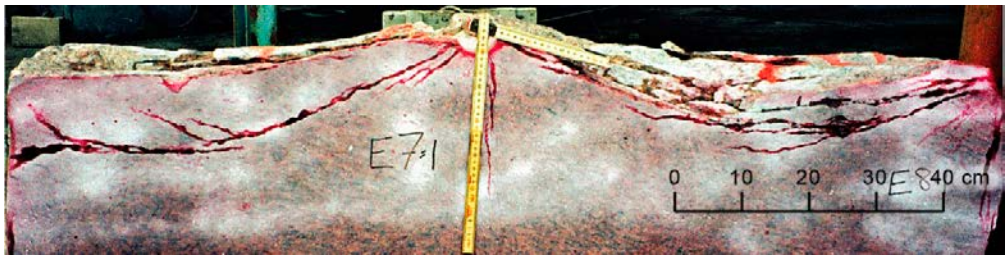

Figure 9-12. *A cross-cut through a bench in a quarry (Olsson and Bergqvist 1996).*

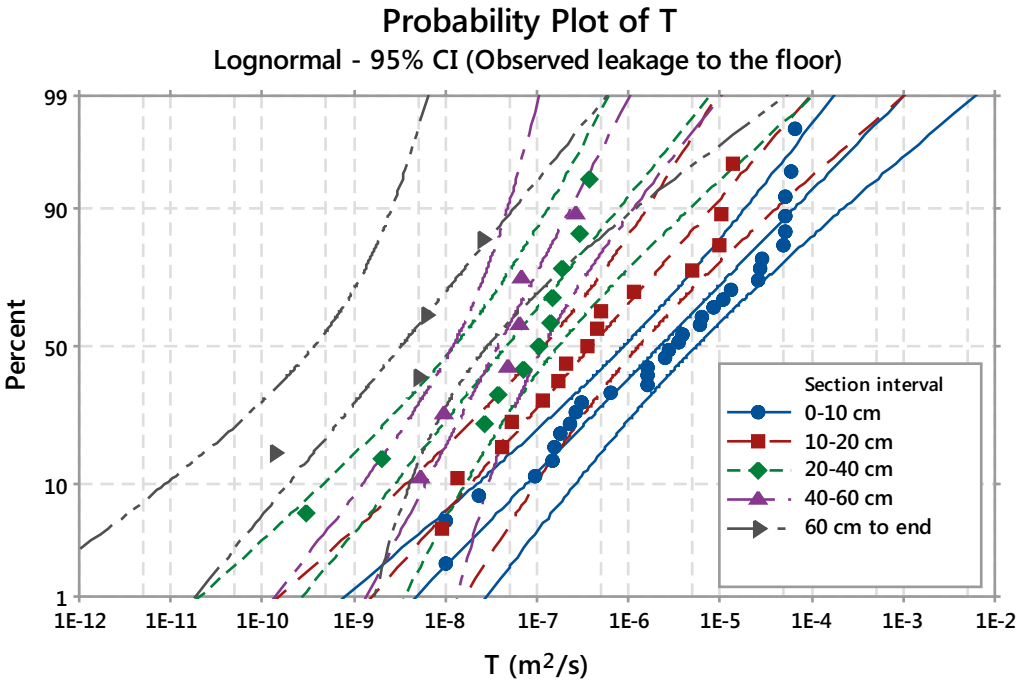

Figure 9-13. *Probability plot of the transmissivity with 95% confidence interval of all injection tests where leakage to the tunnel floor was observed, see Figure 8-13.*

9.6 Geology versus geophysics

Fractures mapped from the tunnel surface (floor) or short, non-oriented boreholes are most often steeply dipping in the data set from TAS04. GPR is best at detecting horizontal or sub-horizontal features, making a comparison of the interpreted results difficult. Furthermore, the use of different cut-offs in the methods – 1 m in surface mapping vs. 0.3 m in GPR reflector interpretation – makes the datasets look different.

In borehole mapping, the information gained from mapped features is limited to the borehole diameter, while GPR results are more extensive. Even though the cut-off used in GPR interpretation was as low as 0.3 m, there are a significantly smaller number of reflectors penetrating the boreholes than mapped fractures, probably because many of the fractures mapped from cores are small and/or their properties are not suitable for reflection. Reflectors that penetrate a borehole may be correlated to a core-mapped fracture, but in this case only the angle between fractures and the vertical cores was measured. This made a detailed correlation between GPR reflectors and mapped fractures impossible.

Drilling was done using a single drill tube, which often produces mechanical breaks in the core that are difficult to distinguish from other fresh fractures caused by blasting (if no fracture filling is present). In the case of a fracture with filling minerals, it is also difficult to separate blast-induced

re-opening from mechanical breaks during core handling if there is no evidence of movement in the fracture surface that would indicate the existence of the open fracture prior to blasting. In GPR, the reflections are caused by contrast in conductivity and dielectric permittivity, which in fractures are usually correlated with water in the fractures or electrically conductive fracture-filling minerals (e.g. clays, pyrite, pyrrhotite and graphite), or even air in the case of fractures close to tunnel surfaces. Normally, GPR information cannot be used to determine the fracture-filling material, which makes it difficult to compare these two datasets.

The rock type contacts and larger structures in the area are steeply dipping, which means that a direct indication in the form of a reflector is difficult to obtain from the GPR results. The interpreted sub-horizontal reflectors do not follow the rock type contacts, which could mean that these structures are younger than the steeply dipping structures. This is in line with the common understanding at Äspö.

The correlation between the GPR EDZ depth image and the lithology of the floor is in part quite good. At some locations, the more fractured fine-grained granite appears as an anomaly in the GPR EDZ image. An example of this is shown in Figure 9-14, where the photograph from section 27–30 m is compared with the GPR EDZ result. The section includes a deformation zone that is limited by cataclasite fractures/bands filled with epidote, delimited between the light blue lines in the photo. Inside the zone there are enclaves/fragments of less transformed Äspödiorite, which is not as broken-up as in the more oxidized part of the zone. The more broken-up part is visible in the GPR EDZ image (circled with yellow). Outside the zone, the fine- and medium-grained granite is more fractured with short fractures than other rock types. This can also be seen in anomalies in the GPR EDZ image, marked with red circles in the figure.

In general, both geological mapping of cores and GPR results indicate that the uppermost part of the floor is more fractured than the deeper parts. The uppermost 20–30 cm in the GPR image, and in drill core mapping the upper 20 cm, seems to be more fractured.

Later, Ittner and Bouvin (2015) conducted investigations of fractures in wire-sawed slots at the tunnel surfaces, Figure 9-26. In that study, a total of 5 slots were made, four of which were in the TAS04 tunnel and two were in the tunnel floor in the same area as in this study.

Fracture mapping in the slots was done by applying a dye penetrant to the sawed surface, which makes the fractures more visible and permits mapping of even small, fractures,Figure 9-27. The fractures were divided in the interpretation into two groups, excavation fractures and natural fractures, and are marked with different colours in the resulting photographs.

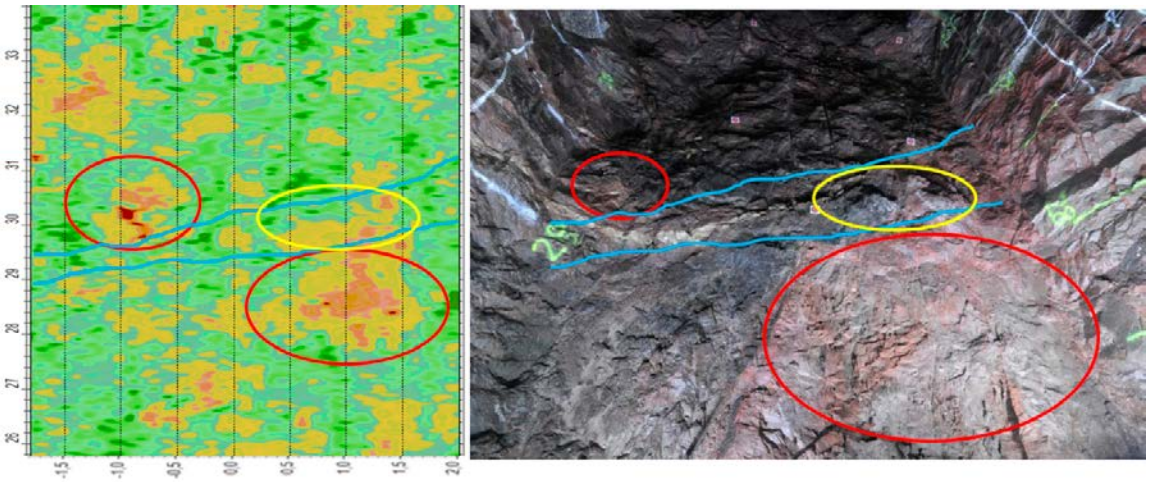

Figure 9-14. *Photograph of the floor in section 27–30 m in TAS04 compared with GPR EDZ depth image.*

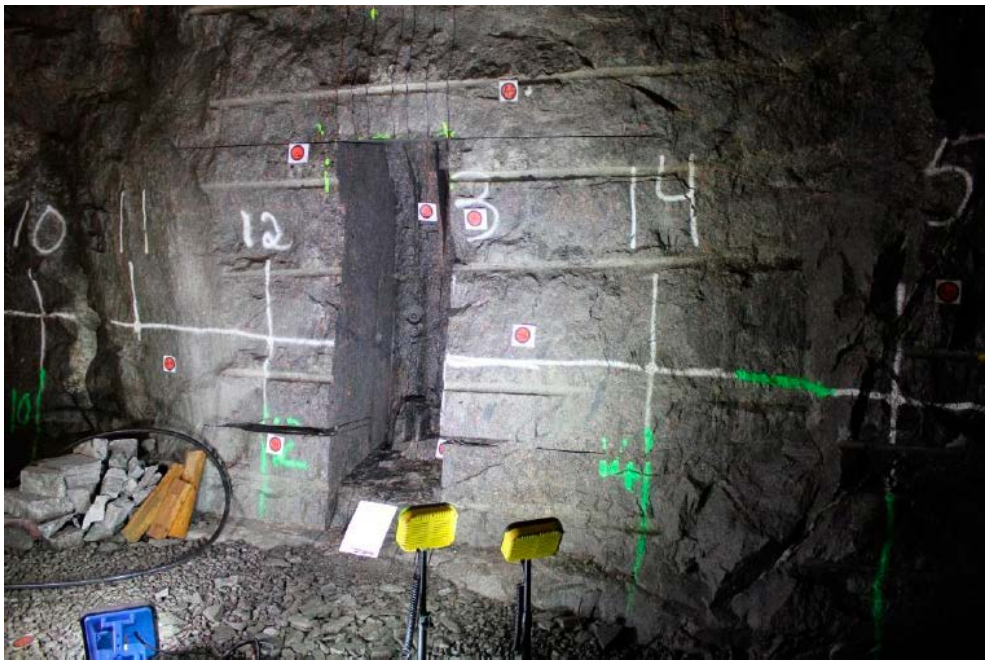

Figure 9-15. *Photograph of a sawed slot at tunnel wall in TASN (Ittner and Bouvin 2015).*

When the fractures interpreted from the sawed surfaces are viewed together with the interpreted reflectors from the GPR results, some observations can be made. From Figure 9-16 it is obvious that more features are visible in the sawed surface than can be interpreted from GPR. The resolution in GPR does not allow detection of small and very tight fractures, which use of the dye penetrant does. Looking at the right-hand side of Figure 9-16 there seems to be a continuous sub-horizontal fracture (marked with yellow arrow) that is not detected by the GPR. This could be explained by two facts. First, the fracture seems to be dry at this part of the cut. On the left part of the surface (marked by the yellow circle) there is a similar fracture, but wet, and an interpreted reflector coincides with it. Second, above this fracture there is a fracture swarm as well as excavation fractures that could attenuate the GPR signal and thus prevent detection. The attenuation effect can also be seen at the left below the previously mentioned fracture, where no reflector exists.

Looking closer at the large sub-horizontal fracture marked by a yellow circle, we see a small difference in the location of the reflector. This may be due to the dip error discussed in Section 7.2, but it may also result from the fact that the radar wave velocity used in GPR interpretation is too high in this case.

Figure 9-16. *A photograph showing a sawed slot in the floor of TAS04 at tunnel length 34 m. The interpreted fractures from Ittner and Bouvin (2015) are marked with green (natural fractures) and yellow (excavation fractures). The light blue lines are reflectors that intersect this section.*

9.7 Geology versus hydrogeology

A map of the rock types in the floor of TAS04 is presented in Figure 6-2. The main rock types are fine-grained granite, diorite and granodiorite.In the boreholes, the fine-to-medium-grained granite is divided into two different types based on colour differences, red versus lighter red. Although "red granite, fine-to-medium-grained" usually has more fractures than "light red granite, fine-to–medium-grained", the estimated transmissivity properties do not seem to support this, assuming that these fractures are conductive. Furthermore, the Äspö diorite and Ävrö granodiorite usually contain open fractures with fracture fillings. The estimated transmissivity properties in boreholes with these rock types do not appear to differ markedly from those of boreholes in other rock types, see Figure 9-17.

The terminology used in Boremap mapping (in boreholes) differs somewhat from that used in RoCS mapping (at the tunnel floor), especially when it comes to fractures, see Section 6.1. This should be taken into account when comparisons are made between different types of fractures and their hydraulic properties.

One of the possible explanations for the observations of high transmissivities in sections with "no fractures" is that the tunnel mapping procedure (RoCS mapping) applied a cut-off and only mapped visible fractures that were 1 m or longer in length. Many shorter fractures are therefore not mapped, and some of them may very well be open and interconnected, explaining the transmissivity. As explained before, RoCS mapping designates sealed fractures as tight, while the same fractures are called unbroken in Boremap mapping (one of the differences between core mapping and surface mapping). One of the explanations for the transmissivity in sections with unbroken fractures in the core is of course hydraulic channels, but whether they are in the form of short minor fractures in the adjacent rock or partly broken/open fractures is an open question.

Figure 9-18 below presents an interpretation of the same data as reported above based on an examination of the fracture's geometricdistribution along the holes and its position relative to the sectional boundaries, together with hydraulic responses in the surrounding holes and leakages to the tunnel floor. This interpretation is, however, only made for transmissivity values > $1.0 \cdot 10^{-9}$ m^2/s. Values below this limit are relatively close to the lower measurement limit for the measurements.

A large fraction of the superficial sections have fractures that are in contact with the tunnel floor and have high transmissivities for that reason. In the water-conducting sections, transmissivity decreases with depth. The graph shows that a high percentage of sections down to a depth of c. 0.5 m (section 0.4–0.5 m) are categorized as "Unbroken fractures", but are nevertheless water-conducting. The water is probably transported in small channels

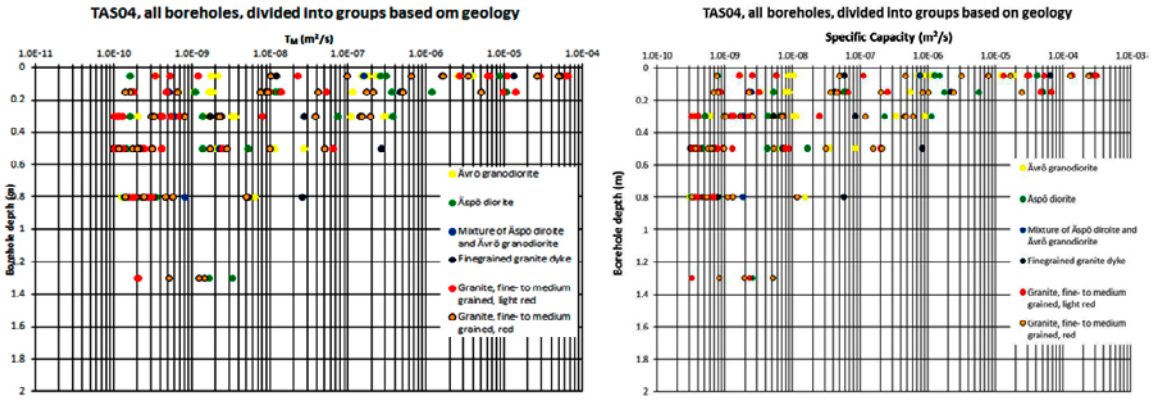

Figure 9-17. *Section transmissivity and specific capacity versus depth for different types of rocks.*

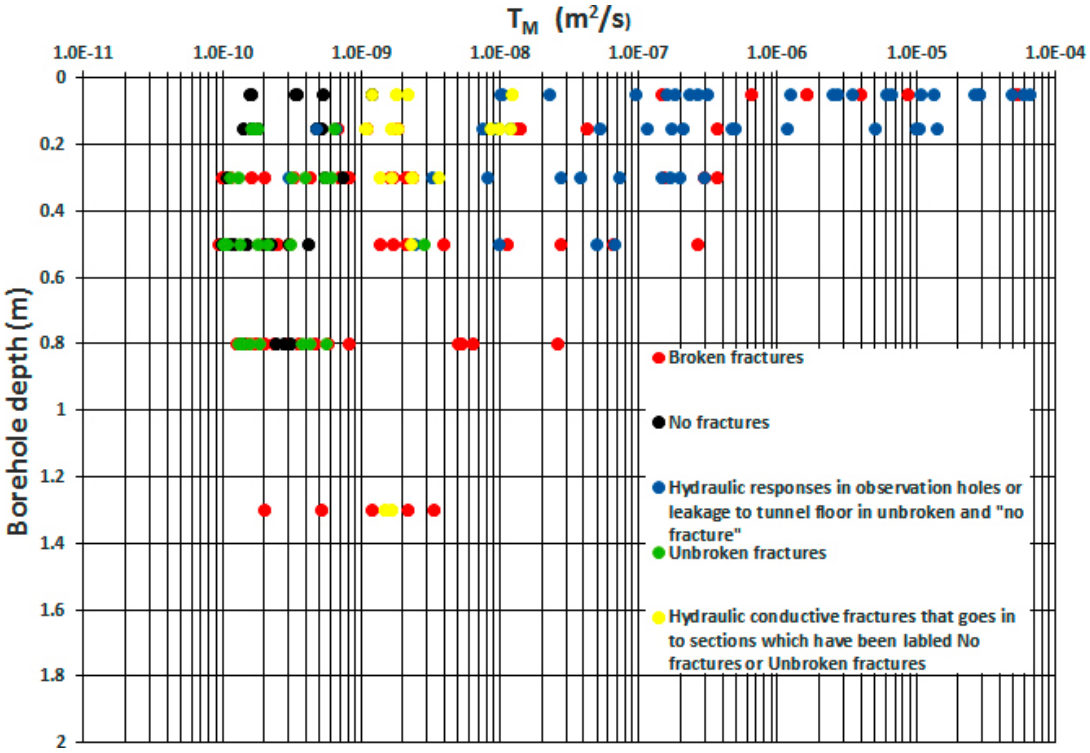

Figure 9-18. *Section transmissivity versus depth. The groups are based on: mapped type of fractures, distribution of fractures along holes and hydraulic responses in the observation sections or in the tunnel floor.*

In the mapping of fractures in the tunnel floor, the fractures were classified as “tight” (sealed) and “open”. The fractures that were mapped in the tunnel floor had lengths of one metre or longer. Figure 9-19 shows mapped fractures in the tunnel floor with marked leakage points (black lines with blue dots).

Figure 9-19 is a plan map, which means that the various leakage points reported for a borehole may come from different sections of the boreholes. However, no leakages are indicated in the figure at the edge of the borehole extender seal.

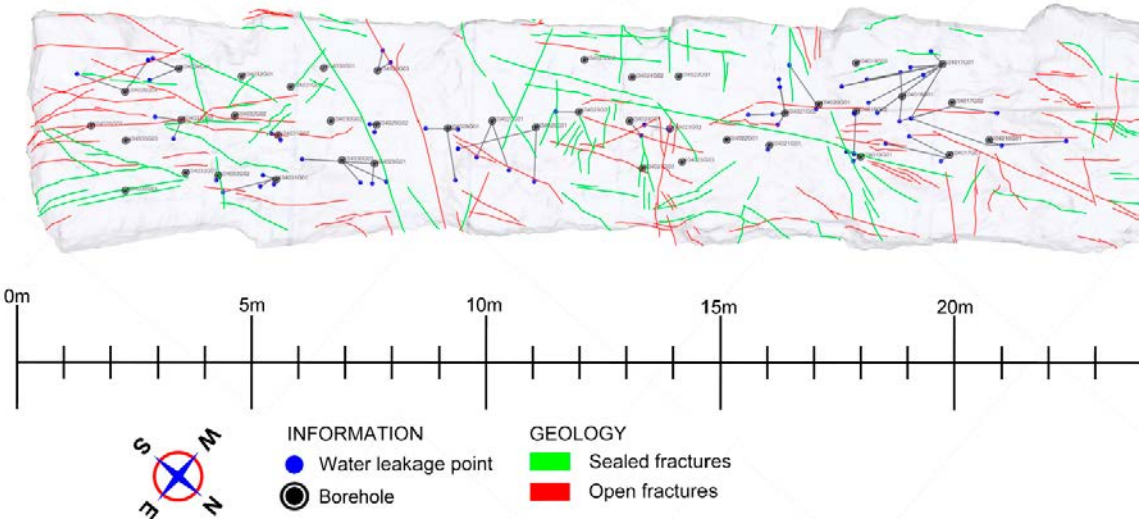

Figure 9-19. *Mapped fractures in the test area together with leakage points obtained by injection tests in the boreholes. The leakage points shown are located outside the sealing unit of the borehole extender.*

The RoCS mapping only mapped fractures that were visible to the naked eye (i.e. fractures with an aperture and/or mineral filing) and more than 1 m in length on the tunnel floor. The EDZ fractures were probably not mapped at all. The EDZ fractures form as a result of blasting and are therefore mostly, or at least in many cases, short, showing little aperture and often without any mineral fillings. The interpretation of leakage points in Figure 9-19 is:

- there are leakage points in parts of open fractures as mapped in the RoCS mapping,
- there are leakage points in close proximity to tight fractures in the RoCS mapping. The reason for this is probably that water comes up in fractures in close proximity to these tight fractures, which have a shorter length in the tunnel floor than 1 m and/or are not documented, and
- there are leakage points at places where no fractures are mapped. The reason for this is that water comes up in fractures that have a shorter length in the tunnel floor than 1 m.

In Section 6.2.3 a network of fractures is reported from the current rock volume. It is based on mapped fractures from the tunnel floor, where fracture properties as well as strike and dip are noted. Relatively steep fractures dominate the obtained mapping results. Since the boreholes are mainly vertical, correlating fractures mapped in the tunnel floor to fractures in the boreholes is difficult.

9.8 Geophysics versus hydrogeology

In this study, the hydraulic responses are visualized in the 3D model (Appendix 2) as straight lines between boreholes or between boreholes and leakage points in the tunnel floor, see Figure 9-20. The line is shown in the middle of the test section. In observation holes the connection line is at a depth of 0.55 m in 1 m deep boreholes and at a depth of 0.95 m in 2 m deep boreholes. In reality hydraulic connections follow fracture surfaces or channels, which means that the actual connection might not be as straight. This must be taken into account when comparing GPR results with hydro tests.

Figure 9-20 shows a figure combining hydraulic responses and interpreted distinct reflectors from GPR results in a plan view The figure includes all reflectors and all pressure responses from different depths. The map shows a good fit between areas with more GPR features and areas with hydraulic connections. Features close to the surface are underrepresented in GPR results, making it is difficult to compare hydraulic connections in the uppermost section (0–0.10 m) or connections to the surface. The map also shows that most of the boreholes without hydraulic responses are outside the areas covered by reflectors, or if a reflector exists it is an isolated, single reflector. This could indicate that the hydraulic responses and intersecting reflectors are correlated.

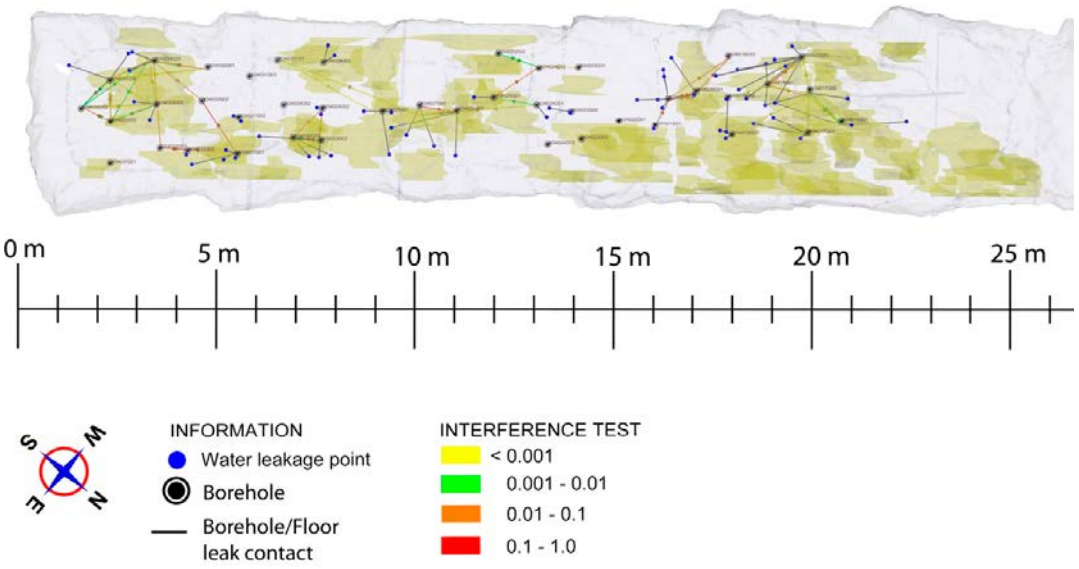

Figure 9-20. *Plan view showing areas where interpreted GPR reflectors exist (green patches), together with classified relative pressure responses, dP_{obs}/dP_{inj}.*

If GPR EDZ results are compared with hydraulic response information (Figure 9-21). similar conclusions can be drawn. Areas where the GPR EDZ response indicates a deeper EDZ often coincide with borehole responses.

The depth determination for reflectors is based on the radar wave velocity (travel time) in the medium, which is governed by the medium's dielectric properties (see Section 7.1). In the case of inclined structures, the reflection from each source point comes from the direction normal to the structure. This means that the true location and inclination of inclined reflectors are not correct. The error is greater for more inclined reflectors. This error is not corrected for in the reflector interpretation, but has been taken into account when comparing GPR and hydrogeology.

Observations from hydro tests and geological mapping in core boreholes can be used to evaluate the capability of GPR to determine the position and extent of structures. In order to analyze possible connections, diagrams were made showing the correlation between reflectors and section transmissivities. The same section intervals were used as those used in the hydrogeological tests (0–0.10, 0.10–0.20, 0.20–0.40, 0.40–0.60 m), and the diagrams show the number of borehole test sections penetrated by GPR reflectors and the section transmissivity distribution in sections (Figure 9-22).

In the case of the uppermost section (section 0–0.10 m), it is difficult for GPR to show representative results. This can also be seen in the diagrams below. Only roughly half (or fewer) of these shallow sections are penetrated by any reflector for all transmissivity intervals. In the deeper sections the situation is somewhat different.

The diagrams show that in section 0.10–0.20 m, GPR detected at least one reflector intersecting all 17 boreholes where the transmissivity is greater than 10^{-9} m^2/s. Furthermore, GPR detected a reflector in 82% (14 of 17) of all sections where the transmissivity is higher than 10^{-9} m^2/s. The corresponding figure for sections with a transmissivity higher than 10^{-8} m^2/s is 91% (10 sections of 11).

In borehole section 0.20–0.40 m, all 10 holes where the transmissivity is higher than 10^{-9} m^2/s were indicated by GPR. In sections where the transmissivity is 10^{-9} m^2/s or higher, a reflector intersects the section in 70% (7 out of 10) of the cases. In sections where the transmissivity is higher than 10^{-8} m^2/s, a reflector intersects the section in 6 out of 7 cases (86%).

In borehole section 0.40–0.60 m, all 6 holes where the transmissivity is higher than 10^{-9} m^2/s were indicated by GPR. In sections where the transmissivity is 10^{-9} m^2/s or higher, a reflector intersects the section in 33% (2 out of 6) of the cases. In sections where the transmissivity is higher than 10^{-8} m^2/s, no reflector intersects the section. This section is not taken into account in the general conclusions below due to the small number of cases.

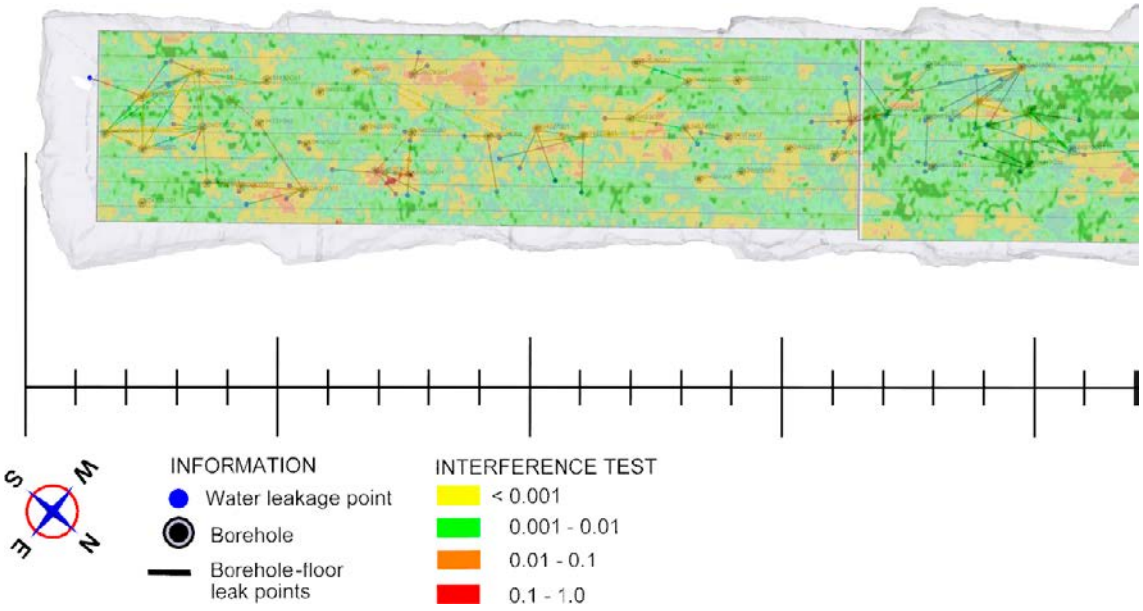

Figure 9-21. *GPR EDZ topographical map shown together with relative pressure response results.*

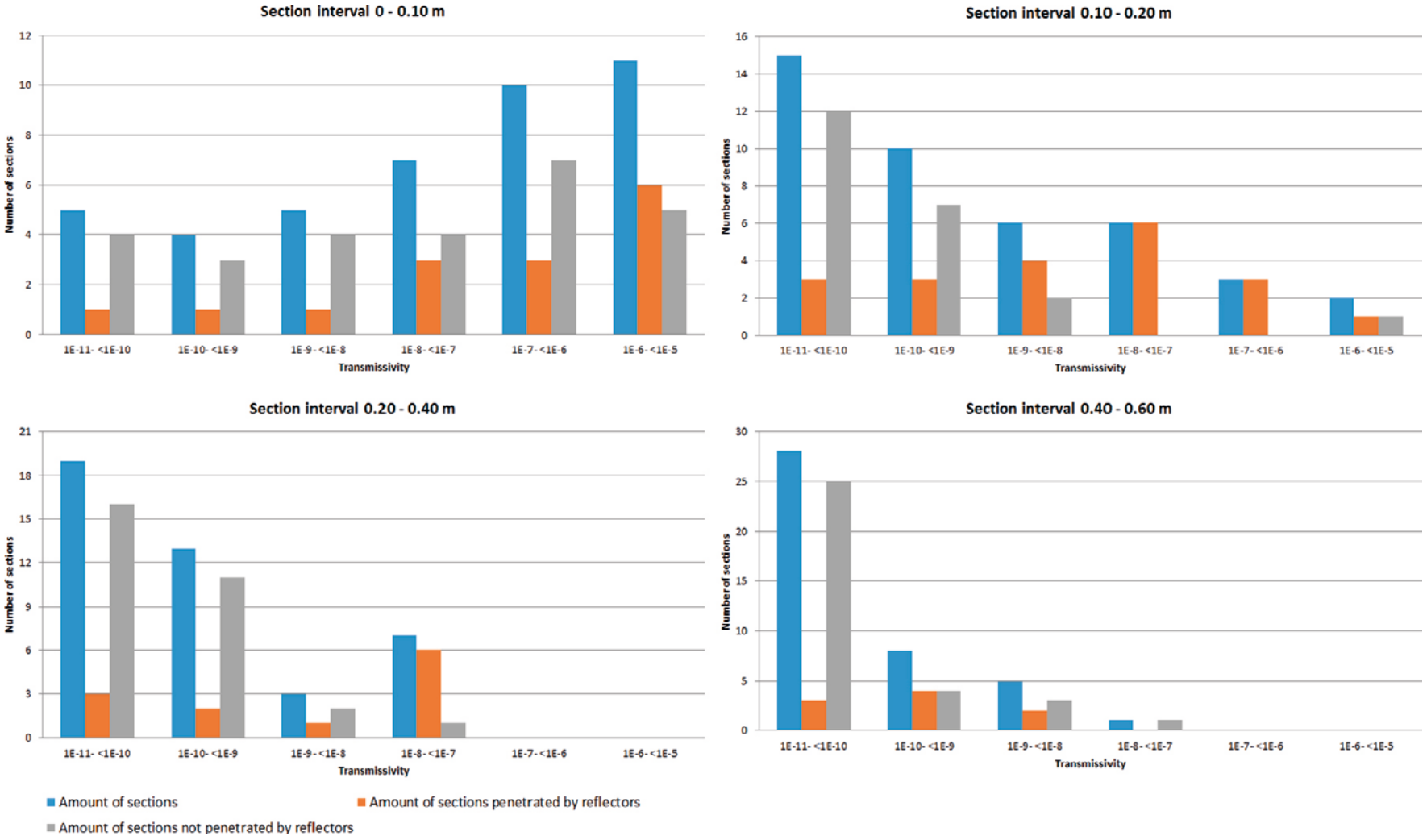

Figure 9-22. *Diagrams for sections 0–0.10, 0.10–0.20, 0.20–0.40, 0.40–0.60 m in boreholes showing number of sections for transmissivity intervals 10^{-11}–10^{-10} m^2/s, 10^{-10}–10^{-9} m^2/s, 10^{-9}–10^{-8} m^2/s, 10^{-8}–10^{-7} m^2/s, 10^{-7}–10^{-6} m^2/s, 10^{-6}–10^{-5} m^2/s. Dark blue marks the number of sections per transmissivity interval, orange marks the number of sections penetrated by at least one reflector. Grey marks the number of sections in boreholes that are not penetrated by a reflector.*

The following conclusions can be drawn from the results presented above and the existing location of the boreholes at the site for depth intervals 0.1–0.2 m and 0.2–0.4 m:

- There is a clear indication of a correlation between transmissivities higher than 10^{-9} m^2/s and interpreted reflectors.
- The GPR measurements can with high probability indicate where to locate boreholes to measure the transmissivities of hydraulic conductors with transmissivities higher than 10^{-9} m^2/s. The locations of the holes can be optimized from the information gained from GPR results concerning the location and the extent of the reflectors.
- Areas at the test site where there are several reflectors on top of each other are more likely to have a higher summed transmissivity and be connected over a larger volume than areas with a single reflector.
- Water-conducting structures are good candidates for detection by GPR, provided they have a geometry suitable for GPR (sub-horizontal). It is not possible to assign transmissivity values to the reflectors based solely on GPR data, however.

In order to enable more confident conclusions to be drawn, the dataset should be broadened with new boreholes in areas with and without reflectors.

To study whether the interpreted reflector could be the structure responsible for the measured transmissivity, a visual comparison between hydraulic responses and reflectors was made for some sample cases. Most of the fractures have a limited extent, which means that there are often more fractures involved (intersecting) in the hydraulic responses. If vertical fractures are involved in the hydraulic responses, no reflector can be directly detected from that structure. It is also evident from the GPR results that one reflector is often not enough to explain all responses. The extent of a reflector may be greater in reality than interpreted; the interpretation only shows where it is detected.

Figure 9-23 and Figure 9-24 show the responses in neighbouring boreholes when water is injected into borehole 34G01, section 0.1–0.2 m. A hydraulic response was observed in boreholes 32G01, 33G01, 32G02 and a weaker response in 35G04. Looking at the GPR results, we have a reflector intersecting the injected section which almost reaches 32G01. There are also two other reflectors present that could, together with other structures (smaller, intersecting fractures) explain the responses in 32G02 and 33G01. Between 34G01 and 35G04 there is a reflector that might be a structure for the flow path. In the geological mapping, a smooth joint (fracture 22, strike 197 (RT90), dip 20 degrees) could be part of this fracture system. In the deeper sections no reflectors were detected, even though there are hydraulic responses deeper down. The transmissivity in the section is low, and strong reflectors in the upper part may attenuate the signal from deeper sections, which could explain the lack of reflectors there.

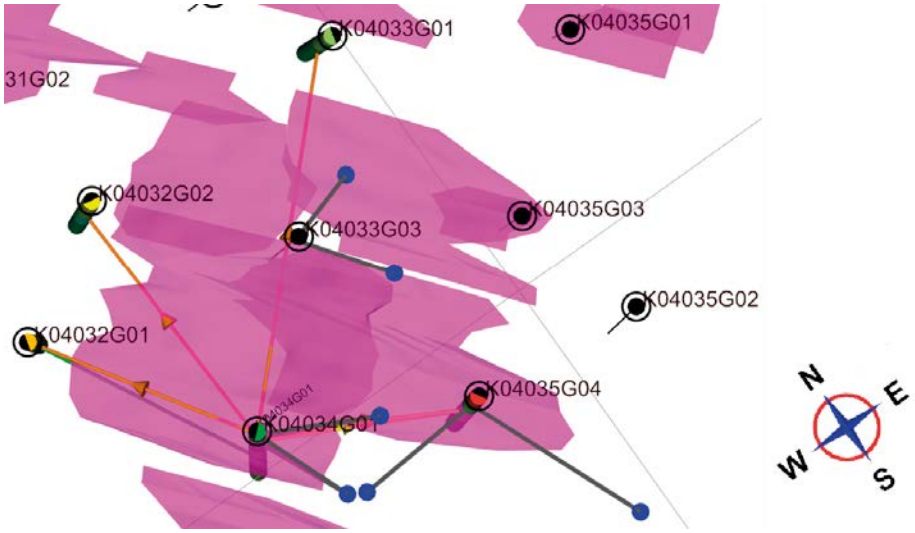

Figure 9-23. *Detailed top view of responses from the injection test in section 0.10–0.20 m in borehole 34G01 together with interpreted reflectors.*

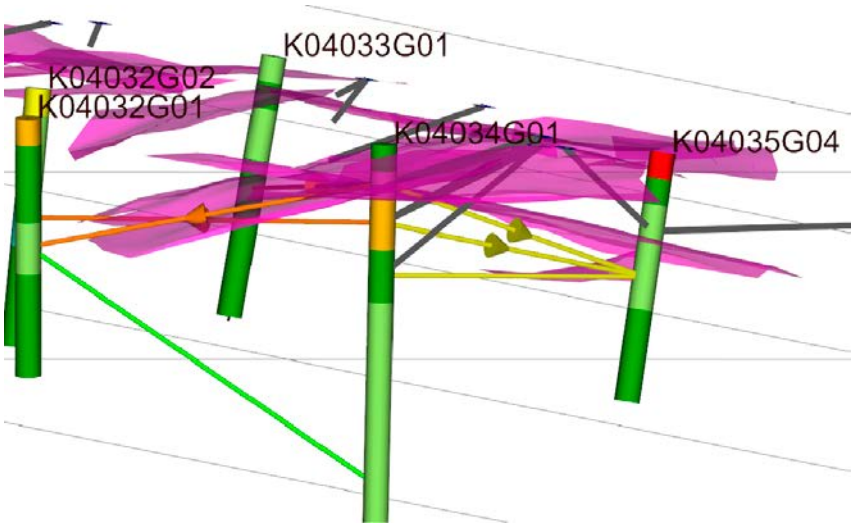

Figure 9-24. *Detailed side view of responses from the injection test in section 0.10–0.20 m in borehole 34G01 together with interpreted reflectors.*

Figure 9-25 shows the hydraulic responses from the injection test in borehole 35G04, section 0.4–0.6 m, together with the interpreted GPR reflectors. Responses were observed in neighbouring boreholes 35G02, 35G03 and 32G01. Between 35G04 and 32G01 there are two sub-horizontal reflectors intersecting each other that may be related to the hydraulic connection. Between 35G04 and 35G03, several reflectors may be related to the connection. No reflector is observed in the vicinity of 35G02.

Responses from the injection test between borehole 29G01 section 0.1–0.2 m and borehole 30G03 are shown in Figure 9-26 (a red arrow indicates this connection). Here a network of reflectors may be in contact with the boreholes and with each other, which could explain the connection response.

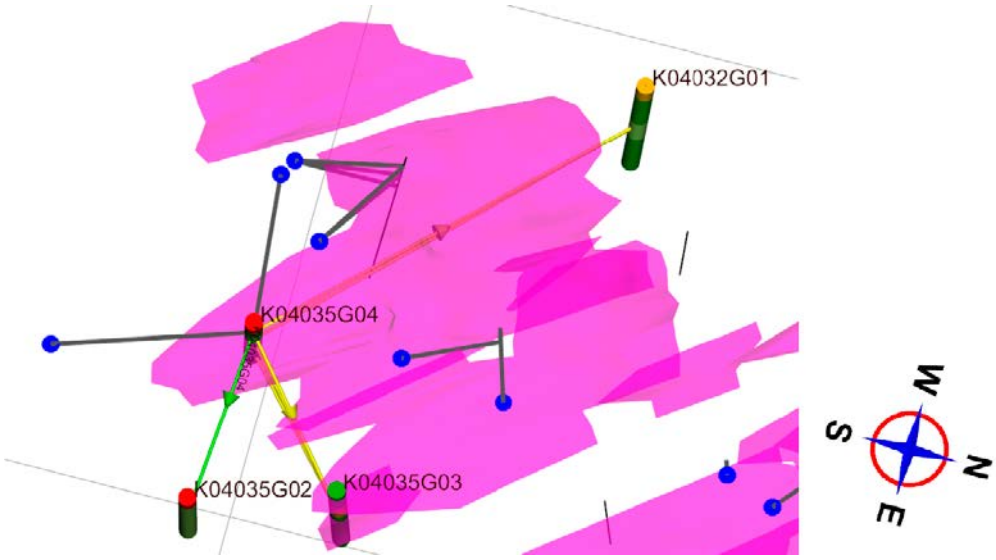

Figure 9-25. *Detailed view of responses from the injection test in section 0.40–0.60 m in borehole 35G04 together with interpreted reflectors.*

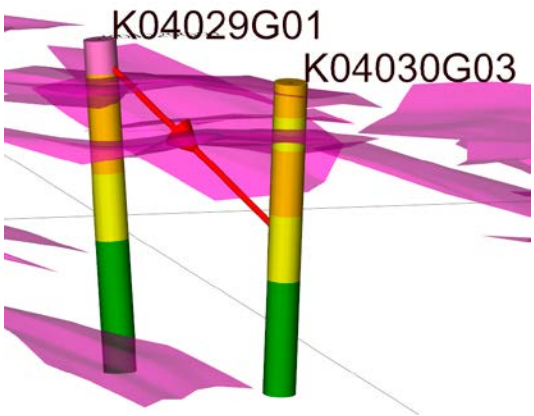

Figure 9-26. *Detailed view of responses from the injection test in section 0.10–0.20 m in borehole 29G01 together with interpreted reflectors.*

Figure 9-27 shows a comparison between the GPR EDZ response depth map and the kriging interpolation results taken from 0 to 0.4 m. This figure shows a weak relationship between the extents of the highly transmissive areas ($T > 10^{-6}$ m^2/s), but a better relationship exists between low-transmissive areas and the superficial responses in the GPR results. This could imply that the location of the weakest anomalies indicates a region where it is likely that a relatively tight rock mass can be found. If this is true, it should be possible to use a co-kriging between the GPR results and the kriging (T) results in order to show how the transmissivity varies in those places without hydraulic test results. However, further investigation is needed in order to draw firm conclusions.

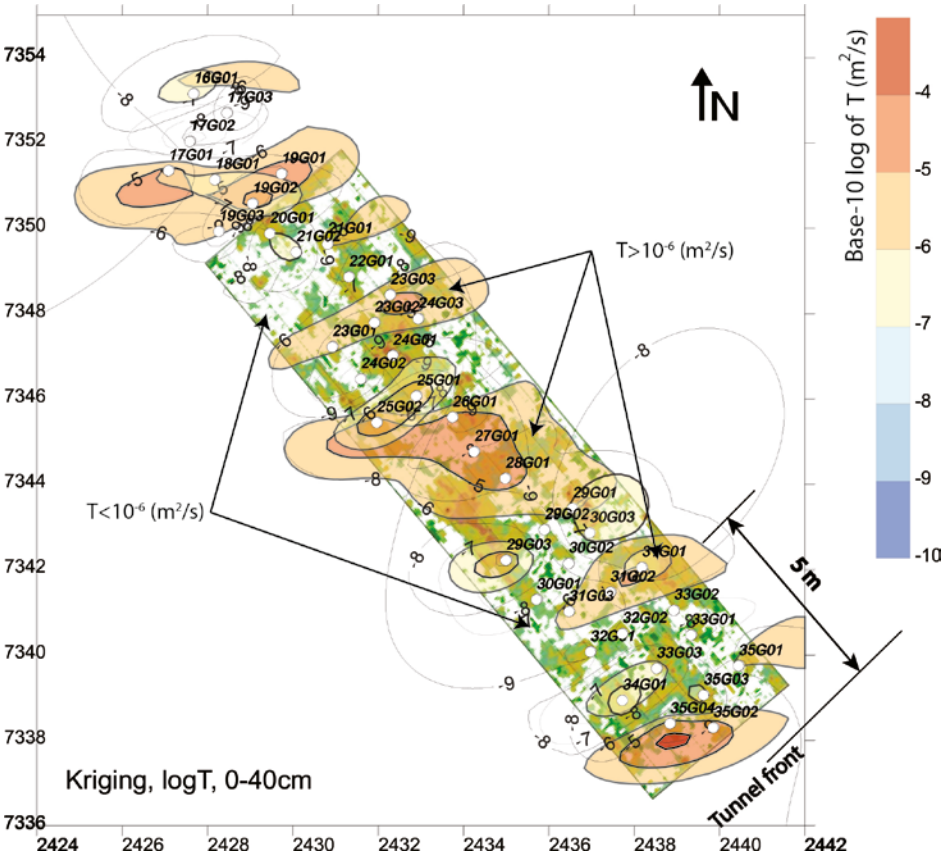

Figure 9-27. *GPR EDZ response depth map shown together with all kriging interpolation results from 0 to 0.4 m. The GPR map shows areas where interpreted GPR reflectors exist (green patches). The kriging interpolation results are superimposed over the GPR response depth map and are indicated by arrows in the figure.*

To conclude this chapter and comparisons between hydraulic tests and GPR results, the following observations can be made:

- Overall, the results from GPR and hydraulic tests show good correlation.
- Of the GPR results, only one cannot assign transmissivity values to reflectors.
- It is difficult to determine whether the indicated fracture (reflector) is caused by blasting or not.
- In order to minimize the number of boreholes and hydraulic tests, GPR can be used as a tool for determining where to drill boreholes for transmissivity measurements of hydraulic connectors with a transmissivity higher than 10^{-9} m^2/s.
- GPR can be used to determine the extent of reflectors and thereby optimize the locations of boreholes.
- In areas where several interpreted reflectors exist and where the GPR EDZ response penetrates deeper, there is likely to be a higher integrated transmissivity representing larger volumes than in areas with a single reflector or in areas where the GPR EDZ response shows shallow penetration depth.

10 Conclusions and recommendations

10.1 General observations

The extensive investigations along 20 m of the TAS04 tunnel floor confirm the studies carried out by Olsson et al. (2009) in another tunnel at the Äspö HRL:

- Blast-induced fractures occur at low frequency. The highest fracture density is in the bottom charge at the end of each blast round due to higher charge weight.
- The depth of the excavation-induced fractures beneath the floor is interpreted to be on average 0.3 m for a column charge of 0.5 kg/m and 0.5 m for the short bottom charge (1.8 kg/m).
- Fracture penetration depth seldom exceeds the empirical design value.
- Both blast-induced and stress-induced fractures will form sub-parallel to the tunnel contour. The full extent and connectivity of the fractures can only be explored by indirect methods, such as hydraulic testing in boreholes or the use of geophysical methods in addition to geological mapping.
- The damage effect due to variation in the amount of explosives (kg/m) should be limited due to the small difference in nominal weight.
- The majority of injection tests with transmissivity > 10^{-8} m^2/s leaked to the tunnel floor. These flow paths are interpreted to be correlated with excavation-induced damage.
- Blast-induced fractures and increased apertures of natural fractures are the main source of the high transmissivity values in injection tests (down to max. 4–5 dm).
- The connectivity between induced fractures is, however, limited.
- Blast-induced fractures in some cores were not “open” (did not break the core). This indicates that there may be small-scale rock bridges in the blast-induced fractures.

10.2 Blast design

It would appear that the empirical blast design first proposed by Olsson and Ouchterlony (2003) may be slightly conservative in predicting the extent of blast-induced damage.

The drilling and charging plan used in the experiment can be considered to be a normal plan that could have been used in any Swedish tunnel project with the same requirements on blast damage. However, some modifications regarding the charge concentration in the stoping holes may have reduced the breakage problems. Such modifications will also provide greater robustness in the execution of future tunnels.

The current blast design used seems to be sufficiently good from the point of view of minimizing the blast-induced damage. However, breakage was not efficient with the current blast design. Oversized boulders and the need for reblasting of some perimeter holes occurred frequently. Greater efforts are required to optimize the blast design for efficient breakage as well as to limit the EDZ. More research is therefore recommended on the fragmentation process in a blast round, especially in brittle crystalline rock under high confinement. Primary parameters to study are probably:

- hole spacing,
- specific charge/specific drilling ratio,
- initiation sequence, and
- modifications of the charge concentration in the stoping holes.

In addition, a greater understanding of the influence of geological conditions (rock brittleness and fracturing) on blast efficiency and development of the EDZ would be valuable.

Improving the quality of the excavation also requires that drilling and charging be carried out according to specifications. This requirement was not fully met in the drilling of the floor in the TAS04 tunnel.

10.3 QA/QC of excavation works

It is recommended that procedures be established for continuous improvements in consultation with the miners if project-specific demands on perimeter control are to be met (Aijling et al. 2014). Implementation of new technologies or measures with the aim of increasing precision in drilling and charging requires sufficient time to analyze and work with the factors that influence the working environment. Identifying and listing the most important factors in checklists from a human factors engineering perspective in a tunnelling project and working systematically with these factors is an important part of ensuring constant improvements in the project. Aijling et al. (2014) also concluded that it is possible to utilize modern automated drilling and charging equipment for improved project control and documentation as long as the technical limitations are understood. However, such an approach imposes new demands on the tunnelling organization and its skills.

It is possible to conclude that high precision in drilling and charging with string emulsion can be achieved and documented using modern logger technology in the drilling and charging equipment.

Further development of the logger systems and processing software is needed in order to verify the results of logged emulsion in individual holes on an industrial scale. Evaluation of the results requires manual interpretation in order to combine data from the drilling and charging logs in the Äspö Expansion project. It is also recommended that development efforts be focused on simplifying interpretation of the charging log, for example by visualization of the results. It would be beneficial if the logger could deliver the concentration in kg/m instead of kg/ hole in chronological order. Automatic identification of each hole in the charging log for the drill plan is also a desired future improvement. Since SKB will stipulate requirements on traceability in the construction documentation to permit verification that all requirements related to post-closure safety are met, this development work will continue.

10.4 Verification methods

The approach of controlling the execution of the excavation works with checklists for the Contractor, use of modern loggers in drilling and charging equipment and Client follow-up inspection is fundamental in verifying that the design requirements on drilling and blasting are met.

This project has developed equipment for hydraulic testing and outlined testing and analysis procedures that have provided data permitting the successful characterization of the hydraulic properties of the rock mass in the tunnel floor. Fracture transmissivity is high in the upper 0.1–0.4 m of the tunnel floor, especially in the inner part of each blast round due to the heavier charge weight in the bottom charge. The connectivity of the most transmissive fractures is short and is normally connected to the tunnel floor. The longest connectivity observed in this project was approximately 7 metres, and it is usually less than 3 m.

Detailed geological mapping of the tunnel and drill cores is of great importance for correlating hydrogeological and geophysical measurements with site conditions. However, the geological documentation cannot capture all fractures of interest due to the limited number of conductive fractures, possible channelling flow and other factors. Other methods such as remote sensing and image processing may capture some of the fracture distribution, at least on the tunnel perimeter.

When the results of reflection and frequency analysis obtained from GPR measurements are considered together, a good estimate of the EDZ can be made within the limits of detectability and resolution. Generally, the results show that the upper 0.20–0.30 m of the tunnel floor is more fractured than the deeper parts. At some locations no increased fracturing is detected, indicating that no excavation-induced damage has occurred. It can also be noted, which can be confirmed by looking at single profiles, that there are locations and areas where there is no increased number of reflectors deeper than 0.1 m from the tunnel floor and where the GPR EDZ response does not show deeper penetration either. This indicates that the EDZ is limited in extent and is not continuous throughout the investigated floor area.

The GPR measurements also show good agreement between observed anomalies and test sections with measured section transmissivities > 10^{-8} m^2/s, indicating that fractures with higher transmissivity are easier to detect with GPR, which is also shown in Section 9.6, where a good correlation was found between a transmissive and gently dipping fracture and a radar reflector. A correlation was also found with borehole sections with even lower transmissivity, see Figure 9-16. However, GPR measurements in the tunnel floor have difficulty identifying steeply dipping (> 45–60 degrees) structures. Such structures are easiest to observe during mapping of the tunnel. Radar wave attenuation may in some cases also prevent features at greater depth from being detected beneath a strong reflector or diffractor.

This study proposes the following strategy to verify the extent and properties of interest of the EDZ:

- QA/QC procedures to verify that the requirements on the excavation works are met are fundamental to minimize the extension of the EDZ (see Section 10.1 and 10.2). Minor random non-conformities probably have no impact on the hydraulic properties of the EDZ.
- Additional hydraulic measurements, e.g. in the pilot holes of the deposition holes are needed to assess the hydraulic properties and continuity of the EDZ along the deposition tunnel.
- The GPR method is proposed to be used for verification of excavation results with regard to the EDZ. The survey should be conducted on a cleaned and dried tunnel surface with high accuracy, both horizontally (dense measurement point spacing) and vertically (dense sampling point interval and high radar frequency). The measurement lines are set parallel to the tunnel and line spacing should be sufficiently dense. The site-specific GPR settings should be determined in advance, allowing the application of the GPR EDZ method for mapping the lateral distribution of the EDZ and the maximum depth of the EDZ. Geological mapping of the tunnel is useful in analyzing the GPR results. Selection of reflectors is useful in order to get an image of the sub-horizontal fracture distribution and lengths.
- A smooth tunnel floor is beneficial for efficiency and quality in GPR measurements.
- Tunnel mapping and GPR surveys ought to be carried out before any pilot holes are drilled. Boreholes can cause reflections in the GPR measurements and change the pattern of water inflow to the tunnel.
- The fracture network in and below the tunnel floor should be co-interpreted with GPR surveying, tunnel mapping and core mapping. It is also recommended that the terminology for tunnel and core mapping be harmonized, especially with regard to open fractures.
- Televiewer investigations in pilot holes or ultrasonic measurements of drill cores provide complementary and supporting information, see e.g. Mustonen et al. (2010) and Ericsson et al. (2009).
- The same test section length should be considered for the boreholes. The length of test sections ought to be 0.4–0.5 m. The use of a borehole extender enables testing directly under the floor. There is however a possibility that the most shallow injection tests leaks to the floor.
- The injection pressure applied in hydraulic tests must be adapted to site conditions so that hydraulic fracturing is avoided.

10.5 Implications for the assessment of post-closure safety

Post closure safety aspects focus on the flow around the deposition hole and the groundwater flow paths and nuclide transport from each deposition hole to the surface.

Engineered flow conduits within a repository include: deposition tunnels, main tunnels, transport tunnels, ramp, shafts, and an excavation-damaged zone, EDZ, around the tunnels created during the construction of the repository. Long-term safety aspects include saturated flow and ensuring that all tunnels have been backfilled to ensure homogeneous properties.

Given the blasting design applied in the present project, the following recommendations for the management of the EDZ in a safety assessment are suggested:

- The rock mechanics situation with stress and strain response to the excavation has to be considered, even although stress-induced spalling is unlikely to occur.
- The relative pressure response may be regarded as a proxy parameter for describing the interference between injection and observation sections, also considering the measuring point distances. The injection test results, of the current study, show that most of the superficial 0–0.1 m sections are hydraulically connected with the tunnel floor. However, below this level the relative pressure responses show a significant decreasing trend versus depth to approximately 0.5 m (section midpoint). The few values below 0.5 m show a more constant relative pressure response. In the context of creating DFN models for the tunnel floor and its surroundings, the relative pressure responses could be used for calibration purposes.
- If the shallowest 10 to 20 centimetres are removed from the floor, transmissivity will be drastically reduced along the tunnel. Appropriate methods could be blasting of a bench or mechanical scaling.
- Conductive conditions due to blasting effects and rock stress redistribution should be considered as superimposed on natural conditions and may increase hydraulic conductivity in the repository tunnel floors.
- Measurement of hydraulic properties should focus on obtaining data on transmissivities or specific capacities using a specified test section length and injection duration time (i.e. equivalent values). Evaluation of the testing should consider initial conditions, hydraulic boundary conditions and test-scale aspects, treating different kinds of uncertainties in a robust way.
- GPR results show that water-saturated/filled gently dipping fractures cause most of the reflectors, and the GPR information makes it possible to estimate the lengths and apparent orientations of the reflectors. The GPR results can be superimposed on fracture mapping results and provide data for statistical fracture analysis and DFN modelling.

References

SKB's (Svensk Kärnbränslehantering AB) publications can be found at www.skb.se/publications.

Aijling G, Christiansson M, Christiansson R, Crilén J, Felldin M, Hogård H, Ittner H, Sturk R, 2014. Kvalitet som styrmedel vid bergschakt under jord. SBUF rapport 12773, Svenska Byggbranschens Utvecklingsfond. (In Swedish.)

Barker J A, 1988. A generalized radial flow model for hydraulic tests in fractured rock. Water Resources Research 24, 1796–1804.

Bernier F, Tsang C-F, Davies C, 2005. Geohydromechanical processes in the excavation damaged zone in crystalline rock, rock salt and indured plastic clays – in the context of radioactive waste disposal. International Journal of Rock Mechanics and Mining Science 42, 109–125.

Bäckblom G, 2008. Excavation damage and disturbance in crystalline rock – results from experiments and analyses. SKB TR-08-08, Svensk Kärnbränslehantering AB.

Bäckblom G, Martin C D, 1999. Recent experiments in hard rocks to study the excavation response. Implications for the performance of a nuclear waste geological repository. Tunnelling and Underground Space Technology 14, 377–394.

Bäckblom G, Christiansson R, Lagerstedt L, 2004. Choice of rock excavation methods for the Swedish deep repository for spent nuclear fuel. SKB R-04-62, Svensk Kärnbränslehantering AB.

Chandler N A, Kozak E T, Martin C D, 1996. Connected pathways in the EDZ and the potential for flow along tunnels. In Martino J B, Martin C D (eds). Designing the excavation disturbed zone for a nuclear repository in hard rock: procceedings of a Canadian Nuclear Society workshop, Winnipeg, Canada, 20 September, 1996. Toronto: Canadian Nuclear Society, 25–34.

Chandler N A, Cournut A, Dixon D A, Fairhurst C, Hansen F, Gray M, Hara K, Ishijima Y, Kozak E, Martino J, Matsumoto K, McCrank G, Sugita Y, Thompson P, Tillerson J, Vignal B, 2002. The five-year report of the Tunnel Sealing Experiment: An international project of AECL, JNC, ANDRA and WIPP. Report AECL-12727, Atomic Energy of Canada Limited.

Christiansson R, Jansson T, 2003. A test of different stress measurement methods in two orthogonal bore holes in Äspö Hard Rock laboratory (HRL), Sweden. International Journal of Rock Mechanics and Mining Sciences 40, 1161–1172.

Christiansson R, Karlzén R, 2010. New developments for careful blasting in hard rock tunnels. In Proceedings of ITA-AITES Word Tunnel Congress, Vancouver, 14–20 May 2010.

Christiansson R, Ericsson L O, Gustafson G, 2009. Hydraulic characterisation and conceptual modelling of the Excavation Disturbed Zone (EDZ). ISRM International Symposium on Rock Mechanics (SINOROCK 2009), Hong Kong, 19–22 May 2009, ISRM-SINOROCK-2009-177.

de Marsily G, 1986. Quantitative hydrogeology: groundwater hydrology for engineers. Orlando, FL: Academic Press.

Drake H, Tullborg E-L, 2004. Oskarshamn site investigation. Fracture mineralogy and wall rock alteration. Results from drill core KSH01A+B. SKB P-04-250, Svensk Kärnbränslehantering AB.

Eliasson T, 1993. Mineralogy, geochemistry and petrophysics of red coloured granite adjacent to fractures. SKB TR 93-06, Svensk Kärnbränslehantering AB.

Emsley S, Olsson O, Stenberg L, Alheid H-J, Falls S, 1997. ZEDEX – A study of damage and disturbance from tunnel excavation by blasting and tunnel boring. SKB TR 97-30, Svensk Kärnbränslehantering AB.

Ericsson L O, 1985. Värmeutbyte mellan berggrund och borrhål vid bergvärmesystem. (Heat exchange between crystalline bedrock and borehole in an energy well system.) PhD thesis. Chalmers University of Technology, Göteborg. (In Swedish with English extended summary.)

Ericsson L O, Brinkhoff P, Gustafson G, Kvartsberg S, 2009. Hydraulic features of the excavated disturbed zone – Laboratory investigations of samples taken from the Q- and S-tunnels at Äspö HRL. SKB R-09-45, Svensk Kärnbränslehantering AB.

Frieg B, Blaser P C (eds), 2012. Grimsel Test Site. Excavation Disturbed Zone Experiment. Nagra Technical Report NTB 98-01, Nagra, Switzerland.

Gray M N, 1993. OECD/NEA International Stripa Project 1980–1992. Overview Volume III, Engineered barriers. Svensk Kärnbränslehantering AB.

Gustafson G, 2012. Hydrogeology for rock engineers. Stockholm: Rock Engineering Research Foundation (BeFo).

Hudson J A, Harrison J P, 1997. Engineering and rock mechanics: an introduction to the principles Oxford: Pergamon.

Hudson J A , Bäckström A, Rutqvist J, Jing L, Backers T, Chijimatsu M, Christiansson R, Feng X-T, Kobayashi A, Koyama T, Lee H-S, Neretnieks I, Pan P-Z, Rinne M, Shen B-T, 2009. Characterising and modelling the excavation damaged zone in crystalline rock in the context of radioactive waste disposal. Environmental Geology 57, 1275–1297.

Ittner H, Bouvin A, 2015. Undersökning av sprängsprickor från mekaniserad laddning med bulkemulsion i bergtunnel. BeFo Report 144, Stiftelsen Bergteknisk forskning (Rock Engineering Research Foundation), Sweden.

Kantia P, Silvast M, Wiljanen B, Heikkinen E, Lehtimäki T, 2010. EDZ assessment in various geological environments using GPR method. Posiva Working Report 2010-04, Posiva Oy, Finland.

Karlzén R, Johansson E, 2010. Slutrapport från drivningen av TASS-tunneln. SKB R-10-31, Svensk Kärnbränslehantering AB.

Ludvigson J-E, Nordqvist R, Ekman L, Hansson K, 1999. Äspö Hard Rock Laboratory. Backfill and Plug Test. Hydraulic testing of core drilled boreholes in the ZEDEX drift. SKB IPR-09-01, Svensk Kärnbränslehantering AB.

Martino J B, Chandler N A, 2004. Excavation-induced damage at the Underground Research Laboratory. International Journal of Rock Mechanics and Mining Sciences 41, 1413–1426.

Martino J B, Kozak E, Woodcock D, Stroes-Gascoyne S, 2004. The blast damage assessment project at the URL. Report 06819-REP-01200-10123-R00, Ontario Power Generation, Nuclear Waste Management Division, Canada.

McEwen T, 2005. Review of the conclusions of previous EDZ workshops. In Impact of excavation disturbed or damaged zone (EDZ) on the performance of radioactive waste geological repositories. Proceedings of European Commission Cluster Conference and Workshop, Luxembourg, 3–5 November, 2003. EUR 21028 EN, European Commission, 137–142.

McWhorter D B, Sunada D K, 1977. Ground-water hydrology and hydraulics. Fort Collins, CO: Water Resources publ.

Moye D G, 1967. Diamond drilling for foundation exploration. Civil Engineering Transactions, Institute of Engineers (Australia), April, 95–100.

Mustonen S, Norokallio J, Mellanen S, Lehtimäki T, Heikkinen E, 2010. EDZ09 project and related EDZ studies in Onkalo 2008–2010. Posiva Working Report 2010-27, Posiva Oy, Finland.

Olofsson I, Christiansson R, Holmberg M, Carlsson A, Martin D, 2014. Application of the observational method in the Äspö Expansion Project. SKB R-13-44, Svensk Kärnbränslehantering AB.

Olsson M, Bergquist I, 1996. Crack lengths from explosives in multiple hole blasting. In Mohanty B (ed). Rock fragmentation by blasting : proceedings of The Fifth International Symposium on Rock Fragmentation by Blasting – Fragblast-5, Montreal, Canada, 25–29 August 1996. Rotterdam: Balkema, 187–191.

Olsson M, Ouchterlony F, 2003. Ny skadezonsformel för skonsam sprängning. SveBeFo Report 65, Stiftelsen Svensk bergteknisk forskning, Sweden. (In Swedish)

Olsson M, Niklasson B, Wilson L, Andersson C, Christiansson R, 2004. Äspö HRL. Experiences of blasting of the TASQ tunnel. SKB Report R-04-73, Svensk Kärnbränslehantering AB.

Olsson M, Markström I, Pettersson A, Sträng M, 2009. Examination of the Excavation Damaged Zone in the TASS tunnel, Äspö HRL. SKB R-09-39, Svensk Kärnbränslehantering AB.

Ouchterlony F, Olsson M, Svärd J, 2010. Crack length or blast damage from string emulsion and electronic detonators. In Sanchidrián J A (ed). Rock fragmentation by blasting: proceedings of the 9th International Symposium on Rock Fragmentation by Blasting – Fragblast 9, Granada, Spain, September 2009. Boca Raton, FL: CRC Press, 469–480.

Singhal B B S, Gupta R P, 1999. Applied hydrogeology of fractured rocks. Dordrecht: Kluwer Academic Publishers.

Sjöberg C, Larsson B, Lindström M, Palmqvist K, 1977. Sprängningsmetod för kontrollerad sprickutbredning och ökad säkerhet under jord. Projekt 77/224, Arbetarskyddsfonden. (In Swedish.)

SKB, 2011. Long-term safety for the final repository for spent nuclear fuel at Forsmark. Main report of the SR-Site project. SKB TR-11-01, Svensk Kärnbränslehantering AB.

SKB, 2013. RD&D Programme 2013. Programme for research, development and demonstration of methods for the management and disposal of nuclear waste. SKB TR-13-18, Svensk Kärnbränslehantering AB.

SSM, 2011. Granskning och utvärdering av SKB:s redovisning av Fud-program 2010. Rapport 2011:10, Strålsäkerhetsmyndigheten (Swedish Radiation Safety Authority). (In Swedish.)

Winberg A, 1991. The role of the disturbed rock zone in radioactive waste repository safety and performance assessment. A topical discussion and international overview. SKB TR 91-25, Svensk Kärnbränslehantering AB.

Zimmerman R W, Bodvarsson G S, 1996. Effective transmissivity of two-dimensional fracture networks. International Journal of Rock Mechanics and Mining Sciences & Geomechanics Abstracts 33, 433–438.